# Investigating Mass Transfer Limitations during Biodegradation of Micropollutants with Compound-Specific Isotope Analysis

**Dissertation**

der Mathematisch-Naturwissenschaftlichen Fakultät

der Eberhard Karls Universität Tübingen

zur Erlangung des Grades eines

Doktors der Naturwissenschaften

(Dr. rer. nat.)

vorgelegt von

Benno Nikolaus Ehrl

aus Gräfelfing

Tübingen

2018

Gedruckt mit Genehmigung der Mathematisch-Naturwissenschaftlichen Fakultät der Eberhard Karls Universität Tübingen.

| | |
|---|---|
| Tag der mündlichen Qualifikation: | 18.07.2018 |
| Dekan: | Prof. Dr. Wolfgang Rosenstiel |
| 1. Berichterstatter: | Prof. Dr. Martin Elsner |
| 2. Berichterstatter: | Prof. Dr. Stefan Haderlein |

## Danksagung — Acknowledgement

In erster Linie gilt mein Dank meinem Doktorvater Prof. Dr. Martin Elsner. Nicht nur für die hervorragende Betreuung, sondern auch dafür, dass ich immer sein Vertrauen genießen konnte. Außerdem sorgte Prof. Dr. Martin Elsner für ein eine wissenschaftliche Atmosphäre, in der die gesamte Gruppe ihre Ideen einbringen konnte, was sehr zum Gelingen dieser Arbeit beitrug.

Ich bedanke mich auch bei Prof. Dr. Stefan Haderlein für seine wertvolle Unterstützung als Betreuer im Thesis Commitee.

Furthermore, I want to thank Prof. Dr. Joel Pedersen for making my research stay at the University of Wisconsin possible and his excellent support.

Mein besonderer Dank gilt Kankana Kundu, Sviatlana Marozava, Mehdi Gharosoo und Kyoungtea Kim für Ihre fast täglich Unterstützung im Labor und ihren wissenschaftlichen Rat.

Ebenso möchte ich mich bei Armin Meyer, Martina Höche, und Aileen Melsbach für Ihre Unterstützung beim Troubleshooting und der Instandhaltung der Isotopenmassenspektrometer bedanken.

Zudem bedanke ich mich bei der gesamten Gruppe der Umweltisotopenchemie, dem Institut für Grundwasserökologie, dem Department of Soil Science und dem Department of Chemistry der UW-Madison.

# Table of Contents

Abstract....1

Zusammenfassung....3

1 Introduction....7

2 Objectives....13

3 Rate limiting mass transfer in micropollutant degradation revealed by isotope fractionation....15

3.1 Abstract....15

3.2 Introduction....16

3.3 Mimicking oligotrophic conditions in chemostat....19

3.4 Isotope fractionation of atrazine degradation in chemostats....19

3.5 Mass transfer limitations revealed by isotope fractionation....20

3.6 Numerical modeling provides a mass transfer estimate for membrane permeation....22

3.7 Adaptation of *A. aurescens* TC1 to oligotrophic conditions....23

3.8 Prominent role of mass transfer limitations in micropollutant degradation....25

3.9 Methods....26

3.9.1 Continuous cultivation....26

3.9.2 Numerical modeling of the chemostat cultivation....26

3.9.3 Calculation of enrichment factors in chemostats....27

3.9.4 Compound specific isotope analysis of atrazine in the bioreactor....28

3.9.5 Concentration measurements, cell counting, and microscopy....29

3.9.6 Statistical treatment of concentration and isotope data....29

4 Isotope fractionation pinpoints membrane permeability as barrier to atrazine biodegradation in Gram-negative *Polaromonas sp.* Nea-C....30

4.1 Abstract....30

4.2 Introduction....31
4.3 Experimental section....34
4.3.1 Chemicals....34
4.3.2 Cultivation of bacteria....34
4.3.3 Atrazine degradation with whole cells of *Polaromonas sp.* Nea-C for isotope analysis....34
4.3.4 Preparation of cell free extracts of *Polaromonas sp.* Nea-C....35
4.3.5 Atrazine degradation with cell free extracts of *Polaromonas sp.* Nea-C for isotope analysis....35
4.3.6 Atrazine degradation rates with and without respiratory chain inhibitor KCN. 35
4.3.7 Determination of the atrazine concentration by HPLC-UV....36
4.3.8 Carbon and nitrogen isotope measurements with GC-IRMS....36
4.3.9 Modelling of the isotope fractionation during the degradation....37
4.4 Results and discussion....38
4.4.1 Atrazine degradation with Gram-negative *Polaromonas sp.* Nea-C induced smaller isotope fractionation than observed with TrzN....38
4.4.2 Strong enzymatic isotope fractionation was masked by mass transfer limitations....41
4.4.3 Passive processes dominate atrazine uptake into the cell....42
4.4.4 Implications for the application of CSIA in field studies....43
4.4.5 Gram Pollutant mass transfer of non-polar pollutants may be rate limiting for biodegradation in Gram-negative bacteria....46
5 High permeation rates in liposome systems explain rapid glyphosate biodegradation associated with strong isotope fractionation....47
5.1 Abstract....47
5.2 Introduction....48
5.3 Experimental Section....51

5.3.1 Chemicals....51
5.3.2 Liposome preparation and characterization....51
5.3.3 Nuclear magnetic resonance spectroscopy....52
5.3.4 Assessing the line broadening due to chemical exchange across the liposome membrane....52
5.3.5 Bacterial isolation and characterization....52
5.3.6 Biodegradation of glyphosate by *Ochrobactrum sp.* FrEM....52
5.4 Results and Discussion....53
5.4.1 Praseodymium(III) ions interact with glyphosate as well as the liposome surface 53
5.4.2 Phosphorus decoupling in $^{1}H\{^{31}P\}$ NMR enabled peak shape analysis to quantify chemical exchange of glyphosate....54
5.4.3 Glyphosate permeation of lipid bilayers depends strongly on pH....56
5.4.4 Membrane permeation can lead to considerable glyphosate uptake into bacterial cells....58
5.4.5 Isolation and glyphosate degradation activity of *Orchrobactrum sp.* FrEM 60
5.4.6 Carbon isotope fractionation revealed rapid glyphosate mass transfer across the cell wall....62
5.4.7 Possibility of mass transfer limitations at low concentrations....63
6 Conclusion....65
6.1 Passive membrane permeation allows rapid atrazine turnover via biotic hydrolysis in the environment at high concentrations....65
6.2 Glyphosate permeates bacterial lipid membranes facilitating its biodegradation in the environment....67
6.3 Bioavailability limitations at trace concentrations in the environment....68
6.3.1 Mass transfer limitations reinforce nutrient scarcity under oligotrophic conditions....68

6.3.2 Bioavailability limitations impair assessment of biodegradation by CSIA in the field....68
6.4 Bacterial life under oligotrophic conditions is affected by bioavailability limitations and physiological adaptation....70
6.4.1 Possible interplay between mass transfer limitations and physiological adaptation....70
6.4.2 Proposed strategies to unravel physiological adaptation to oligotrophic conditions....71
6.4.3 The lower threshold for biodegradation might be determined by the maintenance demand of bacteria....72
Appendix A: Modeling contaminant biodegradation and compound-specific isotope fractionation in chemostats at extremely low dilution rates....73
Appendix B: Kankana....92
Appendix C: Supporting Information Chapter 3....93
Appendix D: Supporting Information Chapter 4....102
Appendix E: Supporting Information Chapter 5....106
Abbreviations....111
References....113

## Abstract

Worldwide, thousands of xenobiotics are discharged into the environment either by accident, e.g. in spills, or on purpose, e.g. when pesticides like atrazine or glyphosate are applied on agricultural fields. Even though most of these chemicals are initially degraded by bacteria, this degradation seems to stall at low concentrations in ground water and surface water. As a consequence, humans are exposed to a large number of these persistent chemical pollutants in drinking water. Two competing paradigms claim that biodegradation is either mass transfer limited or cell physiology limited. While multiple methods, e.g. proteomics, are available to study physiological adaptation, pinpointing mass transfer limitations is challenging, as simple concentration measurements are not sufficient. Therefore, we employed isotope fractionation during biodegradation, a promising concentration independent tool to identify and distinguish different rate determining steps of reactions, to unravel underlying mass transfer limitations during pollutant biodegradation. To mimic oligotrophic conditions where biodegradation seems to stall, we cultivated the atrazine degrader *Arthrobacter aurescens* TC1 in chemostat with atrazine as the sole carbon and nitrogen source. The dilution rate was varied and we observed a decreasing isotope fractionation factor from $\varepsilon^{13}C$ = -5.4 ‰ at 85 µg·L$^{-1}$ atrazine down to $\varepsilon^{13}C$ = -2.3 ‰ at 33 µg·L$^{-1}$ with decreasing residual atrazine concentrations. Thus, we were able to pinpoint a rapid onset of rate limiting mass transfer across the cell envelope when bacteria adapt to oligotrophic conditions and transition to stationary phase at slow growth rates. To further elucidate the role of the cell envelope as barrier to biodegradation, we (i) compared atrazine uptake in Gram-positive *Arthrobacter aurescens* TC1 and Gram-negative *Polaromonas sp.* NeaC and (ii) studied glyphosate permeation in liposome models systems and during biodegradation. The intrinsic enzymatic fractionation factor of atrazine hydrolysis by TrzN $\varepsilon^{13}C$ = -5.3 ‰ was masked in whole cells of *Polaromonas sp.* NeaC $\varepsilon^{13}C$ = -3.5 ‰, but not in Gram-positive *Arthrobacter aurescens* TC1. As the atrazine degradation rates were not reduced after inhibition of active transporter, we identified the outer membrane in Gram-negative *Polaromonas sp.* NeaC as the barrier to atrazine influx. High glyphosate permeation rates in the liposome model system indicate that

passive membrane permeation is also an underestimated uptake pathway for charged pollutants like glyphosate. Additionally, that this glyphosate uptake is not rate determining for glyphosate biodegradation was confirmed by strong isotope fractionation during glyphosate biodegradation by a newly isolated degrader strain *Ochrobactrum sp.* FrEM. To sum up, this thesis not only unravels the role of passive membrane permeation for pollutant degradation but also addresses the environmental implications of rate limiting mass transfer at low concentrations.

## Zusammenfassung

Weltweit werden tausende Xenobiotika in die Umwelt abgesondert. Dies geschieht entweder durch ungewollte Störfälle, z.B. durch Umweltverschmutzung, oder gewollt, z.B. durch Pestizide wie Atrazin oder Glyphosat, die auf landwirtschaftlichen Flächen ausgebracht werden, aber auch durch geklärte und ungeklärte Abwässer. Obgleich die meisten dieser Chemikalien zu Beginn durch Bakterien abgebaut werden, zeigen Forschungsergebnisse, dass dieser Bioabbau bei niedrigen Konzentrationen zu stocken scheint, was dazu führt, dass diese persistenten Schadstoffe unser Oberflächen- und Grundwasser belasten. So wird die Bevölkerung andauernd einer hohen Anzahl von Schadstoffen im niedrigen Konzentrationsbereich ausgesetzt. Zwei gegensätzliche — bis dato nicht unterscheidbare — Theorien versuchen die reduzierte Abbauaktivität bei niedrigen Konzentrationen zu erklären. Danach soll der Bioabbau entweder durch Massentransfer in die Bakterienzelle oder durch die Physiologie der Bakterien selbst limitiert sein. Während die physiologische Anpassung der Bakterien gut untersucht werden kann, z.B. mittels Proteomics, reichen Konzentrationsmessungen nicht aus, um Massentransferlimitierungen nachzuweisen. Deshalb nutzten wir Isotopenfraktionierung während des Bioabbaus von Schadstoffen, um mittels dieses vielversprechenden, konzentrations-unabhängigen Hilfsmittels den geschwindigkeitsbestimmenden Schritt der Abbaureaktion zu bestimmen. So konnten wir latente Massentransferlimitierungen bei der Aufnahme der Schadstoffe in die Bakterienzelle nachweisen. Wir untersuchten den Atrazinabbau durch *Arthrobacter aurescens* TC1 in Chemostat mit Atrazin als einzige Kohlen- und Stickstoffquelle und konnten damit die oligotrophen Bedingungen nachstellen, unter denen der Bioabbau zu stocken beginnt. Die Verdünnungsraten wurden reduziert und mit den entsprechend sinkenden Atrazinkonzentrationen beobachteten wir eine verringerte Isotopenfraktionierung. Die Anreicherungsfaktoren nahmen von $\varepsilon^{13}C$ = -5.4 ‰ bei einer Atrazinkonzentration von 85 µg·L$^{-1}$ auf $\varepsilon^{13}C$ = -2.3 ‰ bei 33 µg·L$^{-1}$ ab. So konnten wir zum einen zeigen, dass bei niedrigen Konzentrationen Massentransfer in die Bakterienzelle überraschend schnell limitierend wurde, und zum anderen, dass diese Massentransferlimitierung von einer Adaptation der Bakterien an die oligotrophen Bedingungen und einem Übergang in die stationäre

Wachstumsphase einherging. Um die Rolle der Zellhülle als Permeationsbarriere genauer zu bestimmen, untersuchten wir außerdem (i) Unterschiede zwischen grampositivem *Arthrobacter aurescens* TC1 und gramnegativem *Polaromonas sp.* NeaC in der Aufnahme von Atrazin und (ii) die Permeation von Glyphosat in Liposomen als Modellsystem und den entsprechenden Glyphosatbioabbau. Der intrinsische enzymatische Fraktionierungsfaktor der Atrazinhydrolyse durch das Enzym TrzN $\varepsilon^{13}C$ = -5.3 ‰ wurde durch die intakte Zellhülle in *Polaromonas sp.* NeaC maskiert $\varepsilon^{13}C$ = -3.5 ‰. Da weder die Isotopenfraktionierung in dem grampositiven *Arthrobacter aurescens* TC1 maskiert war, noch die Atrazinabbauraten durch Inhibierung von aktiven Transportern beeinflusst wurden, bestimmten wir die zusätzliche äußere Bakterienmembran des gramnegativen *Polaromonas sp.* NeaC als Barriere für die passive Membranpermeation. Die Permeation der geladenen Glyphosatmoleküle erfolgte in den Liposomen als Modellsystem deutlich schneller als erwartet. Dies weist darauf hin, dass die Membranpermeation eine unterschätzte Aufnahmeroute in Bakterien auch für geladene Moleküle ist, was auch durch starke Isotopenfraktionierung während des Bioabbaus von Glyphosat bestätigt wurde. Die Anreicherung der schweren Isotope im Medium dient dabei als Nachweis, dass der Glyphosataustausch über die Zellhülle des isolierten *Ochrobactrum sp.* FrEM schneller war als der enzymatische Abbau im Cytosol. So konnten wir in dieser Arbeit die Rolle passiver Membranpermeation für den Bioabbau von Schadstoffen bestimmen und weiter die Auswirkungen von Massentransferlimitierungen bei niedrigen Konzentrationen aufzeigen.

## Declaration according to § 5 Abs. 2 No. 8 of the PromO of the Faculty of Science

### -Share in publications done in team work-

**List of Publications**

1. Benno N. Ehrl, Kankana Kundu, Mehdi Gharasoo, Sviatlana Marozava, and Martin Elsner

   "Rate-limiting mass transfer in micropollutant degradation revealed by isotope fractionation in chemostat"

*Environmental Science & Technology* Just Accepted Manuscript; DOI: 10.1021/acs.est.8b05175.

2. Benno N. Ehrl, Mehdi Gharasoo, and Martin Elsner

   "Isotope Fractionation Pinpoints Membrane Permeability as a Barrier to Atrazine Biodegradation in Gram-negative Polaromonas sp. Nea-C"

*Environmental Science & Technology* 2018 52 (7), 4137-4144

3. Benno N. Ehrl, Emmanuel O. Moguso, Kyoungtea Kim, Heike Hofstetter, Joel A. Pedersen, and Martin Elsner

   "High Permeation Rates in Liposome Systems Explain Rapid Glyphosate Biodegradation Associated with Strong Isotope Fractionation"

*Environmental Science & Technology* 2018 52 (13), 7259-7268.

| Nr. | Accepted for publication yes/no | Number of all authors | Position of the candidate in list of authors | Scientific ideas of candidate (%) | Data generation by candidate (%) | Analysis and Interpretation by candidate (%) | Paper writing by candidate (%) |
|---|---|---|---|---|---|---|---|
| **1** | yes | 5 | 1 | 60 | 80 | 70 | 70 |
| **2** | yes | 3 | 1 | 90 | 100 | 90 | 90 |
| **3** | yes | 6 | 1 | 60 | 50 | 60 | 60 |

# 1 Introduction

Growing production and usage of ever more xenobiotics leads to aggravated discharge into the environment.[1] These anthropogenic contaminants are often mobile in ground water, our main source of drinking water, and directly threaten human health.[2] Past research has prominently focused on typical legacy pollutants like carcinogenic polyaromatic hydrocarbons,[3] petroleum residues,[4] explosives,[5] and halogenated hydrocarbons[6] which originate from industrial spills[7] forming high concentration point sources. In contrast, new challenges are posed by micropollutants, as these emerging contaminants enter the environment in multi-ton scale and with large spatial variability.[8] Industrial chemicals,[9] household chemicals (e.g. pharmaceuticals[10-12]) and personal care products[13] are not completely degraded in wastewater treatment plants and discharged into surface water. Furthermore, toxic and carcinogenic disinfectant byproducts can form during chemical wastewater treatment.[14] In addition, pesticides applied on agricultural fields[15, 16] directly leach into the groundwater with precipitation and groundwater recharge.[17-19]

Therefore, the European Union regulations on drinking water quality set a maximum concentration of 0.1 µg/l for pesticides and their degradation products (European Union Drinking Water Directive, 98/83/EC). However, many pesticides are frequently detected in groundwater above this threshold concentration.[20, 21] For example, the herbicide atrazine is one of the most abundant micropollutants, even though it has been banned in the EU for over a decade.[22, 23] Also, readily degradable pesticides like glyphosate are detected with increasing frequency in surface and groundwater.[19] Both, atrazine and glyphosate were, or still are, widely used herbicides. While atrazine is selective against broadleaf weeds and often used in maize or sugar cane production,[24] glyphosate is a non-selective broad band herbicide.[25] Its success depends on several characteristics: first, glyphosate's acute toxicity to humans is thought to be low.[26] Second, its half life in soil is short, allowing short treatment-planting cycles and even crop desiccation.[27, 28] Third, "glyphosate ready" crops (genetically modified to be glyphosate resistant) are available, which makes glyphosate usage throughout the whole cultivation period

possible.[29] The increasing detection frequency of those pesticides in our drinking water resources leads to growing concerns about their ecological implications and their effect on human health.[30, 31]

While the micropollutant concentrations initially decrease due to sorption[32, 33] and dilution,[34] the most effective and sustainable remediation pathway is natural biodegradation by bacteria, as they break down the pollutants for use as nutrients to gain energy and to build up biomass.[35, 36] However, nutrient scarcity under oligotrophic conditions can limit biodegradation, as the available concentration of nutrients like the electron acceptor,[37] nitrogen,[38] and phosphorus[39] puts a limit microbial growth.[40] Furthermore, even though many persistent micropollutants are frequently detected[41, 42] and thus available as nutrients to bacteria, biodegradation is observed to stall below a certain threshold concentration.[40] The limitations of microbial degradation of micropollutants under oligotrophic conditions have eluded researchers for years. Competing and contradicting models claim that either (i) pollutant uptake into microbial cells is rate limiting for pollutant turnover,[43-45] or (ii) physiological limitations (i.e. downregulation of the degrading enzyme) are responsible.[46] Nutrients can be taken up by bacterial cells either via active transport[47] or passively, i.e. assisted by porins[48] or membrane permeation.[49, 50] Pollutant uptake into bacteria can be rate-limiting for biodegradation if either active transport is slower than the enzyme reaction,[43, 51] or the concentration gradient driving the passive uptake processes becomes too shallow to overcome the cell envelope as a diffusion barrier.[3] On the other hand, bacteria make use of multiple strategies to adapt to low nutrient concentrations. First, at low pollutant concentrations other nutrients might be more favorable and degradation enzymes might be up- or down-regulated under different conditions.[52, 53] Furthermore, bacteria are not only limited by their maintenance demand,[54] but they might actively pursue strategies like reducing their cell size[55] and lowering their DNA content,[56] which allows bacteria to redirect the saved energy to maintain basic cell functions. Due to their low concentrations and the complex processes in the subsurface, investigating the limitations of micropollutant turnover is challenging. As a consequence, targeted strategies to improve the occurring natural attenuation and to ensure the micropollutant

turnover also at trace concentrations are lacking, and innovative research strategies are required to elucidate the true bottleneck of biodegradation.

A systematic approach to investigate pollutant degradation is to study the degrading bacteria (either as isolated bacterial strains[57, 58] or mixed bacterial cultures[59, 60]) in the laboratory, i.e. either as cell suspension cultures[61-63] or even attached to sediment.[64, 65] While experiments including sediment are useful to study bacterial adaptation[66, 67] it is not possible to distinguish mass transfer across the cell envelope from other physical processes (sorption, dispersion, diffusion).[68, 69] Pollutant degradation in batch, when bacteria are exposed to the pollutant and the ongoing degradation is studied over time, leads to conditions which are not comparable with environmental conditions. The initially high pollutant concentration is consumed, leading to varying concentrations and to exponential biomass growth. Furthermore, bacteria eventually reach high cell densities and enter the stationary growth phase which leads to changing biodegradation kinetics. Recently, continuous cultivation in bioreactors (chemostat and retentostat) mimicking environmental conditions has also been introduced to study pollutant degrading bacteria.[52, 70] While in chemostat a steady state in concentration and biomass is balanced by a constant influx of a limiting nutrient and outflow of the degraded nutrient and biomass, the biomass is retained in retentostat. This biomass accumulation leads to a further concentration decrease and, in the end, to a near zero growth rate where most of the pollutant degraded is used for bacterial maintenance. Chemostat cultivation has the advantage that the bacteria are cultivated under steady state conditions for an extended time period. As a consequence, physiological adaptation, and potentially even evolution due to high selection pressure, can be observed.[44, 71, 72] Furthermore, the residual pollutant concentration only depends on the dilution rate, i.e. the inflow and outflow rate divided by the reactor volume. By varying the dilution rate, the steady state residual pollutant concentrations can be adjusted to resemble oligotrophic conditions and bacteria can be kept at low growth rates.[40] As a consequence, the opportunity to study bacterial pollutant degradation at varying steady state concentrations allows pinpointing the threshold concentration below which degradation is limited and elucidating the prevailing bottleneck (mass transfer limitation or physiological limitations). However, concentration measurements are not suitable to provide insight

into why biodegradation stalls. Either there is degradation and the concentration decrease can be observed, or the degradation ceases, leading to constant concentrations. To solve this issue, concentration independent techniques to monitor ongoing biodegradation need to be employed.

Here, the analysis of the stable isotope ratio of the pollutants ($^{13}C/^{12}C$ and $^{15}N/^{14}N$) during biodegradation offers an additional line of evidence. Instrumental advancements by coupling a gas chromatograph for compound separation to an isotope ratio mass spectrometer (GC-IRMS) allowed the assessment of isotope ratios for single compounds in complex mixtures, such as cultivation media, by compound specific isotope analysis (CSIA).[73, 74] The isotope ratio $^{13}C/^{12}C = R_C$ is usually expressed relative to an international standard by the delta notation $\delta^{13}C$ (1) and is denoted in per mil (‰).[75, 76]

$$\delta^{13}C = \frac{R_C - R_C^{Ref}}{R_C^{Ref}} \quad (1)$$

The expression of isotope ratios for nitrogen isotopes is accordingly $\delta^{15}N$. The international reference materials are Vienna Pee Dee Belemnite[77] (VPDB) for carbon and atmospheric air for nitrogen.[78]

The isotope ratios of pollutants undergo changes during biodegradation. The mass differences of the isotopologues lead to small differences in the vibrational energies. Thus, the activation energies for bond breakage differ for the isotopologues and thus also the rate constants for heavy isotopes $^{h}k$ and light isotopes $^{l}k$ are different. As a consequence, the irreversible reaction of a substrate S (2) leads to a primary kinetic isotope effect *KIE* (3) as the reaction proceeds at different rates for the heavy and the light isotopes[79, 80].

$$S \xrightarrow{k} P \quad (2)$$

$$KIE = \frac{^{l}k}{^{h}k} \quad (3)$$

Most chemical reactions lead to a normal isotope effect, i.e. the heavy isotopes react slower as a chemical bond containing a heavy isotope has lower ground state vibrational energy and, thus, a higher activation energy ($^{h}k < {}^{l}k$).[81] In contrast, the rare inverse isotope effect can only be observed if the rate determining step leads to a strengthened bond in the transition state. Here the activation energy for the heavy

isotope is smaller and thus reacts faster than the light isotope ($^{h}k > {}^{l}k$).[81] As the heavy isotopes have a low natural abundance, the enrichment or depletion of heavy isotopes ($R_C(t)/R_C(t=0)$) can be described by the Rayleigh equation where isotope ratios exponentially increase or decrease (normal or inverse isotope effect) with the fraction of the remaining pollutant $f$ (4).[13, 14]

(4)

The enrichment factor $\varepsilon^{13}C$ denoted in per mil describes how much slower (normal isotope effect) or faster (inverse isotope effect) the heavy isotopologue reacts.

Isotope fractionation has also been pioneered to detect pollutant degradation directly in the environment.[82-84] Changing isotope ratios along the flow path of a pollutant or over time can be used to reliably detect ongoing biodegradation where concentration measurements fail and the biodegradation progress is quantified with the Rayleigh equation (4). The prerequisite for precise biodegradation assessment, however, are reliable enrichment factors derived in laboratory experiments which are representative for the isotope fractionation occurring during biodegradation in the environment.

Other processes preceding the enzymatic turnover may mask the isotope fractionation of the degradation reaction. In a multi-step transformation reaction, the observable isotope fractionation depends on reversible individual steps leading up to the irreversible transformation discriminating against the isotopologues. If a preceding step becomes rate determining, the observable isotope fractionation will be smaller, as the downstream isotopic discrimination is not carried back to the initial substrate pool where the isotope ratio is assessed. The phenomenon of such masked isotope fractionation is well known in inorganic reactions like photosynthesis,[85, 86] sulfate reduction,[87-89] and nitrate reduction.[90, 91] The concept that non-polar organic pollutant mass transfer across the cell envelope can be rate limiting as well, has been predicted by Thullner *et al.*.[92] This masking effect has also been demonstrated for bacterial degradation at high pollutant concentrations and artificially high biomass,[93] for slow mass transfer from a donor phase to the water phase,[94] or for rate determining active transport of the pollutant into the cytosol.[51] Also, slow membrane permeation can limit the concentration

gradient dependent influx[48] and mask the enzymatic isotope fractionation.[95] As a consequence, if the mass transfer across the cell envelope constitutes the bottleneck for biodegradation at low concentrations, the observable isotope fractionation will be smaller than at high concentrations.

To investigate membrane permeation processes, various model systems with increasing complexity are available, e.g. the octanol water distribution coefficient, lipid discs, black lipid membranes, liposomes, and synthetic membranes.[49, 96] These model systems are often used to study the diffusion of drugs and cosmetics through human epithelium,[97-99] but little is known about the transport of small hydrophobic molecules like micropollutants through a bacterial membrane.[100] For different molecules active transport,[101] but also passive permeation,[102] have been described. Furthermore, the passive permeation of compounds strongly depends on the membrane fluidity[103] and adjustment of the membrane fluidity is a rapid way of bacterial adaptation to changing environments.[104-106] Therefore, permeation rates valid for natural systems can only be obtained in model systems resembling natural lipid bilayers, e.g. liposomes with natural lipid composition.[103, 107] Passive permeation of the liposome membrane leads to chemical exchange between the inside and the outside of the liposomes. This exchange can be traced by nuclear magnetic resonance (NMR) spectroscopy by adding a non-permeable chemical shift reagent, like lanthanide ions (e.g. $Pr^{3+}$).[98, 108, 109] The chemical shift reagent leads to a change in the resonance frequency Δδ and shifts the peak of the molecules outside the liposomes downfield. When the exchange is slow on the NMR timescale, i.e. the mass transfer coefficient $k_{tr}$ is slower than the frequency shift ($\Delta\delta\ k_{tr}/\Delta\delta < 1$), two distinct peaks appear in the spectrum that can be attributed to molecules which are inside and outside the liposomes.[108] A single combined peak with an averaged chemical shift in the middle appears when the exchange is fast on the NMR timescale ($\Delta\delta\ k_{tr}/\Delta\delta > 1$). Based on the evaluation of associated line broadening in the NMR spectrum, peak shape analysis may subsequently serve to quantify chemical exchange for both cases.[110] Together with the structural properties of the liposome, this can be used to calculate the permeation rate. Then, these permeation rates are an additional line of evidence to elucidate how the mass transfer across the cell envelope is rate limiting for the biodegradation of micropollutants.

# 2 Objectives

This thesis aims to elucidate possible mass transfer limitations during biodegradation of the micropollutants atrazine and glyphosate. Batch degradation of atrazine by *Arthrobacter aurescens* TC1 at high concentrations leads to a pronounced carbon isotope effect.[111] Also, the atrazine degradation with the purified degrading enzyme TrzN[112] and atrazine turnover in an abiotic model reaction[111] showed similar isotope fractionation. This strong isotope fractionation demonstrates that mass transfer across the cell envelope is not rate limiting for atrazine biodegradation, at least at high concentrations. In addition, the reaction mechanism (hydrolysis to hydroxyatrazine catalyzed by TrzN) can easily identified by the combination of nitrogen and carbon isotope analysis.[113, 114] The rate determining step is the protonation of a nitrogen atom in the aromatic ring which stabilizes the C=N bond. This leads to an inverse secondary nitrogen isotope effect ($\varepsilon^{15}N > 0$) and a distinct negative slope in the dual element isotope plot ($\lambda \approx \varepsilon^{15}N / \varepsilon^{13}C$). As a consequence, any non-fractionating step masking the isotope fractionation of TrzN will mask both enrichment factors $\varepsilon^{13}C$ and $\varepsilon^{15}N$ to the same extent, and the dual element isotope slope λ will stay constant. However, bacterial adaptation resulting in a different transition state will likely also affect the primary and secondary isotope effects of the two elements which will lead to an altered dual element isotope slope λ.

Chapter 3 aims to pinpoint possible mass transfer limitations at trace concentrations during biodegradation by cultivating *Arthrobacter aurescens* TC1 in chemostat with atrazine as the only carbon and nitrogen source. The dilution rate was varied to adjust the residual atrazine concentrations mimicking oligotrophic conditions and the bacteria were kept at steady state to allow adaptation to the different conditions. Then samples for isotope analysis were taken, atrazine was extracted and the isotope ratio of atrazine was analyzed by GC-IRMS. The enrichment factors obtained in chemostat were compared with those from atrazine degradation in batch and with the purified enzyme.[111, 112] Furthermore, quantified mass transfer limitations by numerical modelling and thus expanded the existing theoretical framework described by Thullner *et al*..[92]

This numerical model also forms the basis for a related study that is provided in Appendix A. Furthermore, at the same time points when samples for isotope analysis were taken from the chemostat, we also took samples for proteomic analysis. This related study, which can be found in Appendix B, aims to unravel the role of bacterial adaptation under oligotrophic conditions and how maintenance demand constitutes a limiting factor for pollutant biodegradation and bacterial growth.

Chapter 4 of this thesis addresses the role of cell envelope physiology in bioavailability limitations. While the cell envelope of Gram-positive bacteria like *Arthrobacter aurescens* TC1 contains a single inner membrane, Gram-negative bacteria like *Polaromonas sp.* Nea-C possess an additional restrictive outer membrane.[62] This additional barrier is described to reduce the influx of xenobiotics into bacteria[95] which is important for antibiotic resistance.[48] We aim to unravel to what extent the outer membrane in *Polaromonas sp.* Nea-C constitutes a bottleneck for atrazine biodegradation. Therefore, we analyzed isotope fractionation during atrazine degradation with whole cells and cell free extracts of *Polaromonas sp.* Nea-C. To observe how the inhibition of energy dependent active transport affects the atrazine degradation, we used cyanide to inhibit the respiratory chain and analyzed the atrazine degradation rates.

Chapter 5 aims to elucidate whether also charged micropollutants like glyphosate can permeate the cell envelope and if this passive permeation leads to substantial glyphosate uptake into bacteria during biodegradation. Glyphosate membrane permeation with respect to different protonation states of glyphosate was studied in liposome model systems by NMR at varying pH. The derived permeation coefficients were used to estimate the glyphosate influx rates into bacterial cells for comparison with published glyphosate degradation rates.[58] In addition, a glyphosate degrader was isolated from glyphosate amended soil. Then, during glyphosate biodegradation, carbon isotope fractionation was used as diagnostic tool to detect possible mass transfer limitations and thus confirm our theoretical considerations.

# 3 Rate limiting mass transfer in micropollutant degradation revealed by isotope fractionation

Benno N. Ehrl, Kankana Kundu, Mehdi Gharasoo, Sviatlana Marozava, and Martin Elsner

Reproduced in part with permission from *Rate-limiting mass transfer in micropollutant degradation revealed by isotope fractionation in chemostat* Benno N. Ehrl, Kankana Kundu, Mehdi Gharasoo, Sviatlana Marozava, and Martin Elsner; Environmental Science & Technology; Just Accepted Manuscript; DOI: 10.1021/acs.est.8b05175. 

## 3.1 Abstract

Biodegradation of persistent micropollutants like pesticides often stalls at low concentrations (μg/L) in the environment. Mass transfer limitations or physiological adaptation are debated to slow down microbial degradation under these conditions. Although promising, evidence from compound-specific isotope fractionation analysis (CSIA) yet remains unexplored for this low concentration regime. We accomplished CSIA for degradation of the persistent pesticide atrazine during cultivation of *Arthrobacter aurescens* TC1 in chemostat under four different dilution rates leading to 82, 62, 45, and 32 μg/L residual atrazine concentrations. Isotope analysis of atrazine revealed a drastic decrease in isotope fractionation with declining residual substrate concentration from $\varepsilon^{13}C$ = -5.36 ± 0.20‰ at the highest concentration to $\varepsilon^{13}C$ = -2.32 ± 0.28‰ at the lowest concentration. At high concentrations $\varepsilon^{13}C$ of the biodegradation with whole cells fully represented the isotope effect of the enzyme reaction. At low concentrations contrasting, smaller $\varepsilon^{13}C$ indicated that this isotope effect was masked. Supported by numerical modeling, these observations indicate that mass

transfer across the cell membrane became rate-limiting for biodegradation. This onset of mass transfer limitation was observable at concentrations resembling oligotrophic conditions, and was accompanied by physiological adaptations to nutrient limitation. We conclude that mass transfer limitations are important for biodegradation in the environment and that this may bias pollutant turnover estimations by CSIA.

## 3.2 Introduction

Assessing the biodegradation of anthropogenic micropollutants is a prominent challenge of our time. Industrial chemicals,[9] disinfectant byproducts,[14] pharmaceuticals,[10] personal care products,[13] and pesticides[15, 19] are released from non-point sources. They are detected with increasing frequency at trace concentrations (ng/L to µg/L) in the environment with the potential to impact ecosystem and human health.[1, 115] Assessing and understanding their degradation raises two aspects of fundamental importance: first, the identification of the limits of biodegradation and second, an *in-situ* assessment of biodegradation.

First, micropollutants are often quite persistent[41] because biodegradation is observed to stall below a certain threshold concentration.[40] Underlying bottlenecks of biodegradation under such oligotrophic conditions have eluded researchers for years. Competing models claim that it is either mass transfer (uptake into microbial cells) which puts a limit to otherwise rapid enzymatic transformation,[43-45] or that physiological limitations (enzyme activity, maintenance mode) prevail.[46] A current obstacle for management and natural attenuation strategies is, therefore, the missing understanding of the true limitations in pollutant degradation at very low concentrations.

Second, it is a challenge to confidently detect biodegradation in complex natural systems. Environmental micropollutant concentrations decrease not only due to degradation, but also by physical processes (diffusion, sorption, transport). Concentration analysis alone is, therefore, not sufficient. Compound-specific isotope analysis offers an alternative opportunity, because information on degradation is not derived from concentrations, but instead from stable isotope ratios of a pollutant. Due to the isotope effect of enzymatic reactions, biodegradation leads to an enrichment of

heavy isotopes at their natural abundance in the remaining pollutant molecules.[116] These changes in isotope ratios can, therefore, provide evidence as “isotopic footprints” of ongoing biodegradation at contaminated sites.[117-119]

Both research aspects are connected, however: isotope fractionation of an ongoing degradation reaction is influenced by mass transfer limitations as shown in **Figure 1.**[19,20] When mass transfer across a cell membrane becomes increasingly rate-limiting, molecules cannot get out of the cell any longer to make the enzyme’s isotope effect visible in solution where samples are taken for isotope analysis. Hence, degradation-associated isotope fractionating of the pollutant is masked and decreases. This has two consequences. First, if mass transfer limitations prevail at low concentrations, a decrease in isotope fractionation is expected to give evidence of such bioavailability limitation. Second, however, this means that such low isotope fractionation will no longer accurately reflect the true turnover of trace concentrations in natural systems!

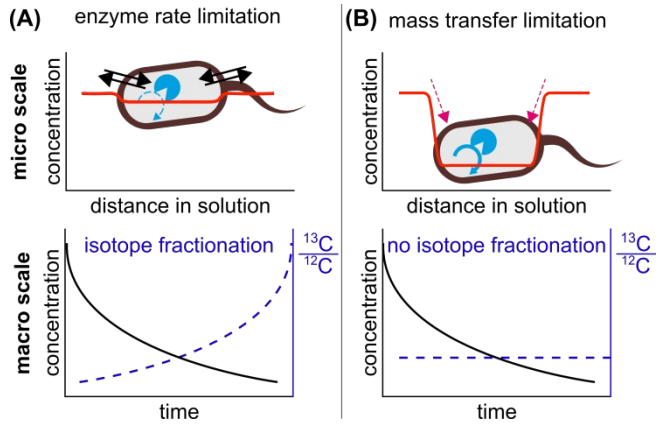


**Figure 1: Isotope fractionation depends on the rate-determining step.** $^{13}C/^{12}C$ isotope ratios are analyzed in the residual, not yet degraded substrate fraction outside the cell in solution. The strong, enzyme-specific isotope fractionation can only be observed if pollutant molecules outside the cell are in rapid exchange with the molecules inside the cell where the comparatively slow enzyme reaction takes place (**Case A: enzyme rate limitation**). In contrast, if mass transfer across the cell membrane is slow in supplying enough substrate molecules for an enzyme reaction that is comparatively fast, this leads to lower substrate concentrations inside the cell (**Case B: mass transfer limitation**). Molecules still diffuse into the cell and are transformed. However, since practically every molecule that enters the cell is degraded,

molecules cannot get out “reporting” on the isotope effect and make it visible in solution. Thus, the mass transfer masks the isotope fractionation of the enzyme reaction.

How cell uptake can mask the isotope fractionation of the enzymatic reaction is well studied for inorganic processes like photosynthesis,[86] sulfate reduction,[88, 89] or nitrate reduction.[91] However, organic pollutants as small non-polar molecules can permeate bacterial cell membranes even without active transport.[48, 120] Indeed, numerous studies have reported high observable isotope fractionation in organic contaminant degradation[111, 121, 122] reflecting the isotope fractionation of the enzymatic reaction.[112] However, practically all of these batch studies suffer from the artifact that – because of the substantial substance amount required for multiple isotope analysis – experiments were conducted at high (>1 mg/L) pollutant concentrations as shown in **Figure 2**. The low concentration range of oligotrophic conditions in the environment (µg/L), in contrast, is practically unexplored territory when it comes to isotope fractionation.[123]

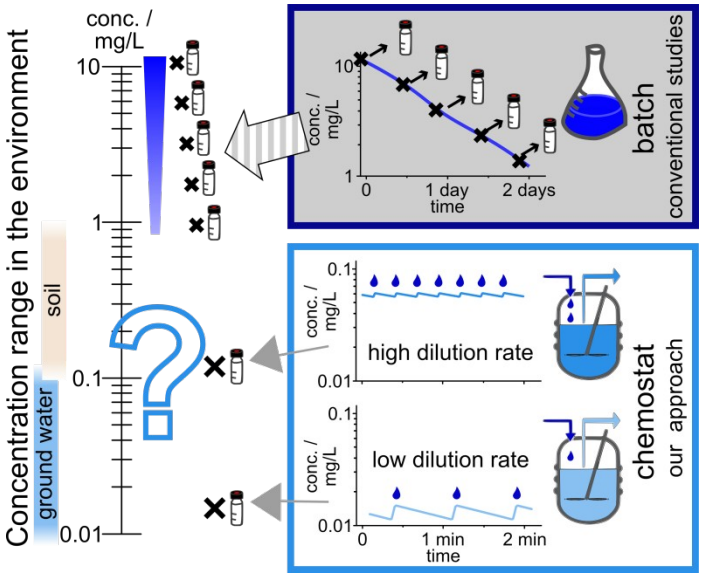


**Figure 2: Conventional isotope fractionation studies have been conducted at high concentrations, whereas the chemostat approach allows measuring isotope fractionation at low, environmentally relevant concentrations.** Typical pesticide and pharmaceutical concentrations in the environment are in the µg/L to sub-µg/L regime, whereas laboratory-based batch studies have consistently investigated degradation-associated isotope fractionation at

much higher (mg/L) concentrations (upper panel). Chemostat experiments (lower panel) close the gap by achieving distinct, small steady-state concentrations through varying the dilution rate. Our numerical modelling validates the approach by demonstrating that the oscillation of the residual substrate concentration - resulting from drop wise addition of the media - is negligible.

## 3.3 Mimicking oligotrophic conditions in chemostat

We established a new approach to explore isotope fractionation during micropollutant degradation by microorganisms adapted to trace contaminant concentrations. Our study is based on the model microorganism *Arthrobacter aurescens* TC1, a pesticide-degrading bacterium which grows on atrazine as sole carbon and nitrogen source.[63] Hydrolysis by the cytoplasmatic enzymes TrzN, AtzB, and AtzC first leads to 2-hydroxyatrazine and subsequently produces cyanuric acid, while the alkylamine sidechains are further mineralized or used to build up biomass as shown in **Figure C1.**[124] These pesticide-degrading bacteria were cultivated in chemostat (**Figure 2**). By lowering the dilution rate of the chemostat stepwise (from 0.023 $h^{-1}$ to 0.006 $h^{-1}$), environmentally relevant steady-state concentrations of pollutants were established (32 µg/L at the lowest dilution rate) and these concentrations were varied to probe for the onset of mass transfer limitations. The chemostat approach allowed withdrawing sufficient amounts of sample at steady-state to facilitate isotope analysis. Simultaneously, bacteria could adapt to low concentrations mimicking oligotrophic conditions.

## 3.4 Isotope fractionation of atrazine degradation in chemostat

Aerobic cultivation of *A. aurescens* TC1 in chemostat at a high dilution rate (0.023 $h^{-1}$; t = 19 days; **Figure C2**) resulted in a steady state residual atrazine concentration of 82.6 ± 2.0 µg/L meaning that more than 99.8 % of the atrazine of the inflow was degraded. Similar atrazine concentrations are also found in US groundwater[125] and resemble oligotrophic conditions.[40, 126] The isotopic signature of atrazine in the bioreactor showed a difference of $\delta^{13}C_{in} - \delta^{13}C_{reac} \approx \varepsilon^{13}C$; $\varepsilon^{13}C$ = -5.36 ± 0.20 ‰ compared to the inflow, which – as we predict (see theoretical treatment in the Methods section) – is identical to the enrichment factors determined in

high concentration batch degradation with resting cells[111] and pure enzyme.[112] This strong isotope fractionation demonstrates that the degradation is not (yet) mass transfer limited at 82 µg/L residual atrazine concentration. In contrast to previous chemostat studies which evaluated isotopic differences between substrate and product,[127, 128] to our knowledge this is the first chemostat experiment which determines isotope enrichment factors with high precision by measurements of the same limiting substrate in inflow and outflow of the bioreactor. This expands chemostat-based isotope fractionation studies to a large number of target compounds, since not all products are amenable to isotope analysis. This chemostat approach has two advantages over batch reactions. First, the result does not depend on concentration measurements. Second and most importantly, a one-time sampling at steady state makes studies at low concentration accessible, where fast degradation or low solubility would not allow withdrawing multiple large-volume samples over time, as needed for typical evaluations of $\varepsilon^{13}C$ by the Rayleigh equation.[129, 130]

## 3.5 Mass transfer limitations revealed by isotope fractionation

We exploited this new opportunity to investigate if, and at what point, mass transfer became limiting when atrazine concentrations were systematically lowered by decreasing dilution rates ($\mu_{med}$ = 0.018 $h^{-1}$, $\mu_{low}$ = 0.009 $h^{-1}$, and $\mu_{min}$ =0.006 $h^{-1}$) over a total cultivation time of 120 days (**Figure 3**). As expected, these lower dilution rates resulted in lower respective residual atrazine concentrations of 61.5 ± 1.3 at $\mu_{med}$, 44. 5 ± 1.0 at $\mu_{low}$, and 31.9 ± 1.0 µg/L at $\mu_{min}$; **Figure 3B**). Remarkably, these lower-concentration experiments also resulted in a dramatic decrease in isotope fractionation compared to batch studies with resting cells[111] and pure enzyme[112] or to chemostat at 83 µg/L (**Figure 3A**). Specifically, the degradation-induced normal carbon isotope effect $((d^{13}C/dt)/(d^{12}C/dt) < 1)$ decreased with lower concentrations to a similar extent (from $\varepsilon^{13}C$ = -4.34 ± 0.13 ‰ at $\mu_{med}$ to -2.12 ± 0.08 ‰ at $\mu_{low}$ and -2.32 ± 0.28 ‰ at $\mu_{min}$) as the simultaneously occurring inverse nitrogen isotope effect $((d^{15}N/dt)/(d^{14}N/dt) > 1)$, which decreased from $\varepsilon^{15}N$ = 1.94 ± 0.06 ‰ to 1.04 ± 0.09 ‰ and 1.27 ± 0.08 ‰ at corresponding dilution rates. This identical masking despite an opposing nature of the isotope effects was also represented in the dual element isotope trend λ defined by the

ratio $\varepsilon^{15}N/\varepsilon^{13}C$. Lambda remained constant with decreasing concentration and dilution rate (-0.45 ± 0.13 at $\mu_{med}$, -0.49 ± 0.15 at $\mu_{low}$, and -0.55 ± 0.15 at $\mu_{min}$) and was similar to previous resting cell and pure enzyme degradation experiments (-0.61 ± 0.06 and -0.54 ± 0.02).[112] Taken together, this provides compelling evidence that the underlying

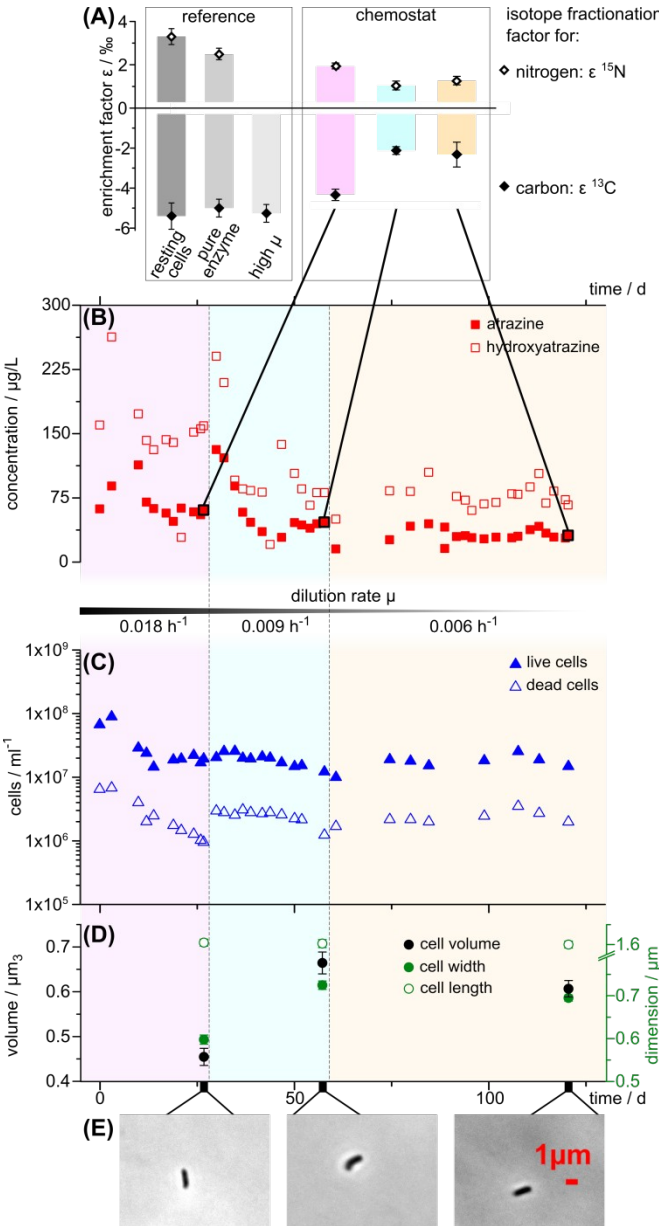


**Figure 3: Isotope fractionation of atrazine and associated cell parameters of *A. aurescens* TC1 when cultivated in aerobic, atrazine limited chemostat with stepwise decreased dilution rates.** Enrichment factors $\varepsilon^{13}C$ in chemostat **(A)** were determined according to equation (6) at different residual atrazine concentrations **(B)** resulting from decreasing dilution/ growth rates (bar in panel **B**) (whiskers show 95 % confidence intervals; N=10). Enrichment factors observed in the absence of mass transfer limitations are drawn for comparison in panel **(A)**: from degradation experiments with resting cells at high atrazine concentration,[111] of the pure enzyme,[112] and at high dilution in chemostat. Negative carbon enrichment factors reflect a normal isotope effect whereas positive nitrogen enrichment factors reflect an inverse isotope effect. Cell numbers are shown in panel **(C)**, cell length and diameter, and cell volumes derived from panel (**E)** are shown in panel **(D)** (whiskers show the standard error; N=50),. Images in **(E)** show typical bacterial cells observed during chemostat operation at the three dilution rates determined by phase contrast microscopy. Concentrations **(B)** and cell numbers **(C)** from one biological replicate are supported by data from a second biological replicate in **Figure C6**.

biochemical degradation mechanism remained the same so that changes in enrichment factors must result from mass transfer limitations that masked the isotope fractionation of the enzymatic reaction of TrzN. Since diffusion of atrazine through the media towards the cells can be ruled out considering the high agitation in the chemostat (600 rpm), the rate limiting step of the degradation must be mass transfer across the cell membrane itself.

## 3.6 Numerical modeling provides a mass transfer estimate for membrane permeation

A numerical model was developed to provide a better insight to the interplay between mass transfer limitation and degradation processes.[131] In the absence of a mass transfer term, those predictions reproduced neither observed isotope ratios nor concentrations when based on Monod parameters derived from our experiments (substrate affinity $K_S$ = 237 ± 57 µg/L; maximum growth rate $\mu_{max}$ = 0.12 ± 0.02 $h^{-1}$). In contrast, the effect of masking on isotope ratios and concentrations could be adequately reproduced by implementing a linear mass transfer term with an estimated mass transfer coefficient of $k_{tr}$ = 0.0025 $s^{-1}$ (**Figure 4, Table C1**). From this value of $k_{tr}$ = 0.0025 $s^{-1}$, the diffusion coefficient through the membrane $D_{mem}$ and the apparent permeability of the cell wall $P_{app}$ calculate to $P_{app} = 3.5 \times 10^{-5}$ $ms^{-1}$ and $D_{mem}$ = 1.9 x $10^{-16}$ $m^2s^{-1}$ (see theoretical treatment in the Methods section), which are values in a typical range of small organic molecules.[98] Interestingly, this onset of mass transfer limitation occurs at a growth rate $\mu_{med}$ = 0.018 $h^{-1}$ which is only 16% of $\mu_{max}$ and the residual substrate concentration 61.5 µg/L is around 25% of $K_S$. Growth under these extremely low substrate concentrations is often accompanied by physiological changes to adapt to oligotrophic conditions.[52, 70]

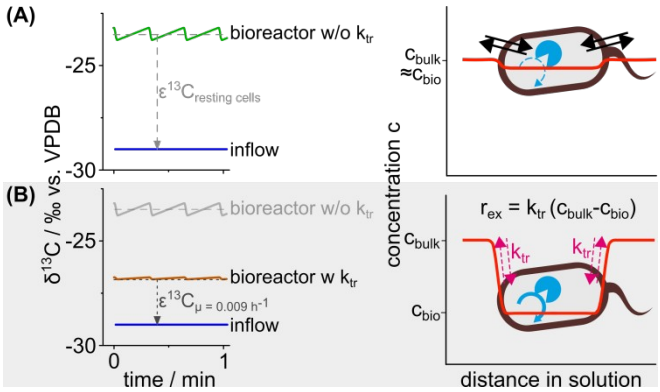


**Figure 4: Numerical modeling validates the chemostat approach and delivers a first estimate of mass transfer rates.** At low dilution rates, only few drops of medium per minute feed the culture so that degradation, and thus isotope enrichment of the substrate occurs in between drops. Numerical modeling demonstrates that the resulting oscillation of residual atrazine concentrations (**Figure 2**) and isotope ratios (**Figure 4A)** in chemostat lies within the uncertainty of $\varepsilon$-values thereby validating the chemostat approach to measure isotope fractionation. **(A)** In the absence of a mass transfer term the model predicts that carbon isotope values $\delta^{13}C$ inside the chemostat differ from those of the inflow by exactly the enrichment factor $\varepsilon^{13}C$ of batch studies, independent of the dilution rate. **(B)** By incorporating a mass transfer term $k_{tr}$ = 0.0025 $s^{-1}$, in contrast, simulated differences decrease to the same extent as observed in our experiments. The mass transfer limitation also predicts a concentration decrease inside the cell: modeled $c_{bio}$ is only 40 % of the concentration outside the cell, $c_{bulk}$.

## 3.7 Adaptation of *A. aurescens* TC1 to oligotrophic conditions

Several observations indicate indeed that some kind of additional adaptive changes took place in our experiments. First, we observed a fast onset of mass transfer limitations within a remarkably small concentration range (from -5.36 ‰ at 83 µg/L to -2.12 ‰ at 44.5 µg/L), whereas a theoretical model by Thullner *et al.* predicts a slower onset over more than one order of magnitude in concentrations.[92] Additionally, a further decrease in concentration (32.9 µg/L) did not lead to a further decrease in observable enrichment factors ($\varepsilon^{13}C$ = -2.32 ‰). Indeed, no significant further decrease in isotope fractionation with decreased concentration may be predicted with our estimated $k_{tr}$ = 0.0025 $s^{-1}$ in combination with Thullner *et al.*'s model. This rare case is only

observable if $k_{tr}$ is in the same range as the affinity of the enzyme for the substrate and thus, the exchange rate over the membrane is just enough to replenish the substrate inside the cell to maintain a certain metabolic flux.[92] This raises the question about underlying drivers triggering such a balance of fluxes. Spontaneous mutations and evolution of *A. aurescens* TC1 during our cultivation can be ruled out because (i) 30 generations are usually not enough for atrazine degrader mutants to evolve[71] and (ii) both biological replicates show the same kind of adaptation. Regulation of TrzN on the enzyme/proteome level is an unlikely reason, since the hydrolytic enzyme is constitutively expressed[132] and does not depend on co-factors.[113] In contrast, we did observe changes in morphology. While – with decreasing dilution rates – the number of live cells decreased (from $2.0 \times 10^7$ cells/mL to $1.4 \times 10^7$ cells/mL, **Figure 3C**), rod-shaped cells maintained their length ($1.61 \pm 0.05$ µm), but increased their diameter (from $0.60 \pm 0.02$ µm at $\mu_{med}$ to $0.71 \pm 0.01$ µm at $\mu_{min}$, **Figure 3E**) leading to a constant calculated dry weight at all dilution rates ($m_{biomass} = 0.56 \pm 0.03$ mg/L; **Figure C3**). This is consistent with the transition to a coccus-like shape in at low nutrient content reported by Strong *et al*..[63] Considering that *A. aurescens* TC1 assimilates only 5 carbon atoms per atrazine molecule (7 $mg_C/L$)[63] the $m_{biomass}$ results in a yield of $Y = 0.08$ $g_{biomass}/g_{carbon}$, which is only 30 % of that in fed-batch growth (**Figure C4**) providing further evidence of adaptation. We describe here for the first time that the physiological changes that are indicative of bacterial adaptation appear to go hand in hand with rate-limiting mass transfer of the substrate atrazine across the cell envelope. Specifically, as the evidence of isotope fractionation reveals slow mass transfer compared to enzymatic turnover, we can model that this affects not only the overall contaminant degradation rate, but that also intracellular substrate concentrations ($c_{bio}$) must be reduced by 40 % compared to those in solution ($c_{bulk}$) (**Figure 4B**). Hence, substrate scarcity is much more severe than apparent from $c_{bulk}$ indicating that there is an interplay of mass transfer limitations and physiological changes at low growth rates which likely plays an important role for the adaptation of *A. aurescens* TC1 to oligotrophic conditions.

## 3.8 Prominent role of mass transfer limitations in micropollutant degradation

The finding that the adaptation to nutrient limited conditions is accompanied by mass transfer limitations affects our understanding of contaminant biodegradation on multiple levels. The observation that bioavailability becomes rate-limiting for the biodegradation at slow growth rates under oligotrophic conditions in chemostat suggests that bioavailability limitation is not an exception, or an artifact of lab experiments, but may rather be the rule for growth and function of bacteria in natural habitats. Further, rate-limiting mass transfer across the cell membrane does not only slow down turnover of micropollutants in the environment but also masks the isotope fractionation of the underlying enzyme reaction, thereby compromising isotope-based assessments of biodegradation. Specifically, since such isotope fractionation at low concentrations is smaller than measured in the lab at high pollutant concentrations, the extent of biodegradation in the environment would be underestimated for turnover of compounds at trace levels.

Finally, mass transfer limitation was found to be accompanied by physiological adaptation to oligotrophic conditions. Transition to near zero growth rate in combination with bioavailable substrate scarcity ($c_{bio} < c_{bulk}$) may, therefore, be the start of an inactivation of the degrading bacterial population. This can bring the biodegradation of micropollutants to a halt even though the degrading bacteria are viable and pollutant molecules are still available to degrade. Future studies targeting (i) the maintenance energy and the threshold concentration at which adaptation is expected to take place and (ii) the role of physiological adaption to oligotrophic conditions, will be instrumental in shedding further light on these limitations of micropollutant degradation at low concentrations.

## 3.9 Methods

### 3.9.1 Continuous cultivation

The atrazine degrading bacterium *A. aurescens* TC1 was cultivated in a 3000 mL glass bioreactor (diameter 130 mm, height 250 mm, and working volume 2000 mL; Applikon Biotechnologie B.V., Netherlands). The cultivation was controlled by myControl (Applikon Biotechnologie B.V., Netherlands) and samples for flow cytometry, concentration analysis by HPLC, and isotope analysis were taken through the reactor's sampling tube. The cultivation media was a mineral salt solution with 30 mg/L atrazine (Cfm Oskar Tropitzsch, Germany). The media preparation, the preparation of the inoculum, and the culture conditions are described in Appendix C. The bacteria were cultivated at dilution rates $\mu$ = 0.023 $h^{-1}$, 0.018 $h^{-1}$, 0.009 $h^{-1}$, and 0.006 $h^{-1}$ over a total cultivation time of 140 d.

### 3.9.2 Numerical modeling of the chemostat cultivation

A numerical model was developed to assess the influence that mass transfer limitations imply on the observed isotopic signature at low steady state concentrations in the chemostat. This model simulates the atrazine degradation, growth, and isotope fractionation in the presence of bioavailability limitations.[133] The kinetic growth parameters for the model were derived from the different dilution rates of the chemostat run and a fed batch growth experiment (**Figure C4**). With a high time resolution of the model, the influence of subsequent droplet addition with the media feed can be analyzed, was found to be negligible under our operating conditions and may only become of relevance at a dilution rate lower than $\mu$ = 0.004 $h^{-1}$ (**Figure 2, Figure 4A**). The model itself has a broader application range which goes beyond the scope of this study. A detailed description of the model was published and the code was made available by Gharasoo *et al.*.[131] The diffusion coefficient through the membrane $D_{mem}$ and the apparent permeability of the cell wall $P_{app}$ can be calculated according to equation (5) where $V_{out}$ is the bioreactor volume (2000 mL) minus the total cell volume ($V_{cells}$).

$$D_{mem} = P_{app}\frac{\delta}{K_{lipw}} = \frac{k_{tr} \times V_{out} \times \delta}{A_{cells} \times K_{lipw}} \quad (5)$$

$V_{cells}$ and $A_{cells}$ - total volume and surface area of all cells - are calculated by the product of the total number of living cells in the bioreactor ($4 \times 10^{10}$) (**Figure 3C**) and the volume, or surface area of a single cell ($1.9 \times 10^{-16}$ m$^3$, or $3.6 \times 10^{-12}$ m$^2$) respectively. The area and the volume of a single cell are calculated assuming a cylindrical shape (**Figure 3D**). $K_{lipw} = 741$ is the lipid-water distribution coefficient of atrazine[134] and $\delta = 4 \times 10^{-9}$ m is a typical value for the membrane thickness.[135]

### 3.9.3 Calculation of enrichment factors in chemostat

The classical way to determine the enrichment factor of a chemical reaction relies on the Rayleigh equation where changes in isotope ratios are monitored with decreasing substrate concentration.[129] In bioreactors at constant steady state concentrations the enrichment factor of the degradation of atrazine must be determined in a different way. The substrate inflow per time $c_{¿} \cdot D$ is equal to the outflow per time $c_{reac} \cdot D$ plus the substrate degraded per time $c_{reac} \cdot k_{deg.}$ (equation (6))

$$c_{¿} \cdot D = c_{reac} \cdot D + c_{reac} \cdot k_{deg.} \quad c_{¿} = c_{reac} \cdot \left(D + k_{deg.}\right) \quad (6)$$

where $c_{in}$ is the atrazine concentration in the inflow, $c_{reac}$ is the atrazine concentration in the bioreactor, $D = \mu$ is the dilution rate, and $k_{deg.}$ is the first order rate constant for the degradation of atrazine. Stating equation (7) for heavy and light isotopes with rate constants $k^h_{deg.}$ and $k^k_{deg}$, respectively, and dividing the equations gives an expression for the isotope ratio $c^h/c^l$

$$\left(\frac{c^h}{c^l}\right)_{¿} = \left(\frac{c^h}{c^l}\right)_{reac} \cdot \frac{D + k^h_{deg.}}{D + k^l_{deg.}} = \left(\frac{c^h}{c^l}\right)_{reac} \cdot \alpha \quad (7)$$

where $\alpha = k^h_{deg}/\ k^l_{deg}$ is the fractionation factor. Here, the observation is taken into account that $c_{reac} << c_{in}$ meaning that $k_{deg} >> D$ (otherwise $c_{reac} \approx c_{in}$). Introducing the more common $\delta$ notation (8)

$$\frac{\left(\frac{c^h}{c^l}\right)_x}{\left(\frac{c^h}{c^l}\right)_{ref}} = \delta_x + 1 \quad (8)$$

where $\left(\frac{c^l}{c^h}\right)_x$ and $\left(\frac{c^h}{c^l}\right)_{ref}$ are isotope ratios of sample and international standard material gives

$$\delta_{¿}+1=\left(\delta_{reac}+1\right)\cdot\alpha=\left(\delta_{reac}+1\right)\cdot\left(\varepsilon+1\right) \quad (9)$$

where $\varepsilon = \alpha$-1 is the enrichment factor, or isotope fractionation[77]. Finally, $\varepsilon$ can be calculated (10) by the difference of the isotope values of inflow and bioreactor because $\delta_{reac} << 1$:

$$\varepsilon=\frac{\delta_{¿}+1-\left(\delta_{reac}+1\right)}{\delta_{reac}+1}\approx\delta_{¿}-\delta_{reac} \quad (10)$$

### 3.9.4 Compound specific isotope analysis of atrazine in the bioreactor.

For each dilution rate (0.023 $h^{-1}$, 0.018 $h^{-1}$, 0.009 $h^{-1}$, and 0.006 $h^{-1}$) samples for isotope analysis (100 mL, 200 mL, 300 mL, and 500 mL respectively) were withdrawn from the bioreactor after three hydrolytic retention times at steady state had passed. Degradation was stopped immediately by sterile filtration with a regenerated cellulose membrane filter (pore size 0.2 µm, diameter 47 mm; GE Healthcare ltd., UK). Immediate removal of the degrading cells is necessary, since the atrazine would otherwise be degraded within minutes. Degradation time courses with fresh sample demonstrated that during our sampling time of 1 min, only 10 % at most of the remaining atrazine was degraded (**Figure C5**). After filtration, the atrazine was extracted with dichloromethane (10 % of the sample volume, three times). The dichloromethane was evaporated under a nitrogen stream and the atrazine was reconstituted in 100 µL ethyl acetate. Simultaneously, 1 mL of the inflow to the chemostat was collected, frozen at -80°C, dried by lyophilization, and the atrazine was reconstituted in 100 µL ethyl acetate, as well. Carbon and nitrogen isotope analysis of atrazine were performed on a GC-IRMS system consisting of a TRACE GC Ultra gas chromatograph (Thermo Fisher Scientific, Italy) equipped with a DB-5 analytical column (60 m, 0.25 mm ID, 1.0 µm film, Agilent Technologies, Germany) coupled to a Finnigan MAT 253 isotope ratio mass spectrometer via a Finnigan GC Combustion III interface (both Thermo Fisher Scientific, Germany). Detailed information about the method adapted from Schreglmann *et al.*[136] is provided in Appendix C.

### 3.9.5 Concentration measurements, cell counting, and microscopy

Atrazine and 2-hydroxyatrazine concentrations were measured using a Prominence HPLC system (Shimadzu Corp., Japan) together with a 100 x 4.6 mm Kinetex 5 µ Biphenyl 100 Å column (Phenomenex Inc., USA). For cell counts, cells were first fixed with 2.5 % glutaraldehyde, then stained with SYBR Green I (total cells) and propidium iodide (dead cells) and analyzed on a Cytomics FC 500 flow cytometer (Beckmann Coulter, USA). The shape of fixed cells was analyzed on agar glass slides by light microscopy with an Axioscope 2 Plus microscope (Carl Zeiss AG, Germany). For a detailed description of these methods see Appendix C.

### 3.9.6 Statistical treatment of concentration and isotope data

The chemostat culture was done in two biological replicates. The steady state concentrations of four days of the individual biological replicates were compared with a two sample t-test (N=4). As they were not statistically different from one another at the 0.05 level for each dilution rate, the concentration values were combined and the average substrate concentration and the standard error for each dilution rate were calculated (N=8). A similar approach was chosen for the determination of the enrichment factors. The enrichment factor for each biological replicate at each dilution rate was determined as described above in five technical replicates which were compared with a two sample t-test (N=5). As they were not statistically different from one another at the 0.05 level, the enrichment factors of the two biological replicates were combined for each dilution rate and the average and the 95 % confidence intervals were calculated (N=10).

# 4 Isotope fractionation pinpoints membrane permeability as barrier to atrazine biodegradation in Gram-negative *Polaromonas sp.* Nea-C

Benno N. Ehrl, Mehdi Gharasoo, and Martin Elsner

## 4.1 Abstract

Biodegradation of persistent pesticides like atrazine often stalls at low concentrations in the environment. While mass transfer does not limit atrazine degradation by the Gram-positive *Arthrobacter aurescens* TC1 at high concentrations, bioavailability limitations have recently been observed at trace concentrations. For this, the roles of cell wall physiology and transporters remain imperfectly understood. Here, compound-specific isotope analysis (CSIA) demonstrates that cell wall physiology (i.e. the difference between Gram-negative and Gram-positive bacteria) imposes mass transfer limitations in atrazine biodegradation even at high concentrations. Atrazine biodegradation by Gram-negative *Polaromonas sp.* Nea-C caused significantly less isotope fractionation ($\varepsilon^{13}C$ = -3.5 ‰) than expected for hydrolysis by the enzyme TrzN ($\varepsilon^{13}C$ = -5.0 ‰) and observed in Gram-positive *Arthrobacter aurescens* TC1 ($\varepsilon^{13}C$ = -5.4 ‰). Isotope fractionation was recovered in cell free extracts ($\varepsilon^{13}C$ = -5.3 ‰) where no cell envelope restricted pollutant uptake. When active transport was inhibited with cyanide, atrazine degradation rates remained constant demonstrating that atrazine mass transfer across the cell envelope does not depend on active transport but is a consequence of passive cell wall permeation. Taken together, our results identify the cell envelope of the Gram-negative bacterium *Polaromonas sp.* Nea-C as relevant barrier for atrazine biodegradation.

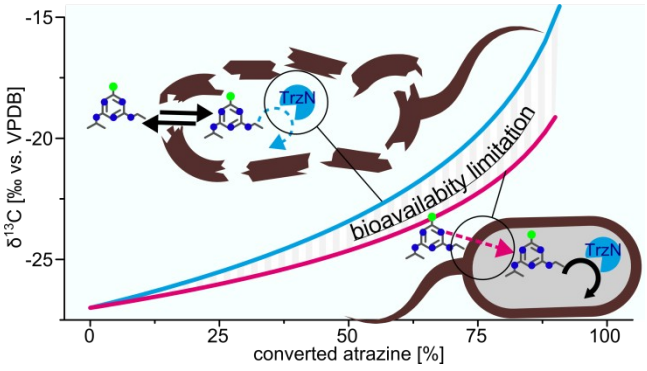


**Figure 5: Abstract art**

## 4.2 Introduction

Groundwater contamination by micropollutants is a prominent challenge of our time. Since ground and surface waters represent an important drinking water resource, the presence of micropollutants is of concern not only for ecosystems, but also for human health.[1] Because of their ubiquitous release and their low concentrations, however, evaluating the fate of micropollutants in the environment is complex. Pharmaceuticals are discharged into the environment with wastewater treatment effluents[10, 13, 14] and pesticides used in agriculture even directly leach into groundwater on a large scale.[19, 137] EU regulations on drinking water quality set a maximum concentration of 0.1 µg/L for pesticides and their degradation products (European Union Drinking Water Directive, 98/83/EC). How difficult it is, however, to relate successful biodegradation in the lab to the fate of pesticides in the environment, is illustrated by the herbicide atrazine: even though banned in the EU as long ago as 2003, atrazine and its metabolites are still the groundwater contaminants most frequently detected above this threshold concentration.[23] The underlying bottlenecks of biodegradation at trace concentrations which cause this persistence have eluded researchers for years. Even though atrazine is initially adsorbed and retained to some extent on soil and sediment[138] it becomes available at low concentrations (µg/L) for atrazine degrading bacteria.[21, 125] For such a situation, competing models claim that it is either mass transfer (uptake into microbial cells) which puts a limit to otherwise rapid enzymatic transformation,[45, 139] or that physiological limitations (enzyme activity, downregulation) prevail.[140] Compound-specific isotope analysis (CSIA) provides a way to directly visualize the rate-determining step of pollutant biodegradation:[141] Chemical bond breakage during pollutant degradation is slower when the bond contains a heavy isotope since the respective activation energy is higher. Therefore, the remaining pollutant molecules contain on average increasingly more heavy isotopes as an enzymatic reaction proceeds.[116] This trend can be described by relating the change in isotope ratios ($R_t/R_o$) to the fraction of the remaining pollutant *f* according to the Rayleigh equation (11)[129, 142]

$$\ln\left(\frac{R_t}{R_0}\right) = \varepsilon \times \ln(f) \qquad (11)$$

where the enrichment factor $\varepsilon$ reflects the incremental isotope fractionation during transformation. This isotope effect, however, can only be observed if substrate molecules experiencing the isotopic discrimination during the enzymatic reaction in the cytosol diffuse back out into the bulk solution, where the isotope ratio is assessed. Thus, any partially rate-determining step preceding the irreversible enzymatic turnover (e.g. mass transfer) will lead to a reduced exchange of "enriched" substrate molecules to the outside of the cell. As a consequence, the observable isotope enrichment factor ε will be smaller, since the reduced exchange masks the isotope fractionation of the enzymatic reaction.[143, 144] Masked isotope fractionation due to mass transfer limitations is well understood from photosynthesis,[85, 86] sulfate reduction,[87-89] or nitrate reduction.[90, 91] The same effect has previously been demonstrated for organic pollutants taken up by active transport[51] and for non-polar chlorinated ethenes.[95, 144] A conceptual framework has been brought forward by Thullner *et al.* to mathematically predict the effect for passive permeation of organic pollutants through a biological double membrane.[92, 145] Based on these studies, we recently discovered that cell wall permeation was not relevant for atrazine biodegradation by *Arthrobacter aurescens* TC1 at high concentrations, but became suddenly rate-limiting at low concentrations (low µg/L range).[146] This finding is challenged by earlier observations by Meyer *et al.* that even at high concentrations, isotope fractionation in atrazine degradation varied significantly between bacterial strains catalyzing the same reaction.[111] Usually, the isotope fractionation factor is assumed to be characteristic for a specific transformation pathway if the underlying enzyme reaction is identical.[147-149] A compelling clue to explain the results of Meyer *et al.*, is, therefore, the fact that differences exist between Gram-negative and Gram-positive bacterial strains. The additional outer membrane in Gram-negative strains possibly constitutes an additional barrier for mass transfer which can mask the enzymatic isotope fractionation. Indeed, Renpenning *et al.* observed that carbon isotope fractionation during chlorinated ethene degradation differed for Gram-positive and Gram-negative bacteria and depended on the integrity of the cell envelope.[95] In the case of Meyer *et al.*, however, this proposed causal relationship could not be uniquely pinpointed because different enzymes of the same family (AtzA vs. TrzN) were involved. Consequently, it could not be excluded that the observed

variability may, alternatively, be attributable to subtle variations in transition state structures.

We, therefore, systematically addressed the question in our study by exploiting the opportunity that the Gram-negative bacterium, *Polaromonas sp.* Nea-C, harbors the same set of intracellular atrazine degrading enzymes[113] as the Gram-positive *A. aurescens* TC1 (TrzN, AtzB, AtzC).[111, 150] Atrazine hydrolysis by TrzN ($K_M$ = 19 µM, $k_{cat}$ = 5.5 $s^{-1}$) proceeds via initial protonation of the ring nitrogen and subsequent hydrolysis of the C-Cl bond.[112, 113] Further, enrichment factors of the degradation reaction in whole cells are similar to those of the degradation with purified TrzN without cell envelope meaning that atrazine degradation by whole cells of Gram-positive *A. aurescens* TC1 is not mass transfer limited.[112] We compared the isotope fractionation during atrazine degradation with intact cells of Gram-negative *Polaromonas sp.* Nea-C – a scenario in which mass transfer across the cell envelope can matter – relative to degradation with Gram-positive *A. aurescens* TC1, cell free extracts of Gram-negative *Polaromonas sp.* Nea-C or purified TrzN enzyme,[112] three scenarios in which mass transfer is absent. Furthermore, we addressed the possibility of active transport to clarify whether passive membrane permeation of atrazine is sufficient to provide enough influx for those bacteria to sustain growth. To this end, we investigated whether atrazine degradation rates of *Polaromonas sp.* Nea-C and *A. aurescens* TC1 were affected when active transport was inhibited by the respiratory chain inhibitor potassium cyanide (KCN).

## 4.3 Experimental section

### 4.3.1 Chemicals

A list of chemicals used can be found in Appendix D.

### 4.3.2 Cultivation of bacteria

*Polaromonas sp.* Nea-C was kindly provided by Fabrice Martin-Laurent (Microbiologie du Sol et de l'Environnement, INRA, France) and *Arthrobacter aurescens* TC1 was kindly provided by Larry Wackett (The BioTechnology Institute, University of Minnesota,

USA). All strains were grown in liquid mineral salt medium (MSM) containing a nitrogen source (composition see Appendix D). Excess atrazine above the solubility limit was added in solid form to a concentration of 500 mg/L to provide enough nutrient for high cell densities. Cultures were incubated at room temperature (25°C).

### 4.3.3 Atrazine degradation with whole cells of *Polaromonas sp.* Nea-C for isotope analysis.

Growth of a freshly inoculated culture (500 mL) of *Polaromonas sp.* Nea-C was followed by monitoring the optical density ($OD_{600}$). During exponential phase ($OD_{600}$ = 0.05) cells were pelleted by centrifugation (Heraeus Megafuge 40R, Thermo Scientific, TX-1000 rotor, 3700 *g*, 30 min, 4°C) and washed twice in 50 mL MSM to remove the remaining atrazine. After those washing steps, the cell pellet was resuspended in 500 mL of fresh MSM containing 30 mg/L atrazine. The atrazine concentration was close to the solubility limit of 33 mg/L (see media preparation in Appendix D) to maximize the amount of substance per volume and, hence, to minimize the necessary sample volume for reliable isotope analysis (see below).[151] The degradation experiment lasted approximately 24 h and the atrazine concentration was monitored by HPLC-UV (see below). For each of the three biological replicates, 5 samples for isotope analysis were taken (20 mL in the beginning and 50, 70, 150, 200 mL at approximately 50 %, 75 %, 85 %, and 95 % atrazine consumption respectively). The degradation reaction was stopped by sterile filtration with a regenerated cellulose membrane filter (pore size 0.2 µm, diameter 47 mm; GE Healthcare ltd., UK). The biomass and the filter volume were not extracted, as their volume (< 0.5 mL) is negligible compared to the filtrate (> 20 mL). The filtrate was extracted three times with 10 % (v/v) dichloromethane. The combined dichloromethane extracts were evaporated under an air stream and the samples were reconstituted in 100 µL ethyl acetate for GC-IRMS measurements (see below).

### 4.3.4 Preparation of cell free extracts of *Polaromonas sp.* Nea-C.

*Polaromonas sp.* Nea-C cells were grown and harvested as described above. The cell pellet was resuspended in 5 mL of fresh MSM and put on ice. Cell membranes were disrupted in two passages by a French pressure cell (American Instrument Company,

USA, 3/8” piston diameter, 20000 Psi). Remaining whole cells and cell fragments were removed by sterile filtration with a regenerated cellulose membrane filter (pore size 0.2 µm, diameter 47 mm; GE Healthcare ltd., UK) and the extract was stored on ice for a short time for the degradation experiment.

### 4.3.5 Atrazine degradation with cell free extracts of *Polaromonas sp.* Nea-C for isotope analysis.

The 5 mL concentrated cell free extract was diluted in 250 mL of fresh MSM containing 30 mg/L atrazine. The atrazine concentration over time was monitored by HPLC-UV (see below) by taking samples for 4 h. For each of the three biological replicates, 5 samples for isotope analysis were taken (10 mL in the beginning and 15, 35, 60, 120 mL at approximately 60 %, 80 %, 90 %, and 95 % atrazine consumption respectively) and the degradation reaction was stopped by extracting atrazine with three times 10 % (v/v) dichloromethane. The extracts were concentrated for GC-IRMS as described above.

### 4.3.6 Atrazine degradation rates with and without respiratory chain inhibitor KCN.

Freshly inoculated cultures (50 mL) of both, *Polaromonas sp.* Nea-C and *A. aurescens* TC1, was followed by the $OD_{600}$ and cell numbers per mL were estimated for both strains with $8 \cdot 10^8$ cells·mL$^{-1}$·$OD_{600}$. The cells were harvested as described above and the cell pellet was resuspended in 50 mL of fresh MSM. For both species, each of the three biological replicates was split in 2 x 25 mL cell suspensions to get the same biomass for the inhibited and the non-inhibited degradation experiment. To inhibit the respiratory chain, 0.25 mM KCN was added to one cell suspension. Afterwards, atrazine was added to both cell suspensions at a concentration of 3 mg/L. A small initial atrazine concentration was chosen to ensure short degradation times to rule out growth of the non-inhibited cells during the experiment. The atrazine concentration over time was monitored by HPLC-UV for 4 h (see below). Because *Polaromonas sp.* Nea-C and *A. aurescens* TC1 might have different TrzN abundances, we only compared each strain with and without inhibition and not the degradation kinetics of *Polaromonas sp.* Nea-C versus *A. aurescens* TC1.

### 4.3.7 Determination of the atrazine concentration by HPLC-UV.

Atrazine concentrations were measured using a Prominence HPLC system (Shimadzu Corp., Japan) together with a 100 x 4.6 mm Kinetex 5 µ Biphenyl 100 Å column equipped with a SecurityGuard ULTRA Biphenyl cartridge (both Phenomenex Inc., USA). The injected sample volume was 10 µL. Peak separation was achieved by 1 mL/ min isocratic flow of a mixture of 51 % 5 mM $KH_2PO_4$ buffer at pH 7 and 49 % methanol, respectively, for 9 min. The compounds were detected by UV absorbance at 222 nm and the peaks were quantified using LabSolutions V 5.71 SP2 (Shimadzu Corp., Japan). External calibration was conducted with atrazine dissolved in 25 % methanol and 75 % water in the following concentrations: 0.5, 4, 12, and 35 µg/L

### 4.3.8 Carbon and nitrogen isotope measurements with GC-IRMS

The method was adapted from Reinnicke *et al*..[151] The GC-IRMS system consisted of a TRACE GC Ultra gas chromatograph (GC; Thermo Fisher Scientific, Milan, Italy) linked to a Finnigan MAT 253 isotope ratio mass spectrometer (IRMS) (Thermo Fisher Scientific, Germany) by a Finnigan GC Combustion III Interface (Thermo Fisher Scientific, Germany). Helium (grade 5.0) was used as carrier gas and the split injector was kept at 250°C with a 1:10 split at a flow rate of 1.4 mL/min. The samples were injected using a GC Pal autosampler (CTC, Switzerland) onto a 60-m DB-5 (30 m × 0.25 mm; 1 µm film; Restek GmbH, Germany) analytical column. Isotope values were determined as $\delta^{13}C$ and $\delta^{15}N$ values in per mill relative to Vienna PeeDee Belemnite (VPDB),[77] and Air-$N_2$.[78] The $\delta^{13}C$ and $\delta^{15}N$ values were assessed in relation to a monitoring gas ($CO_2$ and $N_2$, respectively) which was measured alongside each run at the beginning and the end. Calibration of monitoring gases was performed in a Finnigan MAT Delta S isotope ratio mass spectrometer with dual inlet system (Thermo Fisher Scientific, Germany). The gases were measured against VPDB and air, respectively, by use of international reference materials: the $CO_2$ gases RM 8562, RM 8563, and RM 8564 for $CO_2$ and NSVEC ($N_2$ gas) for $N_2$. Reference standards were provided by the IAEA. The GC oven started at 65 °C (hold 3 min), ramp 25 °C/min to 190 °C This was followed by a temperature ramp of 15 °C/min to 270 °C which was kept for 20 min.

### 4.3.9 Modelling of the isotope fractionation during the degradation.

In the absence of the cell envelope, the bioavailable concentration is equal to the bulk concentration. Therefore, the biodegradation of both substrate fractions (molecules containing $^{12}C$ and $^{13}C$, short $^{12}S$ and $^{13}S$) follows Michaelis-Menten kinetics[152] and is described by the set of equations (12) and (13):[129]

$$\frac{d[{}^{12}_{\square}S]}{dt} = \frac{q_{max}[{}^{12}_{\square}S]}{[{}^{12}_{\square}S]+[{}^{13}_{\square}S]+K_M} \quad (12)$$

$$\frac{d[{}^{13}_{\square}S]}{dt} = \frac{\alpha\, q_{max}[{}^{13}_{\square}S]}{[{}^{12}_{\square}S]+[{}^{13}_{\square}S]+K_M} \quad (13)$$

where $\alpha$ is the fractionation factor with $\varepsilon = \alpha$-1, $q_{max}$ is the maximum degradation rate, and $K_M$ is the half saturation constant of the Michaelis-Menten kinetics. In the presence of mass transfer limitations across the cell envelope it is necessary to distinguish between substrate concentrations outside the cell, S, and substrate concentrations inside the cell, S(bio), where the exchange rate between these two phases is determined by the mass-transfer coefficient $k_{tr}$.[133, 153] Including the mass transfer limiting term in equation (12) and (13) gives equations (14) and (15) and analogous equations for the heavy fraction, where the last term is multiplied by the fractionation factor $\alpha$:[26]

$$\frac{d[{}^{12}_{\square}S]}{dt} = -k_{tr}([{}^{12}_{\square}S]-[{}^{12}_{\square}S(bio)]) \quad (14)$$

$$\frac{d[{}^{12}_{\square}S(bio)]}{dt} = +k_{tr}\left([{}^{12}_{\square}S]-[{}^{12}_{\square}S(bio)]\right)-\frac{q_{max}[{}^{12}_{\square}S]}{[{}^{12}_{\square}S]+[{}^{13}_{\square}S]+K_M} \quad (15)$$

These equations were solved and fitted to the experimental results to obtain the unknown parameters $k_{tr}$ and the maximum degradation rate $q_{max}$ using a modified version of ReKinSim.[154] The enzymatic fractionation factor $\alpha = \varepsilon + 1$ was determined by the fit of the Rayleigh equation (Eq. (11), Table 1) and the value for $K_M$ = 19 µmol/L was taken from the literature.[113] Equation (16) calculates an estimate of the atrazine diffusion coefficient in lipids, $D_{lip}$,

$$D_{lip} = \frac{k_{tr} \times \delta \times V}{A \times K_{lip-w}} \quad (16)$$

(5 nm each) to mimic the Gram-negative cell wall and $V$ = 0.5 L the volume of the cell suspension. $A$ is the bacterial total surface area calculated from an estimate of

$4 \times 10^7$ cells·mL$^{-1}$ (derived from the $OD_{600}$ = 0.05 with $8 \cdot 10^8$ cells·mL$^{-1}$·$OD_{600}$) and an average bacterial surface of 4 µm$^3$. $K_{lipw}$ = 741 is the lipid-water distribution coefficient of atrazine.[134]

## 4.4 Results and discussion

### 4.4.1 Atrazine degradation with Gram-negative *Polaromonas sp.* Nea-C induced smaller isotope fractionation than observed with TrzN.

Resting cells of Gram-negative *Polaromonas sp.* Nea-C with a $OD_{600}$ = 0.05 degraded 30 mg/L atrazine within 24 h (see **Figure D1**). TrzN-catalyzed atrazine hydrolysis to hydroxyatrazine led to considerable isotope fractionation both for carbon (enrichment of $^{13}C$ relative to $^{12}C$ corresponding to a normal isotope effect) and for nitrogen (depletion of $^{15}N$ relative to $^{14}N$ representing an inverse isotope effect) (**Figure 6**). This inverse nitrogen isotope effect is characteristic of proton-assisted hydrolysis in the transition state of TrzN.[112] The enrichment factors for carbon $\varepsilon^{13}C$ = -3.5‰ ± 0.1‰ and nitrogen $\varepsilon^{15}N$ = 1.9‰ ± 0.1‰ were determined by the Rayleigh equation, as shown in **Figure 7A**, B. These enrichment factors are significantly smaller than those described for atrazine hydrolysis catalyzed by TrzN, i.e. those obtained during biodegradation with Gram-positive *A. aurescens* TC1[111] (**Figure 7 A, B**). We screened for genes analogous to the

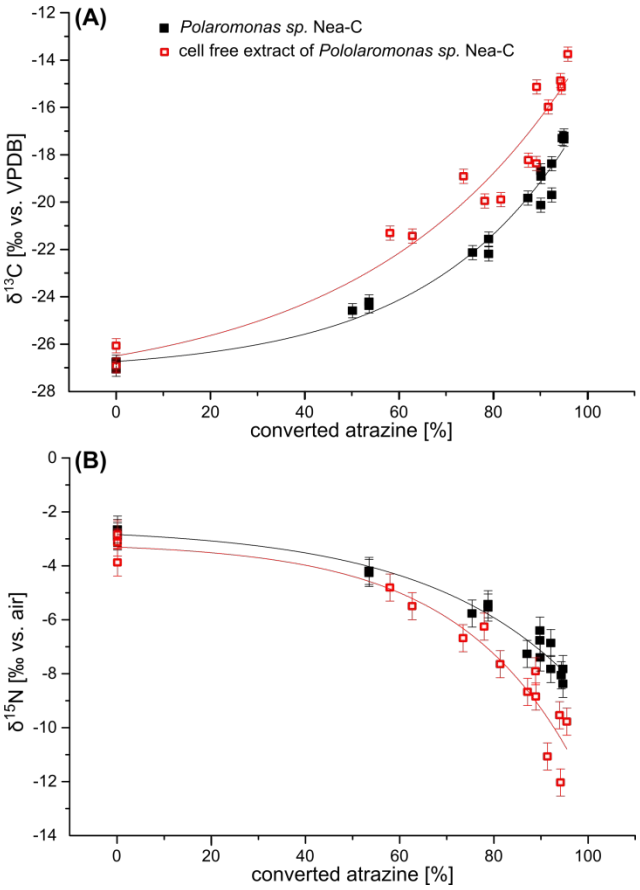


**Figure 6: Isotope fractionation in *Polaromonas sp.* NeaC depends on the integrity of the cell envelope.** The biodegradation of atrazine by the Gram-negative *Polaromonas sp.* Nea-C (black full squares) leads to considerably less isotope fractionation than the atrazine degradation of cell free extracts of *Polaromonas sp.* Nea-C (red empty squares) both for normal carbon **(A)** and inverse nitrogen **(B)** isotope fractionation.

*trzN* gene sequence from *A. aurescens* TC1[132] in the NCBI database by Blast search[155] and found more than 20 sequences coding for TrzN with more than 99% similarity (**Table D1**). Also the isotope fractionation of the abiotic model reaction – acid-catalyzed hydrolysis in water – is stronger than observed in our experiment with *Polaromonas sp.* Nea-C.[111] Taken together, this evidence is consistent with the hypothesis that a different rate determining step – mass transfer across the cell envelope – masked the isotope fractionation of the enzyme in *Polaromonas sp.* Nea-C. Remarkably, the enrichment factors for the Gram-negative *Chelatobacter heintzii* ($\varepsilon^{13}C$ = -3.7 ± 0.2 ‰ and $\varepsilon^{15}N$ = 2.3 ± 0.4 ‰) are statistically indistinguishable from *Polaromonas sp.* Nea-C.

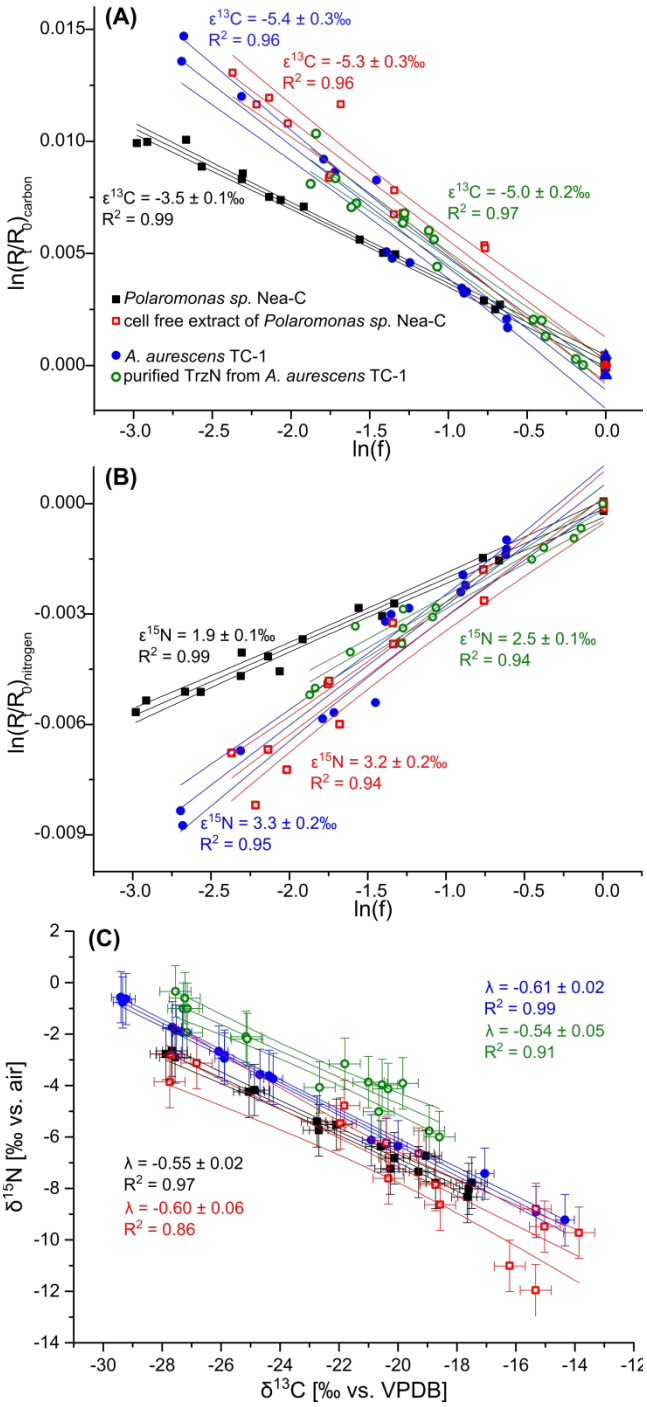


**Figure 7. Rate limiting mass transfer across the Gram-negative cell envelope was revealed by isotope fractionation.** Normal carbon isotope fractionation factors ($\varepsilon^{13}C$) **(A)** and inverse nitrogen isotope fractionation factors ($\varepsilon^{15}N$) **(B)** were determined by the Rayleigh equation. Enrichment factors in cell free extracts of *Polaromonas sp.* Nea-C (red empty squares) were identical to those with whole cells of Gram-positive *A.* aurescens TC1[111] (blue full circles) and purified TrzN[112](green empty circles) indicating that an identical enzyme reaction was at work. In contrast, smaller isotope fractionation was observed in degradation with intact cells of Gram-negative *Polaromonas sp.* Nea-C (black full squares). **(C)** The slope λ in the dual element isotope plot was similar for all degradation experiments, indicating that a common reaction mechanism (acidic hydrolysis) and similar transition state architecture is present in TrzN of both bacteria. Taken together, this indicates that the isotope effect of the enzyme reaction was masked by mass transfer across the cell envelope in *Polaromonas sp.* Nea-C. This non-fractionating step affects carbon and nitrogen fractionation in the same way so that the dual element isotope slope λ stays constant even though the enrichment factors are smaller.

Both are Gram-negative bacteria with the difference that *Chelatobacter heintzii* degrades atrazine with a different enzyme - AtzA[111]- but still via the same acidic hydrolysis (**Table 1**). This raises the question whether these different enzymes from

different species (AtzA, TrzN from *Polaromonas sp.* Nea-C, and TrzN from *A. aurescens* TC1) have different transition states and thus different enrichment factors, or whether the difference in isotope fractionation is attributable to physiological differences in the cell envelope that are characteristic of Gram-positive (*A. aurescens* TC1) versus Gram-negative (*Chelatobacter heintzii* and *Polaromonas sp.* Nea-C) bacterial strains.

**Table 1.** Overview of isotope fractionation during atrazine degradation via acidic hydrolysis in different experimental setups.

| experimental system | enzyme | Gram stain | $\varepsilon^{13}C$ (‰) | $\varepsilon^{15}N$ (‰) | $\lambda \approx \varepsilon^{15}N/\varepsilon^{13}C$ | concentration (mg/L) | Ref. |
|---|---|---|---|---|---|---|---|
| whole cells *Polaromonas sp.* Nea-C | TrzN | negative | -3.5 ± 0.1 | 1.9 ± 0.1 | -0.55 ± 0.02 | 30 - 1.4 | this study |
| cell free extract *Polaromonas sp.* Nea-C | TrzN | negative | -5.3 ± 0.3 | 3.2 ± 0.2 | -0.60 ± 0.06 | 30 - 2.8 | this study |
| whole cells *A. aurescens TC1* | TrzN | positive | -5.4 ± 0.3 | 3.3 ± 0.2 | -0.61 ± 0.02 | 18 - 1.3 | [111] |
| purified *A. aurescens TC1* TrzN | TrzN | positive | -5.0 ± 0.2 | 2.5 ± 0.1 | -0.54 ± 0.02 | 24 - 3 | [112] |
| *Chelatobacter heintzii* | AtzA | negative | -3.7 ± 0.2 | 2.3 ± 0.4 | -0.65 ± 0.08 | 15 - 1.8 | [111] |
| abiotic pH 3 60°C | --- | --- | -4.8 ± 0.4 | 2.5 ± 0.2 | -0.52 ± 0.04 | 24 - 3 | [111] |

### 4.4.2 Strong enzymatic isotope fractionation was masked by mass transfer limitations.

Indeed, although the sequences of *trzN* genes from *Polaromonas sp.* Nea-C versus *A. aurescens* TC1 are highly similar (see above), it cannot be strictly excluded that subtle differences in the protein structure of even TrzN could be responsible for the differences in isotope fractionation. For example, in a recent study by Schürner *et al*.,[112] we observed that single point mutations in the *trzN* gene can lead to subtle changes in isotope fractionation. We therefore prepared cell free extracts of *Polaromonas sp.* Nea-C to degrade atrazine to hydroxyatrazine and followed the degradation with CSIA. As the hydrolysis of the atrazine C-Cl bond does not depend on any cofactors or energy in the form of ATP, the cell free extracts were highly active, atrazine turnover was fast (**Figure D2**), and was accompanied by strong isotope fractionation, as shown in

**Figure 6**. The isotope fractionation in cell free extracts was considerably larger than in whole cells and gave enrichment factors $\varepsilon^{13}C$ = -5.3 ± 0.3 ‰ and $\varepsilon^{15}N$ = 3.2 ± 0.2 ‰ that again were indistinguishable from those of *A. aurescens* TC1 (**Figure 7 A, B**).[111] This isotope fractionation was also similar to that of recombinant TrzN from *A. aurescens* TC1 (instead of cell free extracts), and of abiotic acidic hydrolysis (**Table 1**).[111, 112] Further, the slope of the dual element isotope plot $\lambda \approx \varepsilon^{15}N/\varepsilon^{13}C$ was the same for the degradation with *Polaromonas sp.* Nea-C, *A. aurescens* TC1, and the cell free extract of *Polaromonas sp.* Nea-C (λ = -0.55 ± 0.02, -0.60 ± 0.05, and -0.61 ± 0.02 respectively) (**Figure 7 C**) and was similar to those with recombinant TrzN and abiotic acidic hydrolysis (**Table 1**).[111, 112] This similarity in intrinsic isotope fractionation strongly suggests that the same enzymatic reaction and same transition state prevailed but that this isotope fractionation was masked by a non-isotope fractionating step. This masking occurred only in whole cells with intact cell envelope, but not in cell free extracts of *Polaromonas sp.* Nea-C. Such masking effects have previously be invoked to be attributable to (i) artificial high cell densities,[93] (ii) diffusion through water, or (iii) retention in extracellular polymeric substance (EPS). These alternative explanations can be ruled out since (i) our cell densities were small in comparison with Kampara *et al.*'s study,[93] (ii) the atrazine diffusion in water is fast compared to diffusion in lipid membranes,[146] and (iii) *Polarmonas sp.* NeaC does not form EPS. Consequently, we conclude that it was mass transfer across the cell envelope that was the partially rate-limiting step in biodegradation of atrazine by the Gram-negative *Polaromonas sp.* Nea-C, but not by the Gram-positive *A. aurescens* TC1.

### 4.4.3 Passive processes dominate atrazine uptake into the cell.

The phenomenon that organic pollutant uptake can mask isotope fractionation has already been described by Qiu *et al.* where active transport along the proton motive force was the rate-determining step for phenoxy acid degradation at high concentrations.[51] However, no specific transporters for atrazine are known and non-polar molecules like atrazine with a relatively high log *P* value of 2.6 can even permeate the phospholipid bilayer directly.[50, 156] A phosphotransferase uptake system[157] can be ruled out, as atrazine does not undergo phosphorylation. Other plausible uptake

pathways are active transport across the lipid bilayer driven by ATP hydrolysis or by an electrochemical gradient.[47, 158, 159] To explore these hypotheses, atrazine degradation rates with *Polaromonas sp.* Nea-C and *A. aurescens* TC1, were compared for both strains with and without addition of KCN. Cyanide is known to inhibit cytochrome c so that the proton gradient collapses and ATP production ceases. As shown in **Figure 8**, the initial atrazine degradation rates in *Polaromonas sp.* Nea-C and *A. aurescens* TC1 were not influenced by 0.25 mM KCN. We conclude that atrazine degradation does not depend on active transport by ATP or the proton motive force. Thus, passive processes driven by the atrazine gradient led to atrazine uptake, e.g. through facilitated transport with porins or permeation of the membrane itself.[50, 160] Note that we did not study isotope fractionation here, because (i) this concentration range was also covered in the previous degradation (**Figure D1**) and (ii) the isotope fractionation was not concentration dependent in this concentration range (**Figure 7 A, B; Table 1**) so that the same isotopic enrichment factor is expected.

### 4.4.4 Implications for the application of CSIA in field studies.

When mass transfer masks the enzymatic reaction, this does not only limit biodegradation in the environment, but also has implications for the *in situ* assessment of biodegradation based on CSIA: pollutant turnover via the Rayleigh equation can best be estimated if isotope enrichment factors associated with a certain degradation pathway are constant and show little variation. However, as demonstrated in this study and by Renpenning *et al.*,[95] the isotope fractionation does not only depend on the reaction mechanism, but also on masking of the enzymatic reaction by mass transfer across the Gram-negative cell envelope. This leads to subtle differences in enrichment factors even for the same enzymatic reaction and introduces a small additional uncertainty in biodegradation assessments by CSIA in the field.[161] As a consequence, identification of the primary degradation pathway and the primary degrading strain would help to relate isotope fractionation in the field to isotope fractionation in the lab. A different strategy would be to use the enrichment factor determined under optimal conditions where mass transfer limitations are absent as a conservative estimate of biodegradation. This may underestimate biodegradation when the mass transfer

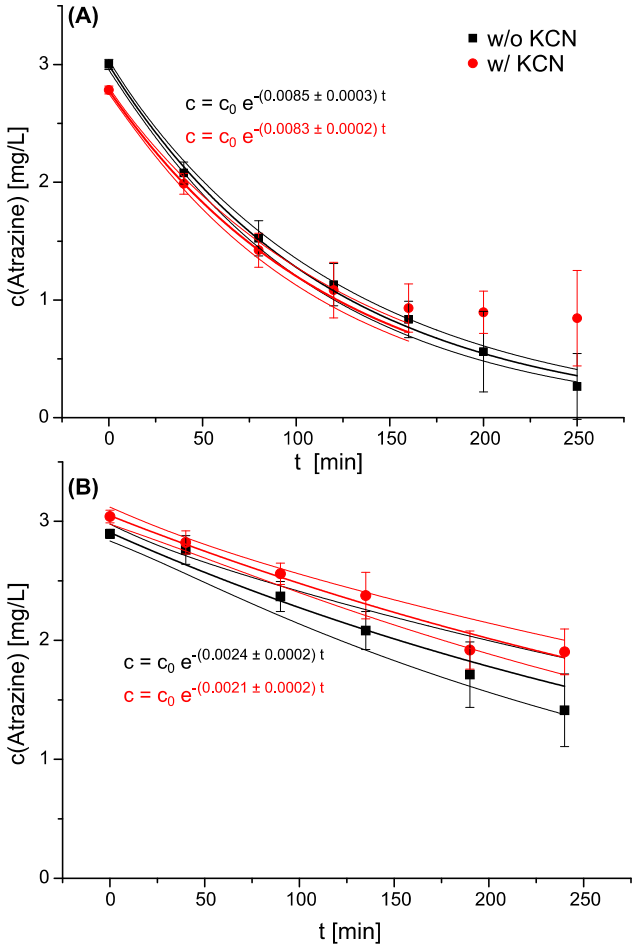


**Figure 8: Mass transfer of atrazine into the cytosol is not mediated by a mode of active transport that depends on energy or the proton gradient.** The degradation rates for both species ((A) *A. aurescens* TC-1 and (B) *Polaromonas sp.* Nea-C) were the same for control cells (black squares) and cells treated with 0.25 mM KCN (red circles). A pseudo first order reaction kinetics was assumed, as the concentration range was well below the Michaelis-Menten constant $K_M$ of TrzN.[113] Cyanide was added to inhibit cytochrome c to prevent formation of a proton gradient so that energy production ceases. The hydrolytic enzyme TrzN does not depend on ATP or other cofactors and is not inhibited. The degradation rates were reduced in *A. aurescens* TC1 150 minutes after KCN addition, indicating endogenous decay of TrzN. The fits of the first order rate constant in (A) and (B) are statistically not different at the 0.05 significance level.

$D = \frac{k_{tr} \times \delta \times V}{A \times K_{lipw}}$ becomes more and more rate limiting at low concentrations.[146] In contrast, the possibility to distinguish different processes and reaction pathways with dual element isotope plots remains valid, as long as the mass transfer across the cell envelope does not mask the enzymatic isotope fractionation completely

Therefore, we analyzed how the isotope fractionation during atrazine degradation by *Polaromonas sp.* Nea-C is affected by decreasing concentrations. This concentration-dependent observable isotope enrichment factor ε* can be modeled with a mathematical framework proposed by Thullner *et al.* for the case that mass transfer masks the intrinsic enzymatic fractionation factor ε.[92] This framework correlates the specific affinity of the enzyme $a = q_{max} \cdot K_M^{-1}$ with the mass transfer coefficient across the cell envelope $k_{tr}$. When the influx (determined by $k_{tr}$) is slower than the enzymatic turnover (determined by a) the fractionation factor ε will be masked which leads to a smaller observable enrichment factor ε* (ε* < ε). We used numerical modeling (see experimental section above) to fit the time-dependent enrichment in $^{13}C$ associated with the atrazine concentration decrease (equations (14) and (15); **Figure D3**). Thus, we were able to estimate the parameters for Thullner *et al*.'s model: $q_{max}$ = 2.7 nmol $L^{-1}s^{-1}$ which gives $a$ = 0.14 $s^{-1}$ and the mass transfer coefficient across the cell envelope $k_{tr}$ = $1.6 \cdot 10^{-4}$ $s^{-1}$. We validated our modeling approach for $k_{tr}$ by calculating the lipid diffusion coefficient $D_{lip}$ according to equation (16) where the cell shape and physiology is taken into account, to compare with literature values. Indeed, the calculated atrazine lipid diffusion coefficient $D_{lip}$ = $1.3 \cdot 10^{-17}$ $m^2 \cdot s^{-1}$ was, as expected, smaller, but in the same range as $D_{lip}$ reported for atrazine in a single lipid bilayer of the Gram-positive *A. aurescens* TC1.[146] This demonstrates, that our modeling approach yields realistic values for $k_{tr}$ allowing us to use $k_{tr}$ to calculate a theoretical further decrease of the observed fractionation factor *ε** with decreasing atrazine concentrations according to Thullner *et al.*.[92] Consistent with our experimental results, at a concentration of 4 mg/L the enzymatic fractionation factor of *ε* = -5.3 ‰ is already reduced to *ε** = -3.5 ‰ and it is predicted to be further reduced to below -3 ‰ already at an atrazine concentration of 1 mg/L.

### 4.4.5 Gram Pollutant mass transfer of non-polar pollutants may be rate limiting for biodegradation in Gram-negative bacteria.

Our results strongly suggest that the specific physiology of the Gram-negative *Polaromonas sp.* Nea-C with its additional restrictive outer membrane limited the influx of atrazine. In contrast, isotope fractionation in the Gram-positive *A. aurescens* TC1 was fully observable, demonstrating the absence of mass transfer limitation. This shows that the permeation of the cell envelope is partially rate-determining for atrazine degradation by *Polaromonas sp.* Nea-C already at high concentrations. Furthermore, Renpenning *et al.* show that the mass transfer across the cell envelope of Gram-negative bacteria affects biodegradation of chlorinated ethenes.[95] Taken together, the difference between Gram-positive and Gram-negative physiology might also affect the nature of non-polar pollutant biodegradation in the environment: while a restrictive outer membrane protects Gram-negative bacteria from xenobiotics[48] and from the toxicity of compounds with high log P values[162, 163] it might also lower the supply of non-polar pollutants as nutrients when transporters are absent.

# 5 High permeation rates in liposome systems explain rapid glyphosate biodegradation associated with strong isotope fractionation

Benno N. Ehrl, Emmanuel O. Mogusus, Kyoungtea Kim, Heike Hofstetter, Joel A. Pedersen, and Martin Elsner

Reproduced in part with permission from *High Permeation Rates in Liposome Systems Explain Rapid Glyphosate Biodegradation Associated with Strong Isotope Fractionation* Benno N. Ehrl, Emmanuel O. Mogusu, Kyoungtea Kim, Heike Hofstetter, Joel A. Pedersen, and Martin Elsner; Environmental Science & Technology 2018 52 (13), 7259-7268. 

## 5.1 Abstract

Bacterial uptake of charged organic pollutants such as the widely used herbicide glyphosate is typically attributed to active transporters, whereas passive membrane permeation as an uptake pathway is usually neglected. For 1-palmitoyl-2-oleoyl-*sn*-glycero-3-phosphocholine (POPC) liposomes, the pH-dependent membrane permeation coefficients ($P_{app}$) of glyphosate, determined by nuclear magnetic resonance (NMR) spectroscopy, varied from $P_{app}$(pH 7.0) = 3.7 ($\pm$ 0.3) × $10^{-7}$ m·$s^{-1}$ to $P_{app}$(pH 4.1) = 4.2 ($\pm$ 0.1) × $10^{-6}$ m·$s^{-1}$. The magnitude of this surprisingly rapid membrane permeation depended on glyphosate speciation and was in the range of polar, non-charged molecules. These findings point to passive membrane permeation as potential uptake pathway during glyphosate biodegradation. To test this hypothesis, a Gram-negative glyphosate degrader, *Ochrobactrum sp.* FrEM, was isolated from glyphosate-treated soil and glyphosate permeation rates inferred from the liposome model system were compared to bacterial degradation rates. Estimated maximum permeation rates were, indeed, two orders of magnitudes higher than degradation rates

of glyphosate. In addition, biodegradation of millimolar glyphosate concentrations gave rise to pronounced carbon isotope fractionation with an apparent kinetic isotope effect, $AKIE_{carbon}$= 1.014 ± 0.003. This value lies in the range typical of unmasked enzymatic isotope fractionation demonstrating that glyphosate biodegradation was little mass transfer-limited and glyphosate exchange across the cell membrane was rapid relative to enzymatic turnover.

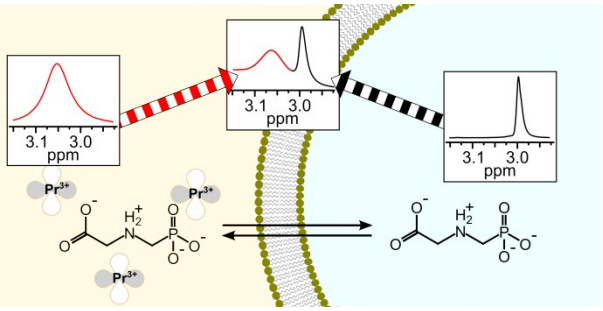


**Figure 9: Abstract art**

## 5.2 Introduction

Glyphosate (*N*-phopshomethylglycine) is a systemic, non-selective, broad-band herbicide widely used in agriculture because of its effective weed control.[25, 26, 164] One component of its success has been the introduction of transgenic, glyphosate-resistant crops.[29, 165] The worldwide market share of glyphosate is estimated at USD 5.6 billion, with production exceeding 620,000 tons in 2008.[164, 166] Historically, the acute toxicity of glyphosate was considered to be low;[26] it appears, however, that the impact of glyphosate on the environment has been underestimated.[31] The ubiquitous use of glyphosate has been found to affect biodiversity,[167] which is aggravated by increased usage due to the planting of glyphosate-resistant crops.[168, 169] The effect of glyphosate on human health is currently disputed. After the World Health Organization classified glyphosate as “probably carcinogenic” to humans (Group 2A),[170] discussion has continued on whether or not glyphosate use poses a cancer risk.[171,172] In addition, the

detection of glyphosate and its metabolite aminomethylphosphonic acid (AMPA) in surface waters and groundwaters at increasing frequencies lends urgency to the need to more thoroughly explore its environmental fate.[19, 173, 174] In particular, an improved understanding is warranted on the key drivers that limit its natural microbial degradation, because biodegradation represents the most effective glyphosate remediation pathway.[58, 175-177]

Recent work highlights the particular role of pollutant mass transfer into microbial cells as a rate limiting step for biodegradation, especially at low pollutant concentrations.[45, 146] The mass transfer of polar and charged species (e.g., zwitterionic glyphosate[28]) into bacterial cells is currently assumed to occur by active transport.[44, 178] Little is known whether charged molecules can directly permeate the cell membrane as non-polar pollutants do,[48, 50] and if so, to what extent the bacterial membrane as diffusion barrier constitutes an even stronger bioavailability limitation for these charged molecules than for non-charged pollutants.[179] Thus, it is not only important to investigate the membrane permeation rate but also to identify whether it is mass transfer across the cell envelope or the enzymatic reaction[44, 140] that is rate-determining in biodegradation of glyphosate (where mass transfer can be facilitated by either membrane permeation[179] or active transport[51]).

To investigate membrane permeation processes, different model systems, ranging from the *n*-octanol-water distribution coefficient as a surrogate to partitioning to membrane lipids to more complex systems like lipid discs and black lipid membranes, to synthetic membranes[49, 96] are used to study the diffusion of drugs and cosmetics through human epithelium.[97-99] However, these model systems typically all contain non-natural lipid phases, or non-natural lipid-water interfaces. Therefore, membranes resembling biological lipid bilayers (e.g., liposomes with natural lipid composition) are currently the best model to approximate permeation rates valid for natural systems.[103, 107] Membrane permeation leads to chemical exchange between the inside and the outside of the liposomes, and this process can be followed by nuclear magnetic resonance (NMR) spectroscopy.[98, 108, 109] The addition of a non-permeating chemical shift reagent like lanthanide ions (e.g., $Pr^{3+}$) separates the glyphosate NMR signal into distinct peaks that

can be attributed to glyphosate inside and outside the liposomes. Peak shape analysis subsequently allows quantification of chemical exchange of glyphosate between both environments based on the evaluation of associated line broadening in the NMR spectrum.[110]

Complementary to these model systems, we recently advanced compound-specific isotope analysis (CSIA) as an analytical approach to trace limitations of mass transfer across the cell envelope directly *in vivo* while pollutant biodegradation is ongoing.[146, 179] The underlying principle is the kinetic isotope effect of the associated enzymatic reaction. As the activation energy during a biochemical reaction is higher for bonds containing a heavy isotope, the turnover of molecules with a heavy isotope in the reactive position is slower. Therefore, as the enzymatic reaction proceeds, molecules containing heavy isotopes become enriched in the residual (non-reacted) substrate relative to those with light isotopes.[116] This trend can be evaluated by relating the change in isotope ratio ($R_t/R_o$) to the fraction of the remaining pollutant *f* according to the Rayleigh equation[129, 142] (17)

$$\ln\left(\frac{R_t}{R_0}\right) = \varepsilon \times \ln(f) \qquad (17)$$

where the enrichment factor ε describes how much slower heavy isotopes react compared to light isotopes. Thullner *et al.* delineated a new angle to use the change in isotope ratio as a diagnostic tool to directly observe mass-transfer limitation: strong isotope fractionation is observable, only if the pollutant exchange across the cell envelope is faster than its enzymatic turnover. Otherwise substrate molecules which experience the isotopic discrimination during the enzymatic reaction in the cytosol are used up completely so that they do not return to the bulk solution where the isotope ratio is assessed.[92, 145, 180] As a consequence, the enzymatic isotope fractionation that is observable in solution becomes masked in the presence of mass transfer limitations – i.e., when active transport (or passive membrane permeation) into and out of the cell is the rate-determining step in biodegradation.[51, 146]

For this study, we used a combined approach to gain insight into the role of passive permeation for biodegradation of the zwitterionic pollutant glyphosate, which carries

either one (pH < 6) or two (pH > 6) net negative charges at circumneutral pH. First, an NMR study was conducted to experimentally determine pH-dependent passive membrane permeation of glyphosate in phosphatidylcholine liposomes as model system. Second, passive permeation rates were extrapolated and compared to biodegradation rates of different glyphosate degraders to elucidate the role of passive membrane permeation of glyphosate for nutrient uptake. To this end, *Ochrobactrum sp.* FrEM, a new glyphosate degrader, was isolated from a vineyard soil treated with glyphosate, characterized, and used for degradation experiments. The isotope fractionation measured during glyphosate biodegradation by *Ochrobactrum sp.* FrEM was explored as a diagnostic tool to directly observe the presence or absence of mass transfer limitations and, thus, to validate the assessment based on the results of the liposome model system and our theoretical considerations.

## 5.3 Experimental Section

### 5.3.1 Chemicals

A list of chemicals used can be found in the Appendix E.

### 5.3.2 Liposome preparation and characterization

A 25 mg·mL$^{-1}$ solution of 1-palmitoyl-2-oleoyl-*sn*-glycero-3-phosphocholine (POPC, transition temperature –2 °C) in chloroform was prepared, and 50 mg POPC (2 mL of the POPC solution) was added to a 3 mL screw cap glass vial. The chloroform was evaporated under a $N_2$ stream, and the lipid film was dried with vacuum for at least 12 h. The dried lipids were hydrated with 1 mL of 20 mM glyphosate in $D_2O$ containing a small amount of 3-(trimethylsilyl)-2,2,3,3-tetradeuteropropionic acid (TSP) as internal reference for NMR. The pH of the solution, ranging from pH 4.1 to pH 7.8, was adjusted prior to hydration with 1 M sodium hydroxide (in $D_2O$). The vial was vortexed thoroughly until the lipids dissolved. Three freeze-thaw cycles (freeze in liquid nitrogen for 5 min, thaw in 40 °C water bath for 5 min, and vortex for 30 s) were followed by extrusion. The liposomes were extruded in 1000 µL syringes with 11 passages through a 0.2 µm polycarbonate filter with an Avanti Mini-Extruder (Avanti Polar Lipids, Inc., USA). The hydrodynamic size and the zeta potential of the vesicles were determined by dynamic

light scattering and laser Doppler electrophoresis with a ZetaSizer Nano ZS (Malvern Instruments Ltd., United Kingdom) in dilutions of 2 µL liposome solution in 800 µL $D_2O$. The temperature of the measurement cell was 25 °C. Ten measurements were averaged for each technical replicate (6 replicates for dynamic light scattering and 5 replicates for laser Doppler electrophoresis).

### 5.3.3 Nuclear magnetic resonance spectroscopy

All measurements were carried out on an Avance III 500 MHz spectrometer equipped with a BBFO+ smartprobe (Bruker, USA) at a sample temperature of 25 °C. NMR spectra were recorded with TopSpin 3.5.6 (Bruker, USA). Apodization, Fourier transformation, phase and baseline corrections, absolute referencing on TSP, spectra analysis, and peak fitting was carried out with MestReNova 11.0.3 (Mestrelab Research, Spain). Standard Bruker pulse sequences were used and the spectra collection parameters are summarized in **Table E1**.

### 5.3.4 Assessing the line broadening due to chemical exchange across the liposome membrane

First, a standard $^{1}H$ spectrum of 550 µL glyphosate liposome solution was collected to assess the pH-dependent chemical shift of the HOD peak and the chemical shift of the phosphorus nucleus was determined by $^{31}P\{^{1}H\}$. Then, a proton spectrum with phosphorus decoupling $^{1}H\{^{31}P\}$ and solvent suppression was recorded. We added 5.5 µL of a 50 mM $PrCl_3$ solution in $D_2O$ to the NMR tube up to a final concentration of 0.5 mM $PrCl_3$. Another $^{1}H\{^{31}P\}$ spectrum with solvent suppression was recorded and the glyphosate peaks prior to and after $PrCl_3$ addition were compared by fitting of the peaks.

### 5.3.5 Bacterial isolation and characterization

A detailed description of the bacterial isolation from vineyard soil can be found in the Appendix E.

### 5.3.6 Biodegradation of glyphosate by *Ochrobactrum sp.* FrEM

The biodegradation of glyphosate by *Ochrobactrum sp.* FrEM was carried out in two biological replicates. We inoculated 50 mL of medium (see Appendix E) with

*Ochrobactrum sp.* FrEM and incubated the culture at 30 °C at 160 rpm overnight. Cells were harvested by centrifugation (2100 *g*, Heraeus Megafuge 1.0R, Germany), washed twice with medium, and transferred to 50 mL fresh medium lacking phosphorus for phosphorus depletion. After incubation at 30 °C for 48 h, cells were harvested by centrifugation (2100 *g*, Heraeus Megafuge 1.0R, Germany) and used to inoculate 150 mL of medium containing 120 µM glyphosate as the only phosphorus source. Bacterial growth was monitored at $OD_{600}$ with a Cary 50 Bio UV-Vis spectrometer (Varian Medical Systems, Inc., USA). During the biodegradation, samples for isotope analysis (10 mL) were taken and the reaction was stopped by adding 1 mL of 2 M sodium hydroxide. The samples were lyophilized and reconstituted in 200 µL water. The isotope ratio in the delta notation ($\delta^{13}C$ in per mil relative to Vienna PeeDee Belemnite (V-PDB)) and the concentration of glyphosate were determined by liquid chromatography Isolink-isotope ratio mass spectrometry (LC-IRMS) (Thermo Fisher, Germany). The method used for carbon isotope analysis of glyphosate was modified from Kujawinski *et al.*[181] as follows: A mixed-phase Primesep 100 column 100 x 5.6 mm, 3 µm particle size (SIELC Technologies, USA) was used as stationary phase and 2.5 mM phosphate buffer at pH 3.1 was used as mobile phase. Separation was achieved with 300 $\mu L \cdot min^{-1}$ isocratic flow. The injection volume was 25 µL. The reagents for the chemical conversion to $CO_2$ at 99.9 °C were 1.5 M phosphoric acid and 0.84 M peroxodisulfate at a flow rate of 50 $\mu L \cdot min^{-1}$ each. The helium (grade 5.0) flow rate in the separation unit was set to 2.3 $mL \cdot min^{-1}$. The glyphosate concentration was determined with the area of the glyphosate $CO_2$ peak in the LC Isolink-IRMS chromatogram via external calibration with glyphosate standards in water (0.03, 0.06, 0.12, and 0.30 µM).

## 5.4 Results and Discussion

### 5.4.1 Praseodymium(III) ions interact with glyphosate as well as the liposome surface

The liposome preparations were of a uniform size with a hydrodynamic diameter of 204 ± 5 nm (median ± standard deviation) ranging from 194 nm to 239 nm. The

median polydispersity index was 0.093 indicating a uniform and narrow size distribution of the individual liposome preparations. The neutral zeta potential of the liposomes composed of lipids bearing zwitterionic phosphatidylcholine headgroups[182] changed to +29 ± 6 mV upon $PrCl_3$ addition, because the strongly positively charged $Pr^{3+}$ associated with the negatively charged phosphate group of POPC. Interaction of glyphosate with the chemical shift agent $Pr^{3+}$ led to a position-specific downfield shift Δδ of the NMR signals: The chemical shift change produced by a 1 mM $PrCl_3$ solution was Δδ = 0.06 ppm for the $PO_3^{2-}$-$CH_2$-$NH_2^+$-$C\underline{H_2}$-$COO^-$ protons and Δδ = 0.16 ppm for the $PO_3^{2-}$-$C\underline{H_2}$-$NH_2^+$-$CH_2$-$COO^-$ protons in the $^1$H-NMR spectrum of glyphosate (**Figure E1**). The phosphorus peak was shifted downfield by Δδ = 1.29 ppm in the $^{31}$P{1H} spectrum (**Figure E1**). This position-specific chemical shift change indicated that $Pr^{3+}$ directly interacted with the negatively charged phosphate group and not with the negatively charged carboxyl group of the zwitterionic glyphosate.

### 5.4.2 Phosphorus decoupling in $^1$H{$^{31}$P} NMR enabled peak shape analysis to quantify chemical exchange of glyphosate

The strong $^2J_{HP}$ coupling of 12.4 Hz between the phosphorus and adjacent protons led to splitting of the peak at 2.99 ppm into a doublet in the $^1$H NMR spectrum (**Figure 10**). This doublet, however, complicated peak shape analysis to quantify the rate of glyphosate permeation across liposomes. In the absence of $Pr^{3+}$, the shape of the separated doublet peaks could be fit. However, addition of $Pr^{3+}$ led to line broadening due to chemical exchange between the inside and the outside of the liposomes.

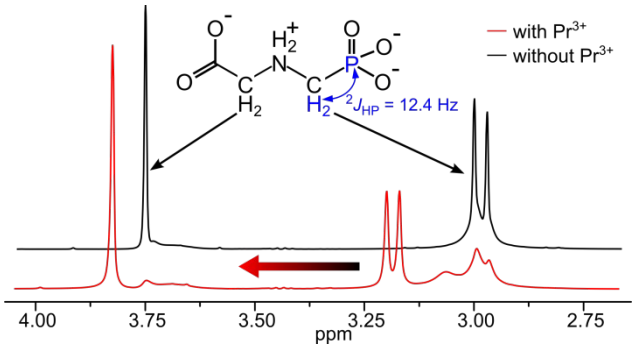


**Figure 10: $^2J_{HP}$ coupling prevents direct measurement of glyphosate permeation of liposomes with standard $^1$H-spectra.** Glyphosate showed one singlet at 3.74 ppm and one

doublet at 2.99 ppm in the $^{1}$H NMR spectrum with solvent suppression (black line). Strong $^{2}J_{HP}$ coupling led to formation of a doublet centered at 2.99 ppm. Upon $Pr^{3+}$ addition to the liposome suspension, the spectrum changed (red line). The glyphosate peaks outside the liposomes were shifted downfield (doublet at 3.2 ppm and singlet at 3.79 ppm) and the peaks inside the liposomes broadened due to chemical exchange. As a consequence, the individual doublet peaks overlapped, almost coalescing into a singlet and rendering peak shape analysis impossible. Both spectra in this figure were collected at pH 7.5

Thus, the individual peaks of the doublet signal overlapped with each other, rendering peak shape analysis unreliable. We therefore used a $^{1}$H-NMR pulse sequence that combined solvent suppression (watergate W5) with phosphorus decoupling. As a result, the doublet peak collapsed to a well-resolved singlet that was distinguishable from the POPC liposome signals (**Figure 11A**). Subsequent addition of 0.5 mM $Pr^{3+}$ to a glyphosate solution without liposomes moved the chemical shift of the collapsed singlet downfield from 2.99 ppm to 3.06 ppm. Interaction with the paramagnetic $Pr^{3+}$ further led to changes in the local magnetic field and thus to line broadening (**Figure 11B**). Relying on this approach, we observed a similar strong chemical shift change also when adding $Pr^{3+}$ to a glyphosate solution containing liposomes (**Figure 11C**). While the non-permeable $Pr^{3+}$ interacted with glyphosate outside of the liposomes influencing the chemical shift, the shift agent could not enter the liposomes leaving the glyphosate chemical shift inside unchanged. As a consequence, two distinct peaks appeared in the spectrum, and the glyphosate peak outside the liposomes was well resolved from the peak inside. This indicated that the exchange was slow on the NMR timescale; that is, the ratio $k_{tr}/\Delta\delta$ is smaller than one ($k_{tr}/\Delta\delta < 1$), where $k_{tr}$ is the rate constant of exchange and $\Delta\delta$ is the chemical shift difference.[110] The glyphosate exchange across the liposome bilayer was fast enough, however, to lead to considerable line broadening, $\Delta\upsilon$, of the inside peak. The line broadening $\Delta\upsilon$ depends on the rate constant of exchange $k_{tr}$ according to equation (18)[98] and ranged from $\Delta\upsilon$ = 2.6 Hz at neutral pH to $\Delta\upsilon$ = 40.8 Hz at pH 4.

$$\Delta\upsilon = \frac{k_{tr}}{\pi} \qquad (18)$$

The glyphosate peaks inside the liposomes were fitted to determine the peak width prior to ($\upsilon_0$) and after addition of $PrCl_3$ ($\upsilon_{ex}$). The resultant line broadening $\Delta\upsilon = \upsilon_{ex} - \upsilon_0$ (**Figure 11C**) was used to calculate $k_{tr}$ for each liposome preparation.

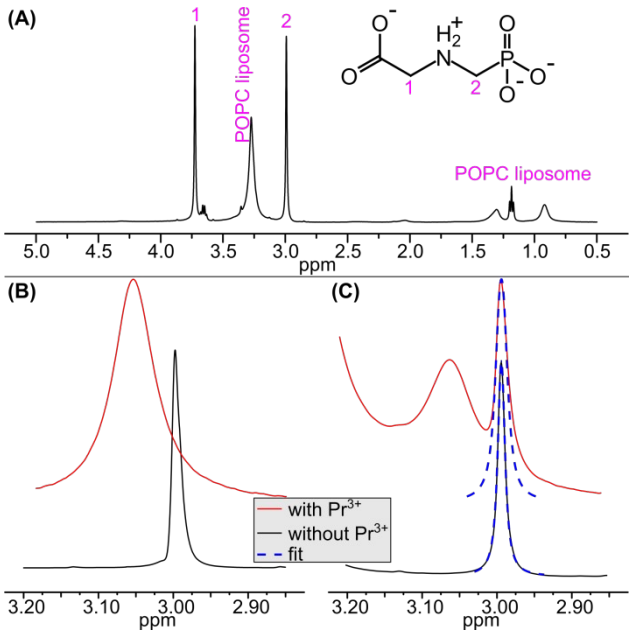


**Figure 11: Peak shape broadening due to exchange can be quantified by fitting the peaks in $^1H\{^{31}P\}$ NMR spectra. (A)** Clear separation of the glyphosate signals from the signals of the POPC liposomes in the $^1H\{^{31}P\}$ NMR spectrum (black line) enabling reliable peak shape analysis. **(B)** Spectral region showing glyphosate protons attached to carbon 2 with (red line) and without $Pr^{3+}$ (black line) in the absence of liposomes. The line broadening upon $Pr^{3+}$ addition was caused by the interaction with the paramagnetic $Pr^{3+}$. Even though the signal without $Pr^{3+}$ slightly overlapped with the broad glyphosate signal in the presence of $Pr^{3+}$, both peaks were well resolved. **(C)** The glyphosate peaks inside and outside the liposomes remained well resolved when POPC liposomes were present. Fitting the peak shape (blue dashed lines) prior (black line) and after (red line) the addition of $PrCl_3$ yielded peak widths and, thus, allowed the line broadening to be quantified. The broadening of the glyphosate peak inside the liposomes (2.99 ppm) was caused by chemical exchange of glyphosate between the inside and the outside of the liposomes, because the non-permeable $Pr^{3+}$ was not able to interact with glyphosate inside the liposomes. All spectra in this figure were collected at pH 7.5.

### 5.4.3 Glyphosate permeation of lipid bilayers depends strongly on pH

Because $k_{tr}$ strongly depends on the surface area and on the size of the liposomes, $k_{tr}$ is not suitable to compare the chemical exchange of different liposome preparations and at different pH values. Therefore, Males *et al*. derived the apparent permeation coefficient $P_{app}$ [m·s$^{-1}$] by including the inner liposome volume and the volume-to-surface ratio according to equation (19),[98] where $d_{lip}$ is the diameter of the respective liposome and δ is the membrane thickness (4 nm).

$$P_{app} = \frac{k_{tr} \times (d_{lip} - 2\delta)}{6} = \frac{\Delta\upsilon \times \pi \times (d_{lip} - 2\delta)}{6} \qquad (19)$$

The permeation coefficient $P_{app}$ describes how fast glyphosate permeates a hypothetical two-dimensional POPC membrane sheet and was much higher than expected (**Figure 12A**). At circumneutral pH the apparent permeation coefficient of glyphosate (double negatively charged, molecular weight $MW$ = 167 g·mol$^{-1}$) $P_{app}$(pH 7.0) = 3.7 (± 0.3) × 10$^{-7}$ m·s$^{-1}$ was considerably higher than the one of maleate[108] (double negatively charged, $MW$ = 114 g·mol$^{-1}$) and in the same range as the permeation coefficient of the non-charged, polar serotonin ($MW$ = 176 g·mol$^{-1}$).[183] With decreasing pH, the permeation rate increased, with an apparent permeation coefficient of $P_{app}$(pH 4.1) = 4.2 (± 0.1) × 10$^{-6}$ m·s$^{-1}$ at pH 4.1. The pH-dependence correlated linearly with the average degree of ionization and thus the average charge of glyphosate (**Figure 12B**). The net charge of –2 (one positive and three negative charges) of glyphosate at neutral pH slowed passive membrane permeation. Protonation of the phosphate group at pH 4.1 reduced the net charge of glyphosate to –1 and, consequently, accelerated membrane permeation. We hypothesize that the zwitterionic structure of glyphosate with its even distribution of charges facilitated permeation of glyphosate across the lipid bilayer by allowing multiple interactions with the zwitterionic POPC headgroup, whereas the increased negative charge at neutral pH slowed passive permeation of glyphosate.

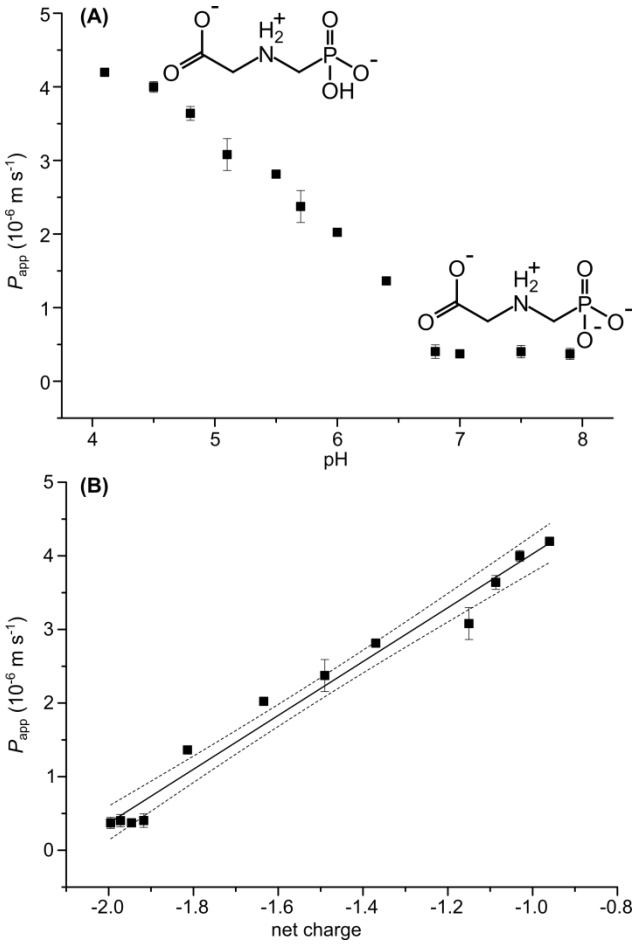


**Figure 12: The pH-dependence of the permeation coefficient $P_{app}$ (black squares) correlated with the net charge of glyphosate. (A)** $P_{app}$ depended strongly on the pH of the liposome solution. The permeation at neutral pH ($P_{app}$(pH 7.0) = 3.7 (± 0.3) × $10^{-7}$ m·$s^{-1}$) was one order of magnitude lower than at slightly acidic pH ($P_{app}$(pH 4.1) = 4.2 (± 0.1) × $10^{-6}$ m·$s^{-1}$). **(B)** Permeation correlated with the ionization of glyphosate which can be explained by two different permeation coefficients of the two different glyphosate species (two negative and one negative charge at the phosphate group, respectively). Both panels show the mean and the error bars depict the standard deviation.

### 5.4.4 Membrane permeation can lead to considerable glyphosate uptake into bacterial cells

Non-polar pollutants' entry of bacterial cells by passive permeation of the cell envelope is well recognized,[50, 156] and charged, polar molecules like glyphosate are commonly

assumed to be taken up almost exclusively by active transport or porin-assisted permeation.[104, 184] Contrary to this expectation, our observations in a liposome model system that lacked transporters or porins gave membrane permeation coefficients of glyphosate in the same range as those of non-charged molecules (see above).[183] This observation suggests that passive membrane permeation of glyphosate mono- and dianions may provide sufficient influx into bacterial cells for it to serve as phosphorus source. The molar amount of substrate outside the liposomes $n_{out}$ is reduced via passive membrane permeation at the rate $(dn_{out}/dt)_{permeation}$ which is driven by the concentration gradient across the membrane and is defined by the linear exchange term in equation (20) as proposed by Males *et al.*.[185]

$$\left(\frac{d\,n_{out}}{dt}\right)_{permeation} = -\left(k¿¿tr\,K_{lip-w}\left[S_{out}\right]\right) + \left(k¿¿tr\,K_{lip-w}\left[S_{¿}\right]\right)¿¿ \qquad (20)$$

Here, $K_{lip\text{-}w}$ is the membrane lipid-water partitioning coefficient, $[S_{out}]$ and $[S_{in}]$ are the glyphosate concentrations outside and inside the bacterial cell, whereas $K_{lip\text{-}w}[S_{out}]$ and $K_{lip\text{-}w}[S_{in}]$ are the concentrations within the lipid membrane (outside and inside), respectively. With the definition of the diffusion coefficient across the membrane (lipid bilayer) $D_{lip}$ (21), the rate constant of exchange $k_{tr}$ can be calculated for a single bacterial cell by equation (22)

$$D_{lip} = \frac{P_{app} \times \delta}{K_{lip-w}} \qquad (21)$$

$$k_{tr} = \frac{D_{lip} \times A_{cell}}{\delta} = \frac{P_{app} \times A_{cell}}{K_{lip-w}} \qquad (22)$$

where $A_{cell} \approx 3\ \mu m^2$ is the estimated surface area of one bacterial cell and δ is the membrane thickness (one 4 nm membrane in Gram-positive and two 4 nm thick membranes (8 nm) in Gram-negative bacteria). Together with equation (23), a term is obtained for the concentration gradient-dependent glyphosate influx of a single bacterial cell:

$$\left(\frac{d\,n_{out}}{dt}\right)_{cel\,l-\,permeation} = -\left(P¿¿\,app\,A_{cell}\left[S_{out}\right]\right) + \left(P¿¿\,app\,A_{cell}\left[S_{¿}\right]\right)¿¿ \qquad (23)$$

The glyphosate influx is at its maximum $(dn_{out}/dt)_{cell\text{-}permeation\text{-}max}$ when the concentration gradient is large ($[S_{in}] = 0$). We compared this maximum permeation rate with the glyphosate degradation rate of *Achromobacter sp.* MPS 12A described by Sviridov *et*

*al*..[58] The glyphosate degradation rate of a single *Achromobacter sp.* MPS 12A cell ($dn/dt)_{deg\text{-}cell} = -1.4 \times 10^{-21}$ mol·s$^{-1}$·cell$^{-1}$ at a concentration of 3 mM[58] was estimated by correlating the number of cells with the optical density $OD_{600}$ ($8 \times 10^8$ cells·mL$^{-1}$·$OD_{600}^{-1}$)[186] and the bulk glyphosate degradation rate. The comparison showed that the calculated maximum membrane permeation rate $(dn_{out}/dt)_{cell\text{-}perm\text{-}max} = -1.9 \times 10^{-18}$ mol·s$^{-1}$·cell$^{-1}$ was two orders of magnitude higher than the degradation rate. As a consequence, even though glyphosate has a net charge of –2 at pH 7, its passive membrane permeation is predicted to be fast enough to provide enough influx for bacterial biodegradation and to serve as phosphorus source. This hypothesis clearly warrants further testing. If true, it should be possible to confirm it (a) by the observation of similarly rapid biodegradation per cell in a different strain and (b) by applying compound-specific isotope fractionation as a diagnostic tool to observe the absence of mass transfer limitations directly. If permeation is indeed faster than enzymatic conversion, glyphosate molecules inside and outside the cell are expected to be in rapid equilibrium. Thus, glyphosate molecules enriched in heavy isotopes due to the enzymatic reaction in the cytosol will get out of the cell into the bulk solution. This would lead to the isotope effect of the enzyme reaction being observable outside the cell, resulting in strong isotope fractionation during biodegradation. A new bacterium was, therefore, isolated from soil, and isotope fractionation was measured during glyphosate degradation.

### 5.4.5 Isolation and glyphosate degradation activity of *Orchrobactrum sp.* FrEM

Repeated subculturing of an inoculum from soil samples in a medium containing 3 mM glyphosate as sole phosphorus source resulted in the isolation of a bacterial strain with glyphosate-degrading activity. The bacteria were rod-shaped as observed by light microscopy (**Figure E2**). Sequence alignment (BLAST) of the 16S rRNA showed a 99% homology with *Ochrobactrum anthropic, O. rhizosphaerae*, *O. pituitosum,* and *O. intermedium*, which all belong to the family of Brucellaceae of Alphaproteobacteria, and 70% homology with *Ochrobactrum haematophilum.* The strain was termed *Ochrobactrum sp.* FrEM (**Figure E3**). The glyphosate degradation rate of *OCHROBACTRUM sp.* FrEM $(dn/dt)_{deg\text{-}cell} = -1.7 \times 10^{-21}$ mol·s$^{-1}$·cell$^{-1}$ at a concentration

of 0.12 mM (**Figure 13A**) was as high as that of *Achromobacter sp.* MPS 12A (see above).[58]

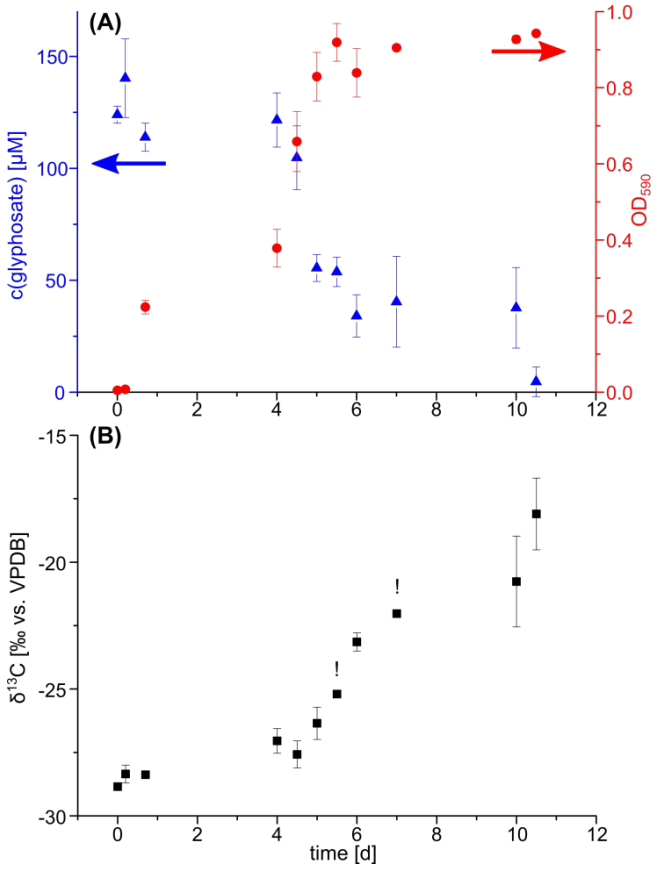


**Figure 13: Glyphosate biodegradation was accompanied by growth and strong isotope fractionation. (A)** Glyphosate degradation by *Ochrobactrum sp.* FrEM. Consumption of glyphosate (blue triangles) as source of phosphorous led to bacterial growth (red circles). **(B)** During this biodegradation, $^{13}C/^{12}C$ ratios of glyphosate increased, as indicated by less negative $\delta^{13}C$ values. All graphs show the mean and the error bars indicate the range of two biological replicates. The exclamation marks (!) above two data points indicate that a reliable isotope value could be measured for only one biological replicate at the respective time points.

Furthermore, just as for *Achromobacter sp.* MPS 12A, the calculated maximum membrane permeation rate $(dn_{out}/dt)_{cell\text{-}perm\text{-}max} = -7.5 \times 10^{-20}$ mol·s$^{-1}$·cell$^{-1}$ at a concentration of 0.12 mM was larger than the degradation rate indicating that passive permeation of the cell envelope is likely not rate limiting for glyphosate biodegradation. We subsequently aimed to verify this hypothesis by compound-specific isotope fractionation analysis.

### 5.4.6 Carbon isotope fractionation revealed rapid glyphosate mass transfer across the cell wall

Glyphosate biodegradation by *OCHROBACTRUM sp.* FrEM was accompanied by significant carbon isotope fractionation (**Figure 13B**). Carbon isotope values $\delta^{13}C$ of glyphosate increased from –28 (± 0.5) ‰ in the beginning to –19 (± 0.5) ‰ after 90% glyphosate conversion reflecting an enrichment of $^{13}C$ over $^{12}C$. The corresponding enrichment factor $\varepsilon^{13}C$ = –4.5 (± 0.5) ‰ was determined according to the Rayleigh equation (**Figure 14**, and equation (1)). The primary apparent kinetic isotope effect *AKIE*, a measure for the isotope effect at the reactive position, allows the direct comparison of isotope effects of different reactions and reactants and was calculated according to equation (24)[187]

$$AKIE_{carbon} = \frac{1}{\frac{n}{x}\varepsilon^{13}C + 1} \qquad (24)$$

where *n* denotes the total number of carbon atoms and *x* the number of carbon atoms at the reactive position. With *n* = 3 and *x* = 1, the primary apparent kinetic isotope effect for glyphosate degradation was $AKIE_{carbon}$ = 1.014 ± 0.003, which is in the range of chemical reactions that involve bond cleavage to a carbon atom.[187, 188]

This suggests that any additional rate determining steps like active transport[51] or slow passive membrane permeation[179] masked the enzymatic isotope fractionation only to a small extent, if at all. As a consequence, we conclude that, indeed, glyphosate exchanged rapidly across the cell envelope consistent with our hypothesis that passive permeation across the cell envelope may be an important, and until now underestimated, driver of glyphosate biodegradation.

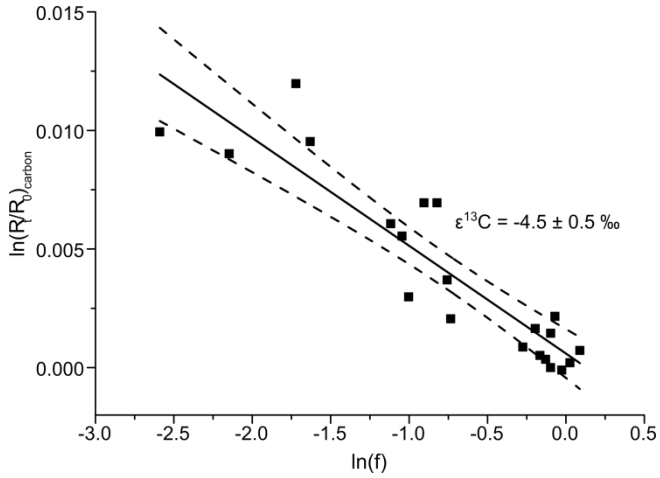


**Figure 14: Pronounced isotope fractionation indicated rapid glyphosate exchange across the bacterial cell envelope.** The carbon isotope fractionation factor ($\varepsilon^{13}C$ = –4.5 (± 0.5) ‰) was determined according to the Rayleigh equation (equation (1)). The corresponding $AKIE_{carbon}$ = 1.014 ± 0.003 (equation (8)) was in the range of typical carbon isotope effects. This indicated that the enzymatic isotope fractionation was not masked by mass transfer limitations and that exchange of glyphosate across the cell envelope was comparatively rapid during bacterial degradation by *Ochrobactrum sp.* FrEM.

### 5.4.7 Possibility of mass transfer limitations at low concentrations

While passive membrane permeation has previously been associated with only non-polar molecules, our results suggest that also charged species like glyphosate can permeate the bacterial cell envelope more rapidly than commonly thought. This can facilitate glyphosate biodegradation and lead to rapid turnover at high concentrations in water and soil.[31] A different situation must be considered, however, if the concentration gradient across the cell envelope is shallower, that is, when the outside concentration is lower. We recently demonstrated that mass transfer across the cell membrane becomes rate-limiting for atrazine biodegradation at trace concentrations.[146] Similarly, at a glyphosate concentration of 1 µM, the calculated maximum membrane permeation rate is reduced to only $(dn_{out}/dt)_{cell\text{-}perm\text{-}max}$ = –6.5 × $10^{-22}$ mol·$s^{-1}$·$cell^{-1}$, which is lower than the respective degradation rate per cell. At these concentrations, acceleration of cell wall transfer of glyphosate with high affinity active transporters may become necessary to

boost biodegradation. Interestingly, Pipke *et al.* described such an active glyphosate transporter with an uptake rate of $(dn_{out}/dt)_{cell\text{-}transport} = -1.8 \times 10^{-21}$ mol·s$^{-1}$·cell$^{-1}$ which is just in the range of observed glyphosate degradation rates.[189] However, its affinity constant $K_M$ = 0.125 mM for glyphosate uptake is rather high, resulting in low transporter activity at trace concentrations. This increased mass transfer limitation at trace concentrations may cause biodegradation to stall and might explain the frequent detection of glyphosate in the environment.[173]

# 6 Conclusion

This thesis clearly brings forward compelling evidence for the important role passive membrane permeation plays for the natural biodegradation of micropollutants. This also has broad implications on how bacteria live and survive under oligotrophic conditions in the environment. First of all, passive membrane permeation leads to pollutant uptake into bacteria, even when specific active transporters are absent. This can be a decisive advantage when oligotrophic bacteria are exposed to a new and unfamiliar nutrient, e.g. a pollutant. As the unfamiliar pollutant might enter the cytosol by passive permeation, degradation can start immediately and bacteria can gain energy and build up biomass without the need for energy intensive expression of specific transporter proteins. Furthermore, when nutrient influx does not depend on energy dependent active transport or the expression of transporter proteins, bacteria can use the saved energy to invest in other cell functions and ultimately for the energy cost intensive mitosis, resulting in growth. A drawback of passive membrane permeation is that bacteria also might lose the degradation metabolites, e.g. hydroxyatrazine, as they permeate the cell envelope and diffuse back into the bulk solution. Many copiotrophic bacteria use strategies, e.g. active transport or phosphorylation in the cytosol,[157-159] to scavenge nutrients from their surrounding and trap them inside to sustain fast growth rates. However, when non-polar pollutant metabolites, like hydroxyatrazine, are lost due to membrane permeation anyway, investing energy into uptake for higher intracellular concentrations would not be an efficient strategy anymore. In contrast, pollutants taken up by passive permeation might lead to loss of metabolites during the degradation, but no energy is wasted by non-effective active transport. How passive permeation of the cell envelope affects the biodegradation of atrazine and glyphosate, and the further implications for life in oligotrophic environments is further discussed in this conclusion.

## 6.1 Passive membrane permeation allows rapid atrazine turnover via biotic hydrolysis in the environment at high concentrations

Atrazine permeation of the *Arthrobacter aurescens* TC1 cell envelope at high concentrations is rapid. This is not only demonstrated by the similar isotope fractionation for the batch degradation in whole cells,[111] with purified enzyme,[112] and at a high dilution rate in chemostat ($\varepsilon^{13}C$ = −5.4 ‰), but also by the fact, that the modeled permeation coefficient $P_{app}$ = 3.5 × $10^{-5}$ $ms^{-1}$ of atrazine (*MW* = 216 g/mol) is two orders of magnitude larger than the permeation coefficient of serotonin ($P_{app}$ = 1.4 × $10^{-7}$ $ms^{-1}$; *MW* = 176 g/mol). Probably due to its stronger lipophilic character,[183] atrazine influx into bacterial cells is unhindered allowing fast degradation rates, at least at high concentrations.

That rapid atrazine degradation does not depend on active transporters could also explain the success of hydrolytic atrazine degradation and the rapid proliferation of the specific degradation genes around the globe. Only the genes for the degrading enzymes (TrzN or AtzA, and AtzB, AtzC) and no additional transporter genes have to be transferred to generate new atrazine degrading species. Prior 1993, in the first 35 years after its introduction, bacteria degraded atrazine by oxidative dealkylation and no other degradation pathways were known.[190-192] However, the oxidative degradation catalyzed by cytochrome P450 uses energy in the form of NADH.[193] Then, as described by de Souza *et al*., a new degradation pathway developed which degrades atrazine by hydrolysis to hydroxyatrazine and subsequent hydrolytic cleavage of the side chains. The catalyzing enzymes AtzA, AtzB, and AtzC emerged in different species around the globe with high sequence similarity of the degradation genes.[194, 195] The next evolutionary step, described by Topp *et al.* in the year 2000, was towards the related enzyme TrzN (42 % similarity with AtzA), which opened the energy saving degradation by hydrolysis for many other triazine compounds, such as simazine.[196] Also the *trzN* gene spread around the globe fast and the high sequence similarities of above 99 % argue for a unique evolutionary origin and a global dispersion by gene transfer.[63, 150, 197-200]

Gram-positive and Gram-negative bacteria are affected differently by the fact that atrazine is taken up by degrading bacteria by passive permeation of the cell envelope. The restrictive outer membrane in Gram-negative bacteria is not only protection against antibiotics,[48] but might also limit nutrient influx when transporters are absent. This is also demonstrated by the mass transfer limitation during atrazine biodegradation by Gram-negative *Polaromonas sp.* Nea-C, indicated by the smaller isotope fractionation $\varepsilon^{13}C$ = -3.5 ‰ compared with Gram-positive *Arthrobacter aurescens* TC1 $\varepsilon^{13}C$ = -5.4 ‰. Together with the study from Renpenning *et al.,*[95] we pinpoint the additional outer membrane of Gram-negative bacteria as diffusion barrier for pollutant uptake which might also have further consequences for biodegradation in the environment. Fast permeation of the cell envelope in Gram-positive bacteria leads to rapid nutrient influx which allows Gram-positive bacteria to sustain substantial nutrient degradation to gain energy and build up biomass, also when nutrients are scarce. On the other hand, the additional outer membrane in Gram-negative bacteria offering additional protection against toxins in highly contaminated environments[160] restricts the nutrient influx,[133] leading to slower nutrient turnover and thus growth.

## 6.2 Glyphosate permeates bacterial lipid membranes facilitating its biodegradation in the environment

While the non-polar atrazine is expected to permeate lipid bilayers and the high permeation coefficient $P_{app}$ = 3.5 × $10^{-5}$ $ms^{-1}$ is a consequence of its hydrophobicity, the rather fast membrane permeation of the double negatively charged glyphosate with its experimentally determined permeation coefficient $P_{app}$(pH 7.0) = 3.7 x $10^{-7}$ $ms^{-1}$ was unexpected. That this passive membrane permeation can even sustain glyphosate influx into bacteria to sustain biodegradation might explain its fast turnover in the environment.[26, 28] Passive glyphosate uptake might be important in oligotrophic environments when bacteria are desperate for phosphate.

However, the experimental system in chapter 5 of this thesis is not targeted to elucidate the possible role of glyphosate transporters and further experiments have to be carried out. That rate determining active transport along the proton gradient results in negligible

isotope fractionation was shown by Qiu *et al*. for charged phenoxy acid degradation.[51] In contrast, the strong isotope fractionation *AKIE* = 1.014 demonstrates, that glyphosate influx is not the rate determining step for biodegradation by *Ochrobactrum sp.* FrEM. However, as shown for sulfate reduction during anaerobic methane oxidation, catabolic processes with low yield can also be, at least partially, reversible.[201] Thus, even though sulfate is taken up by active transport along the proton gradient, strong isotope fractionation is associated with sulfate reduction.[88] A similar situation could also arise during glyphosate degradation when a slow, low yield enzymatic turnover leads to a reversible glyphosate influx, even though glyphosate might be taken up by active transport.[202] To unravel the possibility of reversible transport which does not mask the enzymatic isotope fractionation, further insight into the uptake pathway and the rate determining step for glyphosate biodegradation is needed.

## 6.3 Bioavailability limitations at trace concentrations in the environment

### 6.3.1 Mass transfer limitations reinforce nutrient scarcity under oligotrophic conditions

When mass transfer becomes the rate determining step for biodegradation at low concentrations, the degradation rate *R* decreases according to the Best equation (25)[133] where a mass exchange term is combined with the enzymatic Michaelis-Menten kinetics.[152]

$$R = \frac{k_{tr}}{2}\left([S] + K_M + \frac{q_{max}}{k_{tr}}\right)\left(1 - \sqrt{\frac{4[S]\frac{q_{max}}{k_{tr}}}{\left([S] + K_M + \frac{q_{max}}{k_{tr}}\right)^2}}\right) \quad (25)$$

Thus, even though mass transfer does not limit biodegradation of micropollutants at high concentrations, the degradation stalls at low concentrations, e.g. in ground water. Furthermore, mass transfer limitations might also affect growth and competition in bacterial communities. Bacteria capable of pollutant degradation have a competitive advantage. Not only can the degradation of pollutant generate energy, but also carbon and especially heteroatoms are scarce in the environment. However, this advantage disappears if the pollutant influx ceases at trace concentrations. As a consequence,

growth of pollutant degrading bacteria might be reduced as well, further lowering pollutant turnover rates, possibly causing the persistence of micropollutants.

### 6.3.2 Bioavailability limitations impair assessment of biodegradation by CSIA in the field

Complex physical processes in contaminated aquifers (mixing, sorption, diffusion, and dispersion) result in spatial and temporal variation in the concentration and, therefore, the biodegradation is often investigated *in situ* with the concentration independent tool CSIA.[82-84] However, the results of this thesis and the study of Renpenning *et al*.[95] clearly indicate, that this approach is prone to error because of the masking effect of mass transfer limitations across the cell envelope. That biodegradation enrichment factors may vary for different strains even for the same enzyme and degradation pathway has been shown by Meyer *et al*..[111] This difference was pinpointed to the difference in between Gram-positive and Gram-negative bacteria and the role of the restrictive outer membrane in Gram-negative bacteria as barrier in chapter 4. Thus, for reliable biodegradation assessment with CSIA, not only the degradation pathway, but also the main degrader strain has to be identified, e.g. by stable isotope probing.[203, 204] If this approach is not suitable, the enrichment factor has to be estimated, e.g. by the median of all published enrichment factors for different degradation pathways, with the risk of overestimating the success of biodegradation if the chosen enrichment factor is too small. Contrasting, if the chosen enrichment factor is too large, the extent of biodegradation will be underestimated, or even no isotope fractionation can be detected at all. This might lead to the application of a different, more expensive remediation strategy, e.g. chemical remediation with zero valent iron.[205, 206]

The biodegradation activity is also underestimated, if the isotope fractionation becomes increasingly masked by mass transfer limitations at low concentrations, as demonstrated in chapter 3 and chapter 5. Such decreasing isotope fractionation with decreasing concentrations is also suggested by experimental evidence during sulfate reduction at a hydrocarbon contamination plume at an old gasworks site.[207] That isotope fractionation can be masked by bioavailability limitations at low concentrations has been brought forward in a study by Thullner *et al.* where the authors implemented isotope

fractionation into the Best equation (see above, (25)), which allows the calculation of observable enrichment factors ε* at different pollutant concentrations.[92] This tool could be used to predict enrichment factors valid for low concentrations by adjusting enrichment factors determined at high concentrations in the laboratory. However, the rapid onset of rate limiting mass transfer in chapter 3 was faster than predicted by Thullner *et al*..[92] As a consequence, when bacterial adaptation to oligotrophic conditions leads to changes in the cell envelope or in the abundance of degrading enzymes, the predictions on the fractionation factor will be incorrect. Thus, enrichment factors determined in bioreactors, where bacteria have time for adaptation, will be more precise.

## 6.4 Bacterial life under oligotrophic conditions is affected by bioavailability limitations and physiological adaptation

### 6.4.1 Possible interplay between mass transfer limitations and physiological adaptation

How bacteria adjust to mass transfer limitations and how this physiological adaptation affects the mass transfer of nutrients across the cell envelope is poorly understood. Therefore, to be able to design effective remediation strategies, further research focusing on the interplay of mass transfer limitations and physiological adaptation is needed. Interestingly, as described in chapter 3, the atrazine degradation in chemostat at steady state concentrations around 25 % of $K_M$ led to changes in bacterial physiology and, simultaneously, we were able to detect mass transfer limitations with CSIA. These mass transfer limitations lead to reduced intracellular concentrations and a reduced metabolic flux. Kotte *et al.* describes, that such metabolic flux changes are used by bacteria to sense changing environmental conditions without the need for upstream sensing and signaling networks.[208] As a consequence, bioavailability limitations might be used by bacteria to sense nutrient scarcity and indirectly lead to physiological adaptation. Furthermore, upon changing carbon sources or concentration changes, *Arthrobacter* species have been demonstrated to exhibit a rapid change in membrane fluidity by changing their *anteiso* to *iso* fatty acid composition.[104, 209] However, changes in

the membrane fluidity immediately affect the permeability and, thus, might also affect mass transfer limitations.[103] In conclusion, this hypothesized feedback mechanism between mass transfer limitations and physiological adaptation should be addressed by future research.

### 6.4.2 Proposed strategies to unravel physiological adaptation to oligotrophic conditions

The *Arthrobacter aurescens* TC1 genome was sequenced by Mongodin *et al.,*[132] which enables researchers to study the relative protein abundances by label free proteomics.[210] Proteomics were also the key to investigate the physiological changes of *Arthrobacter aurescens* TC1 during transition from exponential growth in chemostat to stationary growth in retentostat, as shown in the related study in Appendix B. Here, the accompanying observation of decreased isotope fractionation allowed the first observation of the interplay between mass transfer limitations and physiological adaptation.

A novel strategy to study the immediate response of bacteria to changes in the environment is to analyze newly synthesized proteins by bioorthogonal noncanonical amino acid tagging (BONCAT) proteomics.[211] Upon an imposed change in the culitivation conditions, newly synthesized proteins incorporate an added artificial amino acid instead of methionine. This artificial amino acid can be functionalized with click chemistry in a way that newly synthesized proteins can be purified with an affinity tag and analyzed by high throughput mass spectrometry.[212, 213] BONCAT could also be used to complement and improve *in situ* proteomics and *in situ* RNA analysis to study biodegradation activity in field studies.[214, 215]

Unell *et al.* described a decreased membrane fluidity at toxic 4-chlorophenol concentrations[209] which could lead to a reduced permeation rate and slower uptake of 4-chlorophenol. Thus, 4-chlorophenol biodegradation by *Arthrobacter chlorophenolicus* A6 is the ideal system to study how changes in the membrane fluidity affect isotope fractionation. A suitable experimental strategy would be to grow *Arthrobacter chlorophenolicus* A6 with varying 4-chlorophenol concentrations in

chemostat and in batch, extract the fatty acids[216] and convert them to fatty acid methyl esters for GC analysis.[217] Complementary, underlying mass transfer limitations can be detected with CSIA.

### 6.4.3 The lower threshold for biodegradation might be determined by the maintenance demand of bacteria

Bacteria need to maintain basic cell functions (i.e. the proton motive force, osmoregulation, macromolecule turnover, RNA synthesis, and DNA repair) to remain viable and active even at trace concentrations.[218, 219] When the nutrient supply is not enough to fulfill the maintenance energy demand, bacteria may become dormant and non-active, consequently leading to stalling pollutant biodegradation.[220] However, bacteria might not have constant maintenance energy demand when they adapt to oligotrophic conditions.[221, 222] This will have to be taken into account in future studies to pinpoint the threshold concentration below which biodegradation is not beneficial anymore.

In addition, when the concentration of a single substrate is not enough for bacteria, they metabolize multiple organic substrates which leads to overall lower threshold concentrations for biodegradation.[40] Thus, our experimental setup in chapter 3, where atrazine as single substrate was limiting in chemostat, does not necessarily reflect conditions in ground water, where multiple trace carbon sources and competing bacteria would be present.[223] Thus, future experiments should mimic natural groundwater environment by including (i) additional carbon and nitrogen sources in chemostat and (ii) add additional degrader strains or work with natural groundwater communities.

# Appendix A: Modeling contaminant biodegradation and compound-specific isotope fractionation in chemostat at extremely low dilution rates

Mehdi Gharasoo, Benno N. Ehrl, and Martin Elsner

in preparation for submission to *Ecological Modeling*;

## Modeling contaminant biodegradation and compound-specific isotope fractionation in chemostats at extremely low dilution rates

Mehdi Gharasoo[1,*], Benno N. Ehrl[1], Olaf A. Cirpka[2], and Martin Elsner[1,3]

[1]Helmholtz Zentrum München, Institute of Groundwater Ecology, Ingolstädter Landstr. 1, 85764 Neuherberg, Germany
[2]University of Tübingen, Center for Applied Geoscience, Hölderlinstr. 12, 72074 Tübingen, Germany
[3]Institute of Hydrochemistry, Technical University of Munich, Marchioninistr. 17, 81377 Munich, Germany
[*]Corresponding author: Tel. +49 89 3187 3498, Fax +49 89 3187 3361, E-mail: mehdi.gharasoo@helmholtz-muenchen.de

February 22, 2018

**Abstract**

We present a framework to model microbial transformations in chemostats and retentostats under transient or quasi-steady state conditions. The model accounts for transformation-induced isotope fractionation and mass-transfer across the cell membrane. We explicitly consider that the feeding of substrate into the reactor by dripping droplets at very low dilution rates leads to highly transient behavior of concentrations and transformation rates even at quasi-steady state. We demonstrate the practicality of the code by modeling a chemostat experiment of atrazine degradation at extremely low dilution/growth rates by the strain *Arthrobacter aurescens* TC1, shedding light to the interplay of processes that control biodegradation of contaminants at very low ($\mu g/l$) concentration levels. With the help of model, the mass-transfer coefficient of atrazine through the cell membrane of this particular strain was estimated to be $0.0025 s^{-1}$.

**Keywords**: *Chemostat and Retentostat, Continuous Stirred-Tank Reactor (CSTR), Transient and Quasi-steady State, Periodic Input, Isotope Fractionation*

# 1 Introduction

Many dissolved organic compounds in groundwater have an adverse effect on human health and are regarded as micropollutants due to their presence at low concentration levels that are still high enough to be of concern (Daughton and Ternes, 1999). Microorganisms' tendency of degrading the micropollutants drastically declines as the concentrations decrease, down to a threshold at which natural attenuation appears to stall. The question whether the physiological adaptation of microorganisms (i.e., down-regulation of catabolic enzymes (Wick et al., 2011)), or bioavailability limitation of substrate (i.e., rate-limiting mass transfer into microbial cells (Best, 1955; Bosma et al., 1997)) is the bottleneck of degradation, has not yet been fully answered.

Previous studies examined the mass transfer effects at relatively high concentration levels where the culture was grown at sufficiently high substrate concentrations and then suddenly exposed to a low substrate concentration (Aeppli et al., 2009; Kampara et al., 2008). The drawback of this method is that cells do not have enough time for adapting themselves to the new conditions and this may complicate the final conclusions. To assess the degree of influence that mass transfer limitations exert at steady low concentrations, an experimental system is required to be continuously maintained at a low and environmentally-related concentration for a reasonably long time so that cells have enough time to adapt to low-energy conditions. This was obviously not possible using batch systems (Meyer et al., 2009) and it might be only accomplished by running chemostats or retentostats at extremely low dilution rates. To this end, Ehrl et al. (2017) have monitored the degradation of atrazine by strain *Arthrobacter aurescens* TC1 in a chemostat at very low dilution rates (and thus low concentration levels) and used analysis of isotope signatures to pinpoint the bioavailability limitation effects. In presence of bioavailability limitations, the slow exchange rate of isotopologues between bioavailable (cell interior) and bulk domains generates different ratios of heavy to light isotopes in these domains. The phenomenon is usually referred to as masking of isotopic signatures meaning the measured isotopic fractionation at bulk phase is notably smaller than actual, transformation-induced isotopic fractionation occurring at bioavailable phase. Carbon and nitrogen isotope fractionation of the micropollutants thus can provide a concentration-independent line of evidence on bioavailability and biodegradation of micropollutants in natural environments and improve our general understanding of their fate and transport.

At very low dilution rates, the chemostat input feed may turn discontinuous due to the extended waiting times between the incoming droplets. Therefore, the typical analyses of



chemostats which are based on the assumption of constant boundary conditions (Fritsch et al., 2015; Stratton et al., 2009) do not correctly grasp the change of isotopic ratios at the times between the input of subsequent droplets. To overcome this issue, in this study we present a chemostat/retentostat model that considers the transient conditions under the rapid changes of boundary conditions (here addressed by a periodic inlet). In addition, the classical model of chemostat was upgraded with the inclusion of the mechanisms of isotope fractionation and its analysis (Elsner et al., 2005; Elsner, 2010; Qiu et al., 2013), allowing to evaluate and interpret the change of isotopic signatures in the system. The transformation-induced isotopic signatures have so far been calculated as a function of remaining substrate in batch experiments. Since the substrate continuously enters and leaves a chemostat, the observed isotope fractionation was determined as the difference between isotopic ratios at the inlet and outlet. We also included the mechanism of mass transfer between the bulk solution monitored and the cell interior across the cells' membrane (Best, 1955) into the chemostat equations, allowing to quantify and illustrate the importance of this process. Due to high stirring speeds in chemostat the effect from other mechanisms of transport (e.g., diffusion and advection) is negligible. Therefore, a new chemostat model was developed which is able to account for the mechanisms of mass transfer and transformation-based isotopic fractionation at low dilution rates and to allow the delineation of the interactions between these processes in a traceable manner. The model has been employed to simulate the chemostat systems at low and discontinuous dilution rates with the specific application to atrazine degradation at low concentrations.

The overall aim of this contribution is thus to introduce a comprehensive modeling tool in order to quantitatively understand the interplay of the following mechanisms: (1) mass transfer limitations through the cells' membrane, (2) in-situ biodegradation, and (3) transformation-induced compound-specific isotope fractionation in chemostats/retentostats with (4) sporadic but periodic input of substrate. Here, we emphasized further on mathematical modeling of such systems and demonstrated the compelling contribution of the model to a learning-oriented assessment of the chemostat experiments.

# 2 Model Description

## 2.1 Model equations

We consider the concentrations of light and heavy isotopologues of a substrate ($^{12}S$ and $^{13}S\,[ML^{-3}]$), and the biomass concentration ($X[ML^{-3}]$) as dynamic state variables. The turnover of substrate is described by Michelis-Menten kinetics (Michaelis and Menten, 1913) with competitive inhi-

bition amongst the isotopologues, and is coupled to the input and output of substrate through the inflow and the outflow of the reactor, respectively. Biomass growth is assumed proportional to the substrate turnover via a yield factor. This leads to the following system of ordinary differential equations:

$$\frac{d[^{12}S]}{dt} = r_D([^{12}S_{in}] - [^{12}S]) - \frac{\mu_{max}[X][^{12}S]}{([^{12}S] + [^{13}S] + K_m)Y} \tag{1a}$$

$$\frac{d[^{13}S]}{dt} = r_D([^{13}S_{in}] - [^{13}S]) - \frac{\alpha\mu_{max}[X][^{13}S]}{([^{12}S] + [^{13}S] + K_m)Y} \tag{1b}$$

$$\frac{d[X]}{dt} = \mu_{max}[X]\frac{[^{12}S] + \alpha[^{13}S]}{[^{12}S] + [^{13}S] + K_m} - fr_D[X] \tag{1c}$$

where $r_D[T^{-1}]$ is the dilution rate coefficient (volumetric input divided by the reactor volume per time), $\mu_{max}[T^{-1}]$ denotes the maximum specific growth rate, $K_m[ML^{-3}]$ is the half-saturation constant, $\alpha$ indicates the isotopic fractionation factor, $Y$ is the yield coefficient, and $f$ denotes the fraction of biomass filtered at the outflow, ranging between zero (biomass leaves the system at the reactor current concentration; chemostat) and one (complete filtration of biomass thus no biomass discharges from the outlet; perfect retentostat)

The chemostat equations accounting for the mass-transfer through the cell membrane are modified such that the concentrations outside the cells ($S$) differ from the concentrations inside the cells ($S_{bio}$). $S$ and $S_{bio}$ are usually referred to as the concentrations of substrate at bulk and bioavailable phases respectively (Best, 1955; Gharasoo et al., 2015). A linear-driving force model with the mass-transfer coefficient $k_{tr}[T^{-1}]$ was assumed to control the exchange between these two phases. Including such mass-transfer limitations, Eqs. (1a) to (1c) change as follows:

$$\frac{d[^{12}S]}{dt} = r_D([^{12}S_{in}] - [^{12}S]) - k_{tr}([^{12}S] - [^{12}S_{bio}]) \tag{2a}$$

$$\frac{d[^{13}S]}{dt} = r_D([^{13}S_{in}] - [^{13}S]) - k_{tr}([^{13}S] - [^{13}S_{bio}]) \tag{2b}$$

$$\frac{d[^{12}S_{bio}]}{dt} = +k_{tr}([^{12}S] - [^{12}S_{bio}]) - \frac{\mu_{max}[X][^{12}S_{bio}]}{([^{12}S_{bio}] + [^{13}S_{bio}] + K_m)Y} \tag{2c}$$

$$\frac{d[^{13}S_{bio}]}{dt} = +k_{tr}([^{13}S] - [^{13}S_{bio}]) - \frac{\alpha\mu_{max}[X][^{13}S_{bio}]}{([^{12}S_{bio}] + [^{13}S_{bio}] + K_m)Y} \tag{2d}$$

$$\frac{d[X]}{dt} = \mu_{max}[X]\frac{[^{12}S_{bio}] + \alpha[^{13}S_{bio}]}{[^{12}S_{bio}] + [^{13}S_{bio}] + K_m} - fr_D[X] \tag{2e}$$

in which the observable isotope fractionation in the bulk phase is affected by the transformations inside the cell and the mass transfer between bulk and bioavailable phases. The initial



concentrations for the substrate and biomass are indicated by $Sini[ML^{-3}]$ and $X_{ini}[ML^{-3}]$. The isotope ratio of the heavy and the light isotopologues of the substrate is evaluated in the common $\delta^{13}C[‰]$ notation:

$$\delta^{13}C = \left(\frac{^{13}S/^{12}S}{R_C} - 1\right) \tag{3}$$

typically expressed in parts per thousand, where $R_C = 0.0112372$ is the reference isotope ratio of VPDB(Vienna Pee Dee Belemnite) between heavy and light carbon.

## 2.2 Model solution

We solved the above systems of ordinary differential equations, ODE, (Eqs. (1a) to (1c) and Eqs. (2a) to (2e)) with the MATLAB ODE suite (e.g., the ode15s solver) (Gharasoo et al., 2017; Shampine and Reichelt, 1997). To avoid unintended numerical instabilities, the input pulses were smoothed using forth-order analytical formulas. For smoothing the pulses, the user can choose the time period over which the pulse is smoothed, which may be interpreted as the mixing time in the system depending on agitation, droplet size, and reactor volume. A higher numerical stability is achieved when the smoothing intervals is larger. However, the smoothing interval should be substantially smaller than the interval between the pulses in order to avoid flattening the periodicity of the incoming droplets. The smoothing type can be chosen between the following two polynomial spike functions:

$$r_D = \frac{630t^4(t/s-1)^4}{s^5} \quad 0 < t < s, \quad r_D = 0 \quad t > s \tag{4a}$$

$$r_D = \frac{256t^4(t/s-1)^4}{s^4} \quad 0 < t < s, \quad r_D = 0 \quad t > s \tag{4b}$$

producing either a smoothed pulses with a constant area underneath (in case of Eq. 4a) or a pulse that is set to reach to a specific peak height (in case of Eq. 4b). $t[T]$ denotes the time variable which varies between zero and the time until next droplet, $s[T]$ denotes the length of the smoothing interval. Although both methodologies are available in the model, we used the first smoothing function Eq. (4a) as the latter leads to entry of more mass into the system than intended. The model parameter values were taken from Ehrl et al. (2017) for degradation of atrazine by the strain *Arthrobacter aurescens* TC1 in chemostat, and are listed in Table 1.

## 3 Results and Discussions

### 3.1 Model results

Originally, this model was build to test whether a limited diffusion of substrate across the cell membrane explains observed differences between isotope fractionation values in chemostat experiments at low dilution rates to those of batch experiments. For the specific case of Atrazine degradation by strain *Arthrobacter aurescens* TC1 in a chemostat at very low dilution rates, Ehrl et al. (2017) observed isotopic fractionation of $\epsilon^{13}C = -2.2‰$. The actual isotopic fractionation $\epsilon^{13}C$ for this particular reaction was determined as $-5.4‰$ in chemostat experiments at sufficiently high dilution rates. A similar isotope fractionation was reported for batch experiments with bacterial cultures degrading atrazine at high concentrations (Meyer et al., 2009) and in the absence of bacterial cell when performing the experiments with pure enzyme (Schürner et al., 2015).

Fig. 1 shows the concentration and isotope time-series for the case considering mass-transfer limitation across the cell membrane (solving Eqs. (2a) to (2c)). Here, low effective enrichment values of $\delta^{13}C$ were obtained in the bulk solution for low values of the mass-transfer coefficient $k_{tr}$ ranging between 0.002 and 0.007 $s^{-1}$. Using $k_{tr}$ value of $0.0025s^{-1}$ we achieved an isotopic enrichment value of $\delta^{13}C - 2.2‰$ which was observed by Ehrl et al. (2017) in their chemostat experiment at a dilution rate of $0.009hr^{-1}$. When incorporating the mass transfer limitation, the simulated concentration inside the cell $S_{bio}$ was about 40% of the concentration outside the cell $S$. Increasing the values of $k_{tr}$ boosts the exchange rate between the bulk and bioavailable phases and causes that steady late-time $\delta^{13}C$-values to basically increase up to the value of actual, transformation-induced, intrinsic isotopic fractionation coefficient $\epsilon^{13}C = -5.4‰$. Therefore, in the absence of a mass transfer term the model predicts that the carbon isotope composition inside the chemostat is enriched compared to the inflow by the exact same enrichment factor $\epsilon^{13}C$ of batch studies, independent of the dilution rate. Fig. 2 shows the simulated time series of concentrations and $\delta$-values for this case (solution of Eqs. (1a) to (1c)) where the concentration inside the cells is equal to the concentration at bulk solution. As shown, the obtained $\delta^{13}C$ values at steady-state are higher than Fig. 1 and eventually reach the actual fractionation coefficient reported from the batch experiments ($\delta^{13}C = 5.4‰$). Fig. 3 displays the same data as Fig. 2 over a short time period when dynamic steady state has been reached. Under these dynamic steady-state conditions the periodic input of droplets causes constant concentration fluctuations.



### 3.2 Sensitivity and uncertainty analyses

#### 3.2.1 Uncertainty propagation analyses

A crude Monte Carlo simulation was used to delineate the propagation of error originating from experimental and analytical variability of the parameters $k_{tr}$, $K_m$, $\mu_{max}$, and $S_{in}$ onto concentrations and isotopic signatures. In order to reduce the total runtime of the Monte Carlo simulations, we reduced the walltime needed for simulating a single scenario to 7.5 seconds on a quad-cores Intel Core i5-4590 CPU at 3.30GHz with 16GB RAM by optimizing the code and performing parallel computations.

Eqs. (2a) to (2c) were solved for 50,000 randomly generated sets of parameters, which took about 105 hours walltime. In each realization, the parameters of Eqs. (2a) to (2c) were perturbed at random, scaled to the experimentally-obtained standard error. Mean values and standard deviations were calculated from repeated replicates ($237 \pm 57 \mu g/l$ for $K_m$, $0.11 \pm 0.02 hr^{-1}$ for $\mu_{max}$, and $30000 \pm 600 \mu g/l$ for $S_{in}$). In case of $k_{tr}$, since the value is not experimentally determined, a relative standard error of 20% was presumed ($0.0025 \pm 0.0005 s^{-1}$). All parameters were drawn from normal distributions and no correlation was assumed between the input parameters.

The Monte Carlo simulations showed probability distributions of the model outputs ($\delta^{13}C$, ${}^{12}S$, ${}^{13}S$, ${}^{12}S_{bio}$, ${}^{13}S_{bio}$, and $X$) as the result of the input parameters variabilities. Fig. 4 shows the 16%-84% probability range of model outcomes which corresponds to $\pm 1$ standard deviation of a normal distribution. Table 2 lists the average and standard deviation of all model predictions at late time. There is a small offset between the mean output of the ensemble calculation and a single run using the mean input parameters values which can be attributed to the nonlinear dependence of model outputs on the parameters. Fig. 4 shows that the parameter uncertainty translates into a large uncertainty of model predictions, with coefficients of variation (that is, relative standard deviations) between 20% and 33% for solute concentrations and $\delta$-values. Only the biomass ($X$) was clearly the less affected by the parameter uncertainty.

The 95% confidence interval of $\delta^{13}C \approx 2.17 \pm 0.92‰$ does not cover the value of $\delta^{13}C = 5.4‰$ expected from the the fractionation coefficient of the reaction (Meyer et al., 2009; Schürner et al., 2015). This clearly illustrates that limitations of mass transfer across the cell membrane masks isotope fractionation in chemostats at low dilution rates. As a result, the observed isotopic signatures ($\delta^{13}C$) are noticeably lower than the expected transformation-induced isotopic signatures. Sources of uncertainty exist that are not addressed by the Monte Carlo simulations, for example, the error measurement of dilution rate or the uncertainties associated with the size

of droplets. The propagation of error due to these factors is assumed to be insignificant and is partly lumped into the uncertainty of the inlet concentration ($S_{in}$).

#### 3.2.2 Local sensitivity analysis

A tornado diagrams is used here to depict the local sensitivity of the simulated $\delta^{13}C$-value at steady state with respect to the changes in the input parameters: $k_{tr}$, $K_m$, $\mu_{max}$, $S_{in}$, and the time between droplets $1/r_D$. To compare the relative importance of the above input parameters, we varied the value of one input parameter at a time by 20% while keeping all the other input parameters at their base values. As expected, the results (Fig. 5) show a strong sensitivity towards the mass-transfer coefficient $k_{tr}$ in the chemostat model accounting for mass-transfer limitations Eqs. (2a) to (2e). The modeled isotope signal shows a similar but weaker sensitivity to $S_{in}$ and $K_m$ whereas variations of $\mu_{max}$ and $1/r_D$ inversely influence the values of $\delta^{13}C$ noting the absolute sensitivity to $\mu_{max}$ is on par with that to $k_{tr}$. The results clearly indicate that the impact of physiological parameters ($K_m$ and $\mu_{max}$) are as significant as that of a physically motivated parameter ($k_{tr}$).

A similar sensitivity analysis was performed with the model neglecting mass-transfer limitations, Eqs. (1a) to (1c). Unlike the previous model, the simulated late-time $\delta^{13}C$-values showed no sensitivity to the changes of the input parameters $K_m$, $\mu_{max}$, $S_{in}$ and $1/r_D$ (data not shown). This implies that in presence of mass transfer limitations, the sensitivity of the observed $\delta^{13}C$-values even to other input parameters (e.g., $K_m$ an $\mu_{max}$) is due to the existence of mass-transfer coefficient $k_{tr}$.

#### 3.2.3 Global sensitivity analysis

We used the variance-based analysis of Sobol (Sobol, 2001) for global sensitivity analysis (GSA). The benefit of a global over local sensitivity analysis is that it accounts for the entire range of all parameter values rather than focusing on one parameter value at a time. As such, GSA offers a more robust solution in elucidating the impact of an individual parameter in the context of considering all other parameters are also uncertain. To this end, a quasi Monte Carlo method (here, a Latin hypercube sequencing sampler) was employed to generate 60,000 sample scenarios that uniformly covered the space of input parameters. The First-order index ($S_i$) and the Total-order index ($ST_i$) were then calculated similar to Pianosi et al. (2015) and Sobol and Levitan (1999). $S_i$ indicates the effect of an individual parameter variation alone on an output variable while $ST_i$ includes also the effects caused by the interactions of that parameter with all other



parameters.

The pie charts in Fig. 6 demonstrate the sensitivity of output variables: $\delta^{13}C$-values, Biomass ($X$), bioavailable ($S_{bio}$) and bulk concentrations ($S$) to the input parameters $S_{in}$, $\mu_{max}$, $K_m$, and $k_{tr}$. The GSA confirms the relatively equal sensitivity of the $\delta^{13}C$-values to $K_m$, $\mu_{max}$ and $k_{tr}$ as previously estimated from the local sensitivity analysis (Fig. 5). Bulk concentration showed a relatively high sensitivity of about 50% to the $k_{tr}$ values which is in the range of the combined sensitivity to all other input parameters. Amongst the model predictions, bulk concentrations are affected the most by mass transfer followed by $\delta^{13}C$-values at the second place. To our surprise, the bioavailable concentrations showed no sensitivity to mass transfer effects. The variation of $K_m$ showed a predominant effect on the variation of all predicted quantities except biomass. In fact, biomass showed no sensitivity to variation of any of the input parameters. This might be due to the reason that in all scenarios the biomass concentration hardly changed over time (see Fig. 4).

The $ST_i$ pie charts provide a measure on the importance of interactions (of any order) between the input parameters. As shown in Table 3, the total order indices $ST_i$ and the first-order indices $S_i$ were almost identical, indicating that the interactions between parameters did not impose any significant effect on variability of the model predictions except for biomass ($X$). We extended our GSA for another 60,000 sample scenarios to the total amount of 120,000 scenarios to check the consistency of the results and to see whether the sensitivity indices can be improved. Similar indices as Table 3 were calculated for all the model outputs except for the biomass (data not shown). This inconsistency which might originate from the insignificant change of biomass over time, indicates that the biomass sensitivity indices may not be entrusted.

### 3.3 Temporal dynamics of biomass growth

The model accounts for the temporal dynamics of biomass growth and washout in the chemostat system Eqs. (1c) and (2e). We assumed standard Monod kinetics (Monod, 1949) in which biomass growth is proportional to turnover rate. Growth depends only on the concentration of a single substrate, indicating that all other compounds required for growth are available in excess. The only removal term is described by washout via outflow. This is a reasonable assumption for a chemostat system, in which the loss due to washout is greater than the biomass death rate. Maintenance terms are also not considered as under quasi steady-state conditions, the energy demand for maintenance is constant and its effect is subsumed in the yield factor. Furthermore,

we did not consider a prescribed carrying capacity, or maximum biomass concentration, since the simulated biomass concentration remained fairly low as a result of limited supply of substrate and continuous washout of cells.

### 3.4 Comparison with the analytical model of Thullner et al. (2008)

We compared our model to the analytical model of Thullner et al. (2008) which estimates the observed isotopic fractionation factor $\alpha$ under steady-state conditions in relation to intrinsic isotropic fractionation of the enzymatic reaction $\mathring{\alpha}$,

$$\alpha = \mathring{\alpha}\frac{1 + T/2 - \sqrt{a/k_{tr} + T^2/4}}{1 + \mathring{\alpha}\left[T/2 + \sqrt{a/k_{tr} + T^2/4}\right]} \tag{5}$$

where $T = (a/k_{tr} - S/K_m - 1)$ is a dimensionless term and $a = \mu_{max}/K_m$ is the specific affinity of the microorganism promoting the enzymatic reaction. For an arbitrary case of $k_{tr} = 0.002s^{-1}$, $K_m = 50\mu g/l$, $\mu_{max} = 0.027hr^{-1}$, $Y = 0.036$, $S_{ini} = 65\mu g/l$, $X_{ini} = 1000\mu g/l$, $\mathring{\alpha} = 0.994$ and $r_D = 2.5e-6s^{-1}$, the observed $\delta^{13}C$ at steady-state was calculated by our model about 2.64‰. Using Eq. (5), the apparent fractionation factor $\alpha$ was calculated as 0.9973 which yields the observed $\delta^{13}C = 2.62$‰. This means that the two models estimated similar observed vs. expected isotopic signatures. It is worth noting that unlike the analytical model (Thullner et al., 2008), the presented numerical model can determine the observed isotopic signatures also under transient conditions.

### 3.5 Implications for natural systems and applications

Our results confirm that slow mass transfer across the cell membrane can mask the true isotope fractionation of a chemical transformation. So far the differences between observed isotopic signatures from laboratory and field were attributed to other factors for example, leakage from other contaminant sources or hydrologically driven mechanisms (e.g., by transverse dispersion at plume fringes Rolle et al., 2010). As shown here, such differences can stem from the bioavailability limitations and caused particularly by mass-transfer limitation across the cells' membrane. The effect from bioavailability limitations is much more pronounced at low concentrations, and therefore is of high relevance for many micro-pollutants of which concentrations typically do not exceed microgram-per-liter. Recognition and understanding of the interplay of bioavailability limitations with other existing processes thus enhance the overall interpretation of isotope signals under field conditions.



Under the influence of other processes the isotopic signatures show no dependency to the enzymatic reaction rates. Thus., one way to distinguish the masking of isotope signatures as the result of mass-transfer through the cell membrane is to focus on the fact that in the presence of bioavailability limitations the isotopic signatures highly differ in response to the enzymatic transformation rates (see the sensitivity of $\delta^{13}C$ to $\mu_{max}$ in presence of $k_{tr}$). Therefore, two strains with different metabolic activities when feeding on a single substrate must exhibit different isotopic signatures under bioavailability limitations, assuming both have an identical isotopic fractionation factor and similar cell membrane characteristics.

### 3.6 Potentials of the presented modeling approach

The presented model improves the mechanistic understanding of contaminant degradation in microbial ecosystems. While the model in its current form is only applied to fully mixed reactors, it can be easily coupled to solute transport equations (Cirpka et al., 1999; Gharasoo et al., 2012) contributing to the development of models that more realistically describe fixed-bed reactors and natural subsurface systems.

A specific practical aspect of our model is its capacity to calculate the membrane permeability of a specific cell in conjugation with chemostat/batch experiments. The differences between the observed isotopic signatures ($\delta^{13}C$) in batch and chemostat experiments are linked to mass-transfer limitations through the cell membrane which is widely referred to as membrane permeability. The formulation on how to obtain the value of membrane permeability $P_{app}[cm.s^{-1}]$ and the diffusion coefficient through the membrane $D_{mem}[m^2.s^{-1}]$ from the mass-transfer limiting coefficient $k_{tr}[s^{-1}]$ is presented and discussed by Ehrl et al. (2017). According to the model results, Atrazine permeation through the cell wall of *Arth. aurescens* TC1 was approximated as $P_{app} = 3.5 \times 10^{-5} ms^{-1}$ and $D_{mem} = 1.9 \times 10^{-16} m^2 s^{-1}$, which are close to the values reported for a typical range of small organic molecules (Males and Herring, 1999; Miyamoto et al., 1986; van Meer et al., 2008). While different techniques are used in pharmaceutical studies to determine the membrane permeability, the present model provides an alternative way of calculating it.

Sensitivity analysis of the model enables users inspecting the influence of different physical and physiological parameters on the observable isotopic signature before performing the experiments. The results provide clarity into the specific features influencing isotopic signatures in chemo- and retentostats. The modeling framework used in this study allows for a delineation of features such as: (i) biodegradation dynamics of a contaminant, (ii) metabolic activity of the microbial degrader, (iii) the role of bioavailability limitations and typical mass-transfer restric-

tions through the cell's membrane, and (iv) whether the interplay between these mechanisms is responsible for observing uncommon isotopic signatures at low concentration levels. As shown above, these results have relevant implications for both theory building and practical application.

### 3.7 Model accuracy and stability

The model accuracy is confirmed by comparing the results with the experiment (Ehrl et al., 2017) and the analytical model of Thullner et al. (2008) (Section 3.4). Extra processes can still be introduced within the existing potentials of the model, for instance, introducing other degradation mechanisms (e.g., first order reaction) instead of Michaelis-Menten kinetics. Use of MATLAB ODE suite as the internal solver increased model stability on handling relatively stiff problems. However, it should be noted that the model can still turn out numerically unstable if the smoothing interval of droplet is not sufficiently large in respect to the periodic time between droplets. As a rule of thumb, the smoothing interval should be around 15% of the period between droplets, that is, the time between each input cycle.

## Acknowledgments

This research has received funding from the European Research Council (ERC) under the European Union's Seventh Framework Programme (FP7/2014-2019) / ERC Grant Agreement No. 192411 (MICRODEGRADE).

## References

Daughton, C. G. and Ternes, T. A. Pharmaceuticals and personal care products in the environment: agents of subtle change? *Environmental Health Perspectives*, 107(Suppl 6):907–938, 1999.

Wick, A., Wagner, M., and Ternes, T. A. Elucidation of the transformation pathway of the opium alkaloid codeine in biological wastewater treatment. *Environ Sci Technol*, 45(8):3374–3385, 2011.

Best, J. The inference of intracellular enzymatic properties from kinetic data obtained on living cells: some kinetic considerations regarding an enzyme enclosed by a diffusion barrier. *J Cell Comp Physiol*, 46:1–27, 1955.

Bosma, T. N. P., Middeldorp, P. J. M., Schraa, G., , and Zehnder, A. J. B. Mass transfer limitation of biotransformation: Quantifying bioavailability. *Environ Sci Technol*, 31(1):248–252, 1997.

Aeppli, C., Berg, M., Cirpka, O. A., Holliger, C., Schwarzenbach, R. P., and Hofstetter, T. B. Influence of mass-transfer limitations on carbon isotope fractionation during microbial dechlorination of trichloroethene. *Environ Sci Technol*, 43 (23):8813–8820, 2009.

Kampara, M., Thullner, M., Richnow, H. H., Harms, H., and Wick, L. Y. Impact of bioavailability restrictions on microbially induced stable isotope fractionation. 2. experimental evidence. *Environ Sci Technol*, 42(17):6552–6558, 2008.

Meyer, A. H., Penning, H., and Elsner, M. C and N isotope fractionation suggests similar mechanisms of microbial Atrazine transformation despite involvement of different enzymes (AtzA and TrzN). *Environ Sci Technol*, 43(21):8079–8085, 2009.

Ehrl, B. N., Kundu, K., Marozava, S., Gharasoo, M., and Elsner, M. Isotope fractionation reveals rate-limiting cell wall permeation of atrazine when degraded by Arthrobacter aurescens TC1 at low concentrations. *Nature Geoscience*, (Submitted), 2017.

Fritsch, C., Harmand, J., and Campillo, F. A modeling approach of the chemostat. *Ecol. Model.*, 299:1–13, 2015.



Stratton, T. R., García, R. E., Applegate, B. M., and Youngblood, J. P. Application of a high throughput bioluminescence-based method and mathematical model for the quantitative comparison of polymer microbicide efficiency. *Biomacromolecules*, 10(5):1173–1180, 2009.

Elsner, M., Zwank, L., Hunkeler, D., and Schwarzenbach, R. P. A new concept linking observable stable isotope fractionation to transformation pathways of organic pollutants. *Environ Sci Technol*, 39(18):6896–6916, 2005.

Elsner, M. Stable isotope fractionation to investigate natural transformation mechanisms of organic contaminants: principles, prospects and limitations. *J Environ Monit*, 12:2005–2031, 2010.

Qiu, S., Eckert, D., Cirpka, O. A., Huenniger, M., Knappett, P., Maloszewski, P., Meckenstock, R. U., Griebler, C., and Elsner, M. Direct experimental evidence of non-first order degradation kinetics and sorption-induced isotopic fractionation in a mesoscale aquifer: 13C/12C analysis of a transient toluene pulse. *Environ Sci Technol*, 47(13):6892–6899, 2013.

Michaelis, L. and Menten, M. Die kinetik der invertinwirkung. *Biochem Z*, 49:333–369, 1913.

Gharasoo, M., Centler, F., Van Cappellen, P., Wick, L. Y., and Thullner, M. Kinetics of substrate biodegradation under the cumulative effects of bioavailability and self-inhibition. *Environ Sci Technol*, 49(9):5529–5537, 2015.

Gharasoo, M., Thullner, M., and Elsner, M. Introduction of a new platform for parameter estimation of kinetically complex environmental systems. *Environ Model Softw*, 98:12–20, 2017.

Shampine, L. F. and Reichelt, M. W. The matlab ode suite. *SIAM J Sci Comput*, 18:1–22, 1997.

Schürner, H. K. V., Seffernick, J. L., Grzybkowska, A., Dybala-Defratyka, A., Wackett, L. P., and Elsner, M. Characteristic isotope fractionation patterns in s-Triazine Degradation Have Their Origin in Multiple Protonation Options in the s-Triazine Hydrolase TrzN. *Environ Sci Technol*, 49(6):3490–3498, 2015.

Sobol, I. Global sensitivity indices for nonlinear mathematical models and their Monte Carlo estimates. *Math Comput Simul*, 55(1):271–280, 2001.

Pianosi, F., Sarrazin, F., and Wagener, T. A matlab toolbox for global sensitivity analysis. *Environ Model Softw*, 70:80–85, 2015.

Sobol, I. and Levitan, Y. On the use of variance reducing multipliers in monte carlo computations of a global sensitivity index. *Computer Physics Communications*, 117(1):52–61, 1999.

Monod, J. The growth of bacterial cultures. *Annu Rev Microbiol*, 3(1):371–394, 1949.

Thullner, M., Kampara, M., Richnow, H. H., Harms, H., and Wick, L. Y. Impact of bioavailability restrictions on microbially induced stable isotope fractionation. 1. theoretical calculation. *Environ Sci Technol*, 42(17):6544–6551, 2008.

Rolle, M., Chiogna, G., Bauer, R., Griebler, C., and Grathwohl, P. Isotopic fractionation by transverse dispersion: Flow-through microcosms and reactive transport modeling study. *Environ Sci Technol*, 44(16):6167–6173, 2010.

Cirpka, O. A., Frind, E. O., and Helmig, R. Numerical methods for reactive transport on rectangular and streamline-oriented grids. *Adv Water Resour*, 22(7):711–728, 1999.

Gharasoo, M., Centler, F., Regnier, P., Harms, H., and Thullner, M. A reactive transport modeling approach to simulate biogeochemical processes in pore structures with pore-scale heterogeneities. *Environ Model Softw*, 30:102–114, 2012.

Males, R. and Herring, F. A 1H-NMR study of the permeation of glycolic acid through phospholipid membranes. *Biochimica et Biophysica Acta (BBA) - Biomembranes*, 1416(1–2):333 – 338, 1999.

Miyamoto, Y., Yuasa, H., Iga, T., and Hanano, M. Determination of the membrane permeability coefficient and the reflection coefficient by the two-dimensional laminar flow model for intestinal perfusion experiments. *Biochim. Biophys. Acta, Biomembr.*, 854(2):191–197, 1986. ISSN 0005-2736.

van Meer, G., Voelker, D., and Feigenson, G. Membrane lipids: where they are and how they behave. *Nat Rev Mol Cell Biol*, 9(2):112–124, 2008.

## Tables

| | |
|---|---|
| Volume of reactor ($V$) | $2000ml$ |
| Dilution rate ($r_D$) | $0.009hr^{-1}$ |
| Average droplet size ($V_d$) | $0.1ml$ |
| Average time between droplets ($t_d$) | $20s$ |
| Atrazine concentration at the inlet ($S_{in}$) | $30000\mu g/l$ |
| Maximum specific growth rate ($\mu_{max}$) | $0.11hr^{-1}$ |
| Half-saturation constant ($K_m$) | $237\mu g/l$ |
| Yield factor ($Y$) | 0.018 |
| Isotopic fractionation factor ($\alpha$) | 0.9946 |
| Initial atrazine concentration in reactor ($S_{ini}$) | $65\mu g/l$ |
| Initial concentration of biomass in reactor ($X_{ini}$) | $550\mu g/l$ |

Table 1: Model solution. Model parameter values taken from Ehrl et al. (2017).

| | $\delta^{13}C$ ‰ | $^{12}S(\mu g/l)$ | $^{13}S(\mu g/l)$ | $^{12}S_{bio}(\mu g/l)$ | $^{13}S_{bio}(\mu g/l)$ | $X(\mu g/l)$ |
|---|---|---|---|---|---|---|
| Model run with mean input parameters | 2.21 | 50.72 | 0.57 | 20.75 | 0.23 | 549.82 |
| Monte Carlo simulations | 2.17±0.47 | 52.89±10.25 | 0.59±0.12 | 21.60±7.18 | 0.24±0.08 | 549.77±0.31 |

Table 2: Uncertainty analysis. The estimated average and standard error of output parameters calculated from Monte Carlo analyses of 50000 randomly generated sample scenarios based on the error variability of input parameters ($K_m = 237 \pm 57\mu g/l$, $\mu_{max} = 0.11 \pm 0.02hr^{-1}$, $S_{in} = 30000 \pm 600\mu g/l$, and $k_{tr} = 0.0025 \pm 0.0005s^{-1}$).

| | $S_i$ | | | | $ST_i$ | | | |
|---|---|---|---|---|---|---|---|---|
| | $\delta^{13}C$ | $X$ | $S_{bio}$ | $S$ | $\delta^{13}C$ | $X$ | $S_{bio}$ | $S$ |
| $S_{in}$ | .0014 | 0 | .0152 | .0377 | 0 | .01119 | .0049 | .0165 |
| $\mu_{max}$ | .2706 | 0 | .4153 | .2663 | .2658 | .2217 | .4108 | .2559 |
| $K_m$ | .4010 | 0 | .5737 | .3584 | .4052 | .3194 | .5914 | .3690 |
| $k_{tr}$ | .3294 | 0 | .0114 | .5780 | .3276 | .1208 | 0 | .5531 |

Table 3: Global sensitivity analysis. The First-order index ($S_i$) and the Total-order index ($ST_i$) of the output parameters ($\delta^{13}C$-values, $X$, $S_{bio}$, and $S$) in respect to the input parameters ($S_{in}$, $\mu_{max}$, $K_m$, and $k_{tr}$). The higher the value, the more impact the input variability exerts on the variance of the output parameter. Note that both heavy and light isotopologues showed a similar sensitivity trend in bulk and bioavailable phases.

## Figures



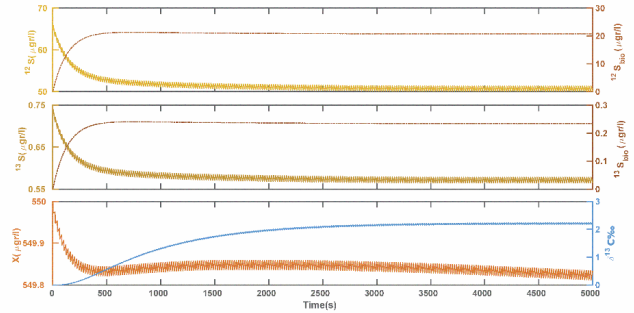


Figure 1: Solution of Eqs. (2a) to (2c) (in the presence of mass-transfer limitations across the cell membrane) for the set of parameter values in Fig. 2 and $k_{tr} = 0.0025s^{-1}$. Note that due to mass-transfer limitations the observed $\delta^{13}C = 2.2‰$ at steady-state notably reduced from 5.4‰ in Fig. 2. It is worth mentioning that inside cells (i.e., at the bioavailable domain) the $\delta^{13}C$ is equal to the expected value of 5.4‰ (data not shown).

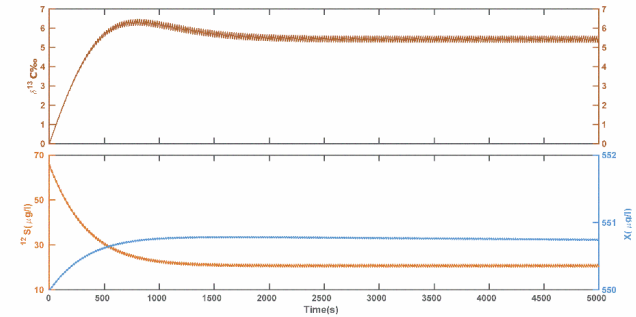


Figure 2: Solution of Eqs. (1a) to (1c) (in the absence of mass-transfer limitations across the cell membrane) for the following set of parameters: $S_{in} = 30000\mu g/l$, $\mu_{max} = 0.11hr^{-1}$, $K_m = 237\mu g/l$, $Y = 0.018$, $\alpha = 0.9946$, $S_{ini} = 65\mu g/l$, $X_{ini} = 550\mu g/l$, and $r_D = 0.009hr^{-1}$. For better illustration of the droplet spikes, the dilution rates together with the changes of concentration, biomass, and $\delta^{13}C$ at steady-state are shown over a short time span (100s) in Fig. 3.

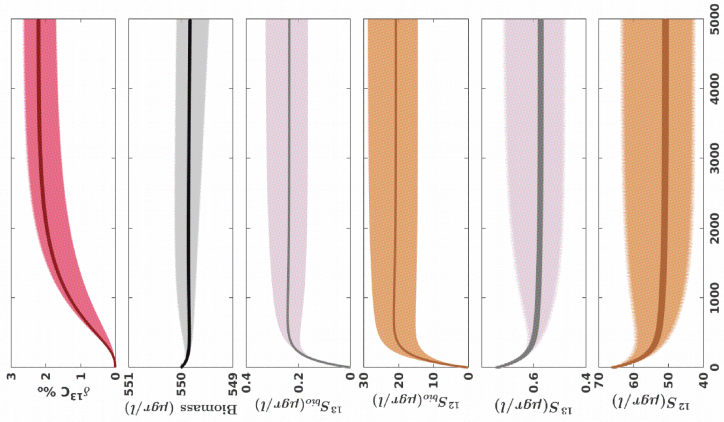


Figure 4: Uncertainty analysis using Monte Carlo simulation. The 68% confidence intervals are shown for all the output parameters, from top to bottom, isotopic signature, biomass concentration, bioavailable and bulk substrate concentrations (for both heavy and light isotopologues respectively). Note that the perturbations resulting from the periodic inlet are more visible at the profiles for bulk concentrations and $\delta^{13}C$-values.





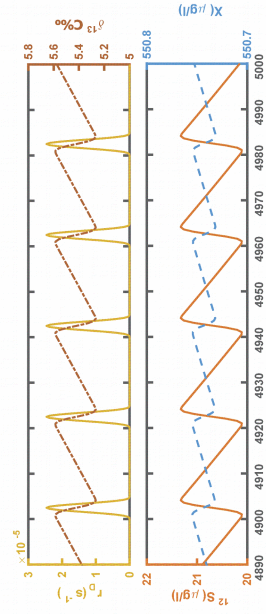


Figure 3: Solution of Eqs. (1a) to (1c) at steady-state. The figure is a close-up snapshot of the last 100 seconds in Fig. 2 at which the system has reached steady-state. Based on size of droplet ($0.1ml$), volume of chemostat ($2l$), and the dilution rate ($r_D = 0.009hr^{-1}$) the droplet frequency is calculated as one drop per every 20 seconds. The smoothing interval is assumed 5 seconds. For this setup, the results at steady-state are averaged as $\delta^{13}C = 5.4‰$, $^{12}S = 20.66\mu g/l$, $X = 550.74\mu g/l$.

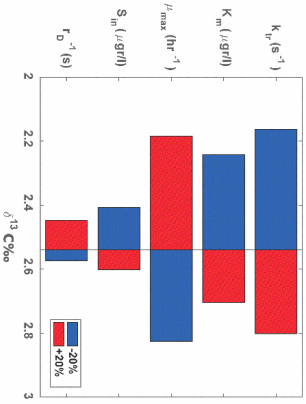


Figure 5: Local sensitivity analysis. Tornado plot showing the sensitivity of the observed $\delta^{13}C$ values to the input variables $k_{tr}$, $K_m$, $\mu_{max}$, $S_{in}$, and the inlet periodic time $(1/\tau_D)$ when mass-transfer limitations across the cell membrane are present Eqs. (2a) to (2e).



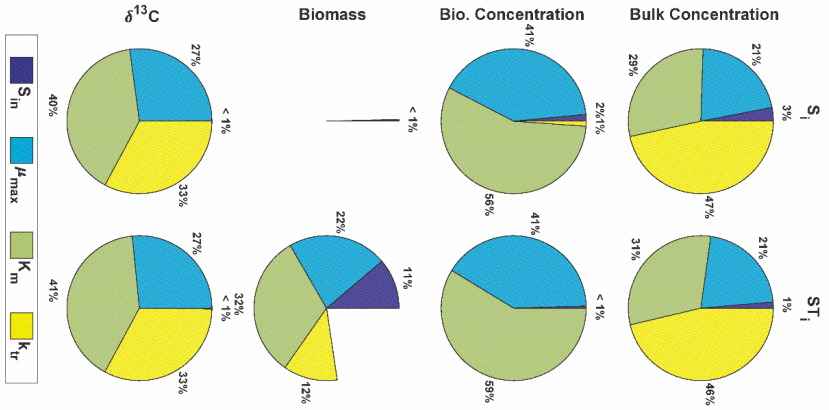


Figure 6: Global sensitivity analysis. The pie charts show the contributions of variability in the parameters $k_{tr}$, $K_m$, $\mu_{max}$, and $S_{in}$ to the steady-state $\delta^{13}C$-values, $X$, $S_{bio}$, and $S$ (Table 3) for the case of considering mass-transfer limitations across the cell membrane Eqs. (2a) to (2e).

# Appendix B: Maintenance demand and physiology of *Arthrobacter aurescens* TC1 define a threshold of atrazine degradation

Kankana Kundu, Sviatlana Marozava, Benno N. Ehrl, Juliane Merl-Pham,

and Martin Elsner

in preparation for submission to *PLOS Biology*;

Maintenance demand and physiology of *Arthrobacter aurescens* TC1 define a threshold of atrazine degradation

Kankana Kundu[a], Sviatlana Marozova[a], Benno Ehrl[a], Juliane Merl-Pham[b], Martin Elsner[a,c]

[a] *Institute of Groundwater Ecology, Helmholtz Zentrum München, Ingolstädter Landstraße 1, 85764 Neuherberg, Bavaria, Germany*

[b] *Core facility Proteomics, Helmholtz Zentrum München, Ingolstädter Landstraße 1, 85764 Neuherberg, Bavaria, Germany*

[c] *Chair of Analytical Chemistry and Water Chemistry, Technical University of Munich, Marchioninistrasse 17, D-81377 Munich, Germany*

## Abstract

Exploring adaptive strategies by which microorganisms function and survive in low-energy natural environments remains a grand goal of microbiology, and may help address a prime challenge of the 21st century: the removal of man-made chemicals at low concentrations ("micropollutants") from the environment. Here the physiological adaptation and maintenance energy requirements of a pesticide-degrading microorganism were for the first time explored with a biomass turn-over on timescales of hours to months under conditions of bioavailability limitation as demonstrated by compound specific isotope fractionation analysis. *Arthrobacter aurescens* TC1 was grown in chemostats and retentostats mimicking environmentally relevant concentration of atrazine, a highly persistent contaminant. Along with kinetic modeling evoking bacterial adaptation under extreme energy limitation by two fold minimization of maintenance energy requirement, proteomics revealed low protein turn-over and low metabolic efficiency as the main factor for this minimization. Under extreme energy limitation at 12±3 μg $L^{-1}$ a low isotope fractionation $\varepsilon^{13}C = -0.45‰ \pm 0.36‰$ indicates abundance of atrazine degradation enzymes is not limiting. This suggests that the channeling of the energy flux to respective substrate degradative enzyme production while slowing other parts of metabolisms is an effective adaptive strategy for survival. Energy supply to sustain maintenance of the viability of cells imposes a physiological threshold of degradation below 10 μg $L^{-1}$ and proton motive force sets an ultimate threshold for cell survival and degradation-like functioning.

**Keywords:**
Arthrobacter, Chemostat, Retentostat, Kinetics, maintenance, physiology

## 1. Introduction

Adaptive strategies of bacteria to cope with extremely low energy input are of utmost importance to understand life on earth and in extreme environments [1], yet remain an underexplored field of microbiology and environmental biotechnology. Of particular relevance is the degradation of man-made chemical contaminants such as pesticides and pharmaceuticals in the environment [2], [3]. An increasing number of anthropogenic chemicals are detected in ground- and surface water in concentrations that are low, but still exceed typical drinking water thresholds (0.1 µg $L^{-1}$). A telling example is atrazine – although competent degraders have been isolated [4], and even though use of atrazine was banned in Germany almost 30 years ago, it is still the most frequently detected herbicide in German groundwater [5]. Finding out why a compound that is in principle biodegradable appears to be persistent at low concentrations ($\mu$g $L^{-1}$) has become a hitherto elusive goal for microbiologists and environmental engineers. Typical regulatory tests, and most laboratory-based degradation tests have been performed at higher concentrations (mg $L^{-1}$) [6] and agricultural studies typically investigate pulses that create "feast and famine conditions" [7]. In groundwater, in contrast, microorganisms face continuous exposure to concentrations (e.g., atrazine over 0.5 $\mu$g $L^{-1}$) that are of similar magnitude as average concentrations of dissolved free organic carbon, or amino acids (10 and 1 $\mu$g $L^{-1}$, respectively) [8]. To develop management strategies fostering natural attenuation of these compounds, it is, therefore, indispensable to explore thresholds of biodegradation, and to understand the underlying drivers behind them.

Two particular drivers are debated to lie at the heart of such thresholds of degradation. Competing paradigms claim that either (i) mass transfer (bioavailability, uptake into microbial cells) puts a limit to otherwise rapid enzymatic transformation [9]; or that (ii) physiological adaptation is responsible meaning that microorganisms switch to maintenance mode and down-regulate their enzymes when - below a threshold concentration - extensive degradation and growth appears to be no longer energetically



favorable. In our previous experiment, we cultivated *Arthrobacter aurescens* TC1 in chemostat system where substrate-containing medium is continuously added and liquid with residual substrate removed so that growth compensates for the bacteria that are washed out. With the advantage of the emerging analytical opportunity of compound-specific isotope fractionation we observed that bioavailability (mass transfer via cell membrane) became limiting at substrate concentrations in solution as high as 30 $\mu$g $L^{-1}$marking the onset of bacterial adaptation (Ehrl et al., in communication). Seminal work by Egli and others [10]–[12], has observed residual concentrations in about the same range of 30-100 $\mu$g $L^{-1}$ in degradation of organic compounds in chemostat experiments. However, this concentration is still ~3-10 times higher than typical concentrations in groundwater and 300 times higher than common drinking water thresholds (100 ng $L^{-1}$). If these were true thresholds concentrations, it would be virtually impossible for living microorganisms to maintain themselves in the aquatic environment contrasting with the observation of significant amounts of bacteria in groundwater ($\simeq 10^5$ $mL^{-1}$). Hence, microorganisms must be able to both metabolize and gain energy for maintaining basic cell functions even at lower carbon concentrations [8]. This calls for exploring the other end member – the threshold imposed by the physiology of bacterial adaptation – and observing concomitant physiological adaptation by further lowering concentrations.

The physiological threshold is defined by the maintenance energy, i.e., the energy requirement to maintain cell's viability: sustaining the proton motive force, osmoregulation, degradation of macromolecules, protein, and RNA repair, etc. Interestingly, reported values of the maintenance energy requirements in chemostat vary by a factor of 10 or more [13]. Besides, chemostat-based data – which is obtained in situations of microbial growth – is *per se* "ill-suited" to describe environmentally relevant no-growth conditions. On the one hand, the high energy fluxes associated with high growth conditions may cause cells to deliberately spill energy by leakage of ions/protons through the cell membrane or by excess motility, rather than supporting actual basic functions [14]. All this "wasted" energy is artificially accounted for as maintenance energy, because it does not contribute to growth, even though it clearly does not represent a true minimum energy requirement of cells. On the other hand, it is debated that synthesis of

alternative proteins may be switched on at low growth so that the apparent maintenance coefficient might even increase under no-growth conditions [15].

A more adequate way to investigate maintenance energy under virtual no-growth conditions are, therefore, retentostat (or recycling reactor) experiments. Here, biomass is retained, whereas substrate is still continuously added and removed (although at very low rates) so that organic substrate transformation can be studied at extremely low growth rates and substrate conversion. Retentostat experiments, therefore, represent a physiological state of the microorganisms close to the natural environment and hold potential to highlight the maintenance demand and threshold of degradation. Retentostat cultivation has a long tradition, and has recently experienced a revival in biotechnological research, because it gives rise to a "twilight" between growth and stationary phase which was found to bring about interesting properties for secondary metabolite production [16]. In environmental research, in contrast, the number of retentostat studies is limited, only few have been conducted with environmentally relevant organisms, and none of them with chemical substrates representative of typical pollutants [17], [18]. Rather, retentostat studies focused on substrates like glucose and lactose, which are very different from organic pollutants- require dedicated transporters, follow fast degradation kinetics and on top, are synthesized endogenously. Hence, these studies cannot mimic degradation of organic micropollutants in the aquatic environment.

Our contribution aims to break ground at this frontier. Chemostat and retentostat experiments were conducted with the relevant organism *Arthrobacter aurescence* TC1 grown on the notorious organic micropollutant atrazine. The particular relevance of the investigated concentration range is stressed by our recent work (Ehrl et al.), which discovered a sudden onset of mass transfer-limitations between 60 µg $L^{-1}$ and 30 µg $L^{-1}$ atrazine, and which obtained first indications that this limiting mass transfer was a trigger for bacterial adaptation. Here, we follow up on this hot lead, explore the nature of this bacterial adaptation when further decreasing concentrations in chemostat and retentostat, and determine the maintenance energy as low-concentration endpoint of atrazine degradation imposed by physiology. The nature of physiological adaptation of bacteria was investigated by flow cytometry, and by comparative proteomics with



retentostat at near-zero growth rate as the end-member of low energy availability. On top, we also measured isotope fractionation of residual atrazine in retentostat to highlight the degradative enzyme regulation at proteome level.

## 2. Materials and methods

### *2.1. Strain, growth condition and media*

The soil bacterium *Arthrobacter aurescens* TC1 [19], was grown on mineral salt medium (MS) supplemented with 30 mg $L^{-1}$ atrazine (Cfm Oskar Tropitzsch, Germany) as a sole source of energy (both as C and N). The media was prepared in MilliQ® water with a low total organic carbon content <10 $\mu$g $L^{-1}$. All salts were prepared in a 100-1000X concentrated solution and diluted with water to have a final concentration of $KH_2PO_4$ (1.36 g $L^{-1}$), $Na_2HPO_4.H_2O$ (1.78 g $L^{-1}$), $MgSO_4.7H_2O$ (0.05 g $L^{-1}$), $CaCl_2$ (0.01 g $L^{-1}$), $H_3BO_4$ (2.86 mg $L^{-1}$), $MnSO_4.4H_2O$ (1.54 mg $L^{-1}$), $CuSO_4.5H_2O$ (0.04 mg $L^{-1}$), $ZnCl_2$ (0.021 mg $L^{-1}$), $CoCl_2.6H_2O$ (0.041 mg $L^{-1}$), $Na_2MoO4.\ 2H_2O$ (0.025 mg $L^{-1}$). The pH of the solution was adjusted to 7.2 with sodium hydroxide (1.0M). The medium solution was autoclaved at 121°C for 20 min. After cooling, powdered atrazine was added to the autoclaved solution and - due to slow dissolution kinetics of atrazine - stirrered vigorously for 48 hours. After complete dissolution of atrazine, filter-sterilized (0.22 $\mu$m) $FeCl_3.6H2O$ solution (5.14 mg $L^{-1}$) was added. The medium was again filter sterilized (0.22 $\mu$m) to remove any solid atrazine residue before using it for sterile cultivations. To prepare the pre-culture for chemostat and retentostat cultivation, *A. aurescens* TC1 was grown on MS media with excess atrazine in a shaken flask until an optical density at 600 nm ($OD_{600}$) of 0.1 was reached.

### *2.2. Chemostat cultivation*

*A. aurescens* TC1 was cultivated in duplicate 3-L bioreactors (Applikon Biotechnologie B.V., Netherlands) operated in chemostat mode. Bioreactors were equipped with pH, aeration, temperature, solution level and agitation controls by myControl® (Applikon Biotechnologie B.V., Netherlands). *A. aurescens* TC1 pre-culture (10% (v/v)) was used for inoculation. Agitation speed was 800 rpm and $\mathbf{pO_2}$ was maintained at 50% throughout cultivation with an air or nitrogen flow of 0.1 L gas $L^{-1}$ $min^{-1}$ as required. The working

volume of the bioreactor was kept constant at 2000 mL by means of a conductivity sensor placed on top of the culture surface which activated a peristaltic pump to remove the effluent. The pH remained constant at 7.2 throughout the cultivation and the bioreactors were operated at 25°C. No foaming was observed eliminating the necessity of adding an antifoaming agent. The bioreactors were operated at eight dilution rates (D) [defined as the ratio of the medium flow rate (mL $h^{-1}$) and culture volume (L)] (0.068, 0.056, 0048, 0.032, 0.023, 0.018, 0.009 and 0.006 $h^{-1}$). Dilution rates were only changed after achieving a steady state at a particular D, where steady state was defined as the condition in which culture parameters such as $\mathbf{OD}_{600}$ or cell concentration, atrazine and 2-hydroxyl atrazine remained constant (<5% and <10% relative variation, respectively) for at least five reactor volume changes.

### *2.3. Retentostat cultivation*

Duplicate retentostat experiments were performed in bioreactors controlled by myControl® (Applikon Biotechnologie B.V., Netherlands) at a dilution rate of 0.02 $h^{-1}$. The bioreactors were identical to the chemostat experiments, but in addition equipped with an autoclavable polyethersulfone cross-flow filter with a pore size of 0.22 $\mu$m (Flownamics, USA) to retain biomass in the reactor. The filtration unit was installed via a head plate port to the bioreactors. An internal sterile filtration loop was established with a connection of level sensor to the myControl® and a peristaltic pump to allow filtration of effluent during level control throughout the cultivation. The retentostats were operated under the same conditions (temperature, aeration, agitation) as the chemostats.

### *2.4. Measurement of biomass, substrate and metabolites*

During chemostat and retentostat cultivations, samples were withdrawn from the bioreactors by a sterile sampling loop (Applikon Biotechnologie B.V., Netherlands) to determine the biomass concentration, as well as atrazine, and 2-hydroxylatrazine concentrations. To minimize the disturbance caused by withdrawal, the sampling volume was kept below 3% of the working volume during routine sampling and below 10% under steady state conditions. For substrate and metabolite analysis, samples were filter-sterilized and stored at −20°C before HPLC analysis. Using a Prominence HPLC system (Shimadzu Corp., Japan) analytes



were separated on a 100 × 4.6 mm Kinetex 5 $\mu$m Biphenyl 100 A°column (Phenomenex Inc., USA) to measure the concentration of atrazine and 2-hydroxyatrazine concentrations as described in detail in Ehrl et al., (in communication). To measure the cell dry weight, samples were centrifuged at 4°C in a pre-weighted tube, washed with 0.9% NaCl and dried overnight at 85°C to constant weight. Additionally, the optical density of the culture was measured at 600 nm.

### *2.5. Estimation of cell numbers and viability*

Cells were fixed with 2.5 % glutaraldehyde and stored at 4°C for a maximum of 20 days prior to measurement. Total cells were determined by staining them with SYBR Green I. To estimate the fraction of dead cells in samples, propidium iodide was used. Viable cells were determined as the difference between total and dead cells. The concentration analysis was performed on a Cytomics FC 500 flow cytometer (Beckmann Coulter, USA) equipped with a 488 nm (40 mW) and a 638 nm (25 mW) laser. Reference beads (**Trucount**$^{TM}$ Absolute Counting Tubes, BD Bioscience, USA) were added to the samples in two control replicates to convert the counts to absolute cell numbers. The data were analyzed with CXP software (version 2.2; Beckman Coulter, Germany).

### *2.6. Compound specific isotope analysis of atrazine in retentostat*

At the end of the retentostat cultivation, samples were withdrawn from two duplicate bioreactors through the 0.22 $\mu$m filter. Atrazine was extracted with dichloromethane (10 % of the sample volume, three times). Carbon and nitrogen isotope analysis of atrazine were performed on a GC-IRMS system consisting of a TRACE GC Ultra gas chromatograph (Thermo Fisher Scientific, Italy) equipped with a DB-5 analytical column (60 m, 0.25 mm ID, 1.0 µm film, Agilent Technologies, Germany) coupled to a Finnigan MAT 253 isotope ratio mass spectrometer via a Finnigan GC Combustion III interface (both Thermo Fisher Scientific, Germany). Details of extraction procedure and analysis is described in Ehrl et al., in communication.

### *2.7. Estimation of growth kinetics parameters*

### 2.7.1. Chemostat

The mass balance for cell mass ($C_x$) and residual substrate ($C_s$) in the chemostat cultivation were calculated as:

$$\frac{dC_x}{dt} = \mu . C_x - D . C_x \quad (1)$$

$$\frac{dC_s}{dt} = D . (C_{s,in} - C_s) - q_s . C_x \quad (2)$$

where $q_s$ is the biomass-specific electron-donor (substrate) consumption rate, and $C_{s,in}$ is the substrate (atrazine) concentration in the media, $C_s$ and $C_x$ denote the steady state substrate and biomass concentration, respectively in the chemostat. Consumption rate $q_s$ was described by a Michaelis-Menten type relation

$$q_s = \frac{q_s^{max} . C_s}{K_s + C_s} \quad (3)$$

where $K_s$ and $q_s^{max}$ are Monod affinity constant and maximal substrate consumption rate. The experimentally measured $q_s$ at each dilution rate at steady state was used to fit the model (eq. 3) to estimate $K_s$ and $q_s^{max}$. To estimate the maintenance demand $m_s$ derived from these chemostat experiments, a modified Herbert-Pirt equation was used [20], [21].

$$\mu = Y_{x/s}^{max} . \left( q_s^{max} . \frac{C_s}{C_s + K_s} - m_s \right) \quad (4)$$

where $q_s^{max} . \frac{C_s}{C_s + K_s} = q_s$ describes the substrate conversion rate, $Y_{x/s}^{max}$ denotes the (hypothetical) maximum growth yield in case all consumed substrate is channeled to biomass only and where $m_s$ is deducted from substrate conversion to account for the maintenance requirement per biomass per time .

### 2.7.2. Retentostat

The dynamic biomass concentration $C_x(t)$ during retentostat cultivation was described by the Van Verseveld equation[22]:



$$C_x(t) = C_{x,0} . e^{-m_s . Y_{\frac{x}{s}}^{max} . t} + \frac{D . (C_{s,in} - C_s)}{m_s} \left( 1 - e^{-m_s . Y_{\frac{x}{s}}^{max} . t} \right) \quad (5)$$

where the first term describes the consumption of the original biomass over time. The second term models how biomass concentration then approaches a long-term value that is sustainable when considering substrate consumption per time ($D^*(C_{s,in}-C_S)$) and taking into account maintenance demand (substrate per biomass per time). Biomass growth rate, finally, was calculated as:

$$\mu = \frac{dC_x^{Total}}{dt . C_x^{viable}} \quad (6)$$

where the concentration of viable cells was determined from staining protocols of flow cytometry (see above).

### 2.8. Parameter estimation

The two parameter estimates $K_s$ and $q_s^{max}$ of substrate the consumption rate model (eq.3) were estimated from the experimentally measured $q_s$ and the residual atrazine concentration ($C_s$) data by minimizing the Root mean squared error (RMSE) as objective function (eq.7).

$$\sqrt{\sum \frac{(\vartheta_{exp} - \vartheta_{sim})^2}{N}} \quad (7)$$

The "brute force" optimization method was used to find the global minimum of the objective function to compute the objective function's value at each point of a multidimensional grid of points, to obtain the global minimum of the function. This multidimensional grid contained ranges of $q_s^{max}$ (0.001 to 10) and $K_s$ (10 to 1000) with linear grid space of 0.005 and 1, respectively. Thereafter, the result of "brute force" minimization was fed as initial guess to obtain a more precise (local) minimum using the downhill simplex algorithm [23]. A similar approach was taken to estimate $Y_{x/s}^{max}$ and $m_s$ for chemostat (equation 4) and retentostat cultivations (equation 5).

### 2.9. Model analysis

The RMSE as a measure of the discrepancy between the experimental data and model prediction is used to indicate an accuracy of the model to describe the kinetics of chemo-stat and retentostat culture. A small RMSE indicates a close fit of the model to the data. Furthermore, to check the functional relation and reliability of estimated parameters, practical identifiability was examined using the collinearity analysis over the complete parameter space $\Re$. If a vector $\beta$ exists among columns $\Re_k$= 1, 2, ..., m, of $\Re$ such that $\| \beta \| \neq 0$ and $\Re\beta \approx 0$, they are near collinear. This collinearity was tested by inspecting the smallest eigenvalue $\lambda_m$ of the normalised sensitivity matrix, $\widetilde{\Re}$ [24]. The collinearity index, $\gamma$ is calculated as

$$\gamma = \frac{1}{\min_{\|\beta\|=0} \| \widetilde{\Re}\beta \|} = \frac{1}{\sqrt{\lambda_m}} \quad (8)$$

Parameter subsets below the collinearity index of 5 are considered as identifiable and above 20 are considered as non-identifiable [24]. The model implementation, fitting parameter estimations and model analysis was performed using Python and employing the built-in functions in scientific libraries NumPy and SciPy [25].

### 2.10. Thermodynamic calculation

Breakdown of atrazine by *A. aurescens* TC1 involves sequential hydrolysis to give ethyl amine, isopropyl amine and cyanuric acid. Subsequently, cyanuric acid is discarded, while the short chain amines serve as further source of energy and growth [19] . Since the initial hydrolysis is energy-neutral, thermodynamic calculations were based on conversion of the short chain amines. Therefore, the Gibbs free energy released during substrate catabolism to $CO_2$ ($\Delta_R G^{0\prime}{}_{cat}$) and the Gibbs free energy released during substrate anabolism for growth ($\Delta_R G^{0\prime}{}_{ana}$) were calculated using the following stoichiometric equations. Free energy values under standard conditions ($\Delta_R G^{0\prime}$) were calculated from published $\Delta_f G^{0\prime}$ values [26], [27].

$$C_2H_5NH_3 + C_3H_7NH_3 + 7.5O_2 \rightarrow 5HCO_3^- + 5H^+ + 2NH_4^+ \qquad \Delta_R G^{0\prime}{}_{cat} = -3338\ kJ.mol^{-1}$$



$$C_2H_5NH_3 + C_3H_7NH_3 + 4O_2 \rightarrow 2.2HCO_3^- + 5H^+ + 1.44NH_4^+ + 2.8CH_{1.8}O_{0.5}N_{0.2}$$

$$\Delta_R G^{0\prime}{}_{ana} = -1838\ kJ.mol^{-1}$$

The calculated $m_s$ was converted to maintenance energy ($m_E$ ) using the correlation of $\Delta_R G^{0\prime}{}_{cat}$ as described by Tijhuis et al., 1993 [13].

### 2.11. Morphology and microscopy

The fixed cells were analyzed on agar glass slides by light microscopy with an Axioscope 2 Plus microscope (Carl Zeiss AG, Germany)[28]. For imaging, pictures were taken with a high-resolution digital camera AxioCam HRm (Carl Zeiss AG, Germany) and the software AxioVision (Version 4.8.2; Carl Zeiss AG, Germany) was used to determine the cell radii and length. Based on this data cell volumes were calculated.

### 2.12. Proteomic analysis

Cells were harvested directly from the bioreactors (approximately, 300 – 400 ml) and centrifuged at 8,000 rpm, 4°C for 20 min in Avanti J-E centrifuge (Beckman Coulter Inc., USA). Then cells were washed once with 1×phosphate buffered saline (PBS) consisting of (per liter) NaCl (8 g), KCl (0.2 g), $KH_2PO_4$ (0.24 g), and $Na_2HPO_4$ (1.44 g). Washed cells were centrifuged again at 15,300 × g for 5 min at 4°C. The cell pellet was dissolved in lysis buffer (9M urea, 2M thiourea, 4% CHAPS, 1% DTT) containing proteinase inhibitor (Complete Mini. EDTA-free (Roche, Germany)) and incubated 30 min at room temperature. Protein extraction was performed via sonication: sonication was applied twice for 1 min (0.3 s per pulse, 30% duty) (ultrasonic processor UP50H, Hielscher Ultrasonics, Germany) with sample cooling on ice between the rounds. DNA/RNase digestion was performed via adding appropriate amount of Nuclease-Mix (GE Healthcare, Germany) to the supernatant and incubating samples for 30 min at room temperature. Protein concentration was determined using the Bradford protein assay (Bio-Rad) with bovine serum albumin as the standard (Bradford, 1976). In total, 10 µg of proteins from each sample was used for trypsin digestion using a modified FASP procedure[29]. LC-MSMS analysis was performed on a QExactive HF mass spectrometer (Thermo Fisher Scientific) online coupled to an Ultimate 3000 RSLC (Dionex). The acquired spectra were loaded to the Progenesis QI software (version 3.0, Nonlinear Dynamics, part of Waters)

for label free quantification and analyzed as described previously [30]. All MS/MS spectra were exported as Mascot generic file and used for peptide identification with Mascot (version 2.5.1) in the Uniprot Arthrobacter aurescens TC1 protein database (1514995 residues, 4566 sequences). Search parameters used were: 10 ppm peptide mass tolerance and 0.02 Da fragment mass tolerance, one missed cleavage allowed, carbamidomethylation was set as fixed modification, methionine oxidation and asparagine or glutamine deamidation were allowed as variable modifications. A Mascot-integrated decoy database search calculated an average false discovery of 0.48% when searches were performed with the mascot percolator algorithm and p<0.05. Peptide assignments were re-imported into the Progenesis QI software and the abundances of all peptides allocated to each protein were normalized and summed up.

### *2.13. Statistical analysis*

Protein abundances were normalized in the software Progenesis QI. Then normalized and log10 transformed protein abundances were used to identify differentially expressed proteins using a linear model for microarray data analysis (LIMMA) (Smyth, 2004) in Bioconductor http://www. bioconductor.org. False discovery rate (FDR) was estimated using Benjamini–Hochberg method [31]. Visualization of hierarchical clustering of z-score normalized protein abundances and conditions was done via creating heatmaps in Perseus 1.5.2.6 (Cox and Mann, 2012). Euclidean distance was used for grouping the observations into groups.

## 3. Results and Discussion

### *3.1. Chemostat cultivation of A. aurescens TC1 indicates a high atrazine degradation capability and a high maintenance demand under growth conditions*

Aerobic cultivation of *A. aurescens* TC1 in chemostat resulted in > 99% degradation of $C_{atrazine,in}$= 30 mg $L^{-1}$ at all investigated dilution / growth rates: $D_{high}$ (0.068 $h^{-1}$, 0.056 $h^{-1}$ and 0.048 $h^{-1}$), $D_{medium}$ (0.032 $h^{-1}$ and 0.023 $h^{-1}$) and $D_{low}$ (0.018 $h^{-1}$, 0.009 $h^{-1}$ and 0.006 $h^{-1}$) (Fig. 1, A). Lower dilution rates D increased substrate and biomass residence time resulting in decreasing concentrations of atrazine and its metabolite 2-hydroxylatrazine (2-OH atrazine) according to a classic chemostat behavior (Fig. 1, A). Cell concentrations did not change



significantly from $D_{high}$ to $D_{medium}$ ($2.2 - 2.69 \times 10^7$, Fig. 1, B), but dropped to $1.31 \times 10^7$ at $D_{low}$ (0.006 and 0.009 $h^{-1}$, Figure 1b). Remarkably, even at $D_{low}$ the viability, as determined by staining protocols of flow cytometry, remained as high as 90% (Fig. 1b). Biomass yield ($Y_{x/s}$) was 0.021 ± 0.004 at all D (Fig. 1, C), which is only 30% of the $Y_{x/s}^{max}$ reported for batch cultivation [25]. At higher dilution rates when more atrazine was supplied per time, also the substrate consumption rate $q_s$ (eq.2) increased (Fig. 1, D, Table S1) reflecting a high atrazine degradation capability of *A. aurescens* TC1. Equation 3 was fitted using measured $q_s$ and Cs to estimate $q_s^{max}$ and $K_s$ as 4.08 ± 0.51 g-S g-$X^{-1}h^{-1}$ and 237±58 μg $L^{-1}$ (~1μM), respectively. The collinearity index (eq. 8) was found to be 4.80, which is sufficiently low to suggest that there was no significant interrelation between parameters $q_s^{max}$ and $K_s$. In comparison to copiotrophic microorganisms, which are reported to have $K_s$ values in the range of 10μM or higher [32], *A. aurescens* TC1, therefore, has a comparatively low $K_s$ (~1 μM). The $K_s$ value plays a major role in the survival and growth of microorganisms at oligotrophic conditions, where a low $K_s$ implies that microorganisms are able to scavenge substrate (i.e, atrazine) at low concentrations in support of growth or a reproductive cycle. The effective value is even lower when considering that only part of the atrazine molecule - the isopropylamine and ethylamine side chains – are used for growth and energy metabolism, corresponding to 5 μM C and 2 μM N. [19]. In addition, we recently discovered (Ehrl et al., in communication) that – due to slow cell membrane permeation – atrazine supply from outside the cell can become rate-limiting at low concentrations so that the intracellular concentration of atrazine amounted to only 60% of measured atrazine concentrations outside. This, in turn, indicates a high substrate affinity of TrZN – the first assimilatory intracellular enzyme responsible for the conversion of atrazine to 2-OH atrazine which created a steep concentration gradient and boosted diffusive atrazine influx at low concentrations.

Hence, growth kinetics of *A. aurescens* TC1 indicates that atrazine can be effectively bio-degraded when present at e concentrations around 1 uM . However, while $q_s^{max}$ and >99%

degradation highlight a high substrate conversion efficiency, the observed low yield suggests a low assimilation into biomass. This may reflect the necessity to sacrifice thermodynamic efficiency in order to increase the thermodynamic driving force for rapid degradation [33]. Alternatively, the consumed substrate which is not utilized to produce biomass may indeed be attributable to maintenance energy requirement [20]. The $m_s$ was calculated by fitting atrazine concentrations at different D and growth rates according to equation 4 (Fig. 1, E). The resultant $m_s$ was 0.25 g-substrate g-biomass$^{-1}$ h$^{-1}$, which was and was converted into $m_E$ = 97±10 kJ C-mol biomass$^{-1}$ h$^{-1}$ based on $\Delta_R G^{0\prime}{}_{cat} = -3338\ kj.mol^{-1}$ for mineralization of the isopropylamine and ethylamine side chains in atrazine (see calculations in the Methods and Materials part according to [13]). This value falls into the upper end of ranges estimated by Tijhuis et al., 1983 [13] for different aerobic microorganisms (7.6-116 kJ Cmol biomass$^{-1}$h$^{-1}$) suggesting that the experimentally determined $m_E$ of *A. aurescens* TC1 was comparatively high. However, we question that chemostat cultivation, where microorganisms are forced to grow at high rates coupled with high metabolic efficiency as reflected by $q_s$ (Fig.1, D), may not be representative of natural conditions. The doubling period ($t_d$) at the lowest D of 0.006h$^{-1}$ was 12 days while in nature microorganisms grow at near-zero growth rate where $m_s$ may change due to a physiological adaptation strategy called "stringent response". Hence, our next step was to explore how $m_s$ changes when *A. aurescens* TC1 adapts to extreme energy limiting conditions in retentostat rather than chemostat cultivation.

### *3.2. Retentostat cultivation results in lower maintenance demand implying adaptation of A. aurescens TC1 at near-zero growth rate*

Two independent retentostat cultivations were successfully performed for 42 days (Fig. 2) at a D of 0.020h$^{-1}$. Wall growth or filter clogging – typical problems when performing retentostat experiments over longer time periods – were not observed. During the first 18 days of cultivation, the biomass (measured in grams dry weight ($g_{dw}$)/L) linearly increased to the concentration at which atrazine supply rate met the maintenance energy requirement of the cells (growth phase) (Fig. 2, A). In this period, μ decreased from 0.018h$^{-1}$ to 0.005h$^{-1}$ and finally, reached a level of 0.0001h$^{-1}$ at the end of cultivation (42 days) corresponding to a doubling time of $t_d$=225 days (Fig. 2, B). During this time, 97% of the



available energy flux was calculated to be directed to the maintainance of basic cell functions (Fig. 3, Table S1). The count of dead cells increased to 4% during the growth phase and later on remained constant implying that the lysis of dead cells can be ruled out as a source of energy for bacterial metabolism. Biomass accumulation in the retentostat cultivations was modeled with the van Verseveld equation (Eq. 5) to estimate the $m_s$ and $Y_{x/s}^{max}$ (collinearity index=1.30). The estimated $m_s$ was 0.11 g-substrateg-biomass$^{-1}$h$^{-1}$ corresponding to $m_E$ (37±8 kJ Cmol biomass$^{-1}$h$^{-1}$), which is ~2 times lower than that of the chemostat. This implies that *A. aurescens* TC1 must undergo further regulation / adaptation to lower its maintenance energy requirement for viability under extreme low-energy conditions.. Notably, the yield $Y_{x/s}^{max}$in retentostat (0.061 ± *0.013 g-biomass.g-substrate*$^{-1}$ ) was higher than in chemostat cultivations. This suggests that the efficiency of converting substrate to cell carbon varies with different energy settings.

### *3.3. Exploring the physiological threshold of degradation*

The concentration of atrazine and 2-OH atrazine was found to be 12 ±3 and 10 ±5 μg L$^{-1}$, respectively at the end of cultivation in retentostat (Fig. 2, C). This concentration of atrazine is an experimentally determined minimum substrate concentration ($\mathbf{S}_{min}$), which corresponds to zero growth conditions. At this concentration of atrazine, the substrate flux is sufficient to meet the cell's maintenance energy demand. Below this concentration, in contrast, energy would be so limited in absolute terms that maintenance of cell viability on the long-term would become impossible and, hence, bioremediation would not be expected to be feasible any longer. Therefore, for the development of a bioremediation strategy, this concentration should be considered as a threshold. However, moving to concentrations below $\mathbf{S}_{min}$ would not necessarily stop degradation immediately as long as substrate can pass through the cell membrane via diffusion or transporters and enzyme kinetics is feasible at that concentration. Hence, another way of defining the threshold of degradation is the concentration at which $q_s$ becomes zero which is mediated by transport phenomenon. In this regard, proton motive force plays a role. If $\Delta_R G^0{}_{cat}$ falls below 10-20 kJ mol$^{-1}$, even extrusion of one proton can not be possible to create pmf and ultimately leading to halt in degradation[21], [34], [35]. However, in case of aerobic process $\Delta_R G^0{}_{cat}$

is so high that the energy required for extrusion of one proton is not limiting. Nevertheless, the challenge may exist in a different direction i.e., to compensate the proton leakage rate. Proton leakage rate has been reported in the range of $1.3\times10^{-5}$-$4.6\times10^{-3}$ μM $H^+$ $min^{-1}$ mg $dryweight^{-1}$ [36], [37]. At low concentrations, microorganisms might change the physiology to adapt to extreme energy limitation[16], however, cannot boost the metabolic rate. If we assume that all protons from catabolic reaction (Section 2.10) are extruded, then at physiological threshold concentration with a low metabolic rate (0.12 g-substrateg-$biomass^{-1}h^{-1}$) the proton extrusion rate $\sim 4.26*10^{-2}$ is close to upper limit of the proton leakage rate. At certain point of low concentrations, low metabolic rate with a slow proton extrusion rate may be similar to the leakage rate resulting a loss of membrane potential. Indeed, frequent detection of non-respiring and depolarized cells under starvation [38] and in the aquatic environment [39] suggest the limitation of sustaining pmf in oligotrophic condition. Hence, below the physiological threshold concentration the limitation of transport would eventually minimize the possibility to undergo further physiological adaptation for survival.

[Table S1 about here.]

[Figure 2 about here.]

[Figure 3 about here.]

### *3.4. Isotope fractionation reveals permeation through cell membrane is slower at physiological threshold concentration*

We took the advantage of compound specific isotope analysis to directly observe the physiological vs mass transfer limitation at physiological threshold concentration [40]. A lower isotope fractionation ($\varepsilon^{13}C$ ) measured in outflow suggests that the transport of substrate to the cell is slower than enzyme kinetics while a high $\varepsilon^{13}C$ indicates that abundance of enzyme in the cell is limiting. We observed a reduction in isotope fractionation in residual atrazine (from $\varepsilon^{13}C$ = -5.36 ± 0.20 ‰ at μ=0.031 to -2.32 ± 0.28 ‰ at μ=0.006 (±SEM, N=2) showing the onset of mass transfer limitation (Ehrl et al., in communication). Interestingly, retentostat experiments also resulted in a drastic



reduction in isotope fractionation compared to chemostat cultivation $\varepsilon^{13}C$ = -0.45‰ ± 0.36‰ indicating the transport of the substrate limits the adaptation to lowering the minimal energy requirement of cells viability. Three proteins involved into hydrolysis of atrazine (triazine hydrolase tzN, hydroxyatrazine hydrolase atzB, and N-isopropylammelide isopropylaminohydrolase atzC) were detected in all chemostats and retentostat (Supporting information, Table S1). No significant down regulation of their abundances in retentostats relative to chemostat was observed which was in agreement with our isotope data suggesting that the abundance of atrazine-hydrolyzing proteins was not limiting at physiological threshold condition. However, under energy limitation a physiological adaptation in terms of down-regulation of proteins is a definite necessity to cope with low energy availability. Hence, in the subsequent section we focus how *A. aurescens TC1* physiologically adapts to extreme energy limitation folded by slower cell membrane permeation.

### *3.5. hanges in physiology of A. aurescens TC1 when adapting from low-energy settings to extreme energy limitation coupled with slow cell membrane permeation*

#### *3.5.1. Morphological adaptation under energy limitation*

In chemostat cultivation, all cells present at a given dilution rate D were of homogeneous morphology. In contrast, shifts in morphology were observed when the dilution rate D was changed (Fig. 4, A). At $D_{high}$, cells were long rods characterized by a smaller aspect ratio (width/length) compared to cells at $D_{low}$, which were shorter rods. This could be evaluated as a drop in cell volume from 1.28 $\mu m^3$ at $D_{high}$ to 0.68 $\mu m^3$ at $D_{low}$.

In the case of retentostat cultivation, cell morphology was more heterogeneous (Fig. 4, B). In the beginning of retentostat cultivation, cells were mainly rod-shaped, whereas both coccoid and shorter rod-shaped cells emerged towards the end of cultivation. This transition in morphology was first observed after 13 days when 38% of cells were smaller in volume (0.1-0.2$\mu m^3$ ) and the morphological change dominated (>50%) at the end of cultivation after 42 days. This kind of morphological adaptation is common for

*Arthrobacter* [19] and bacteria isolated from freshwater and marine habitats including sub-sea floor sediments [1]. Shortening of width and length of rod-shaped cells or transition from rod to coccus shape results in an increase in Surface (S)/Volume (V) ratio, which facilitates scavenging nutrients and substrates under oligotrophic conditions.

[Figure 4 about here.]

*3.5.2. Proteomics reveals slow-down of metabolism in A. aurescens TC1 under extreme energy limitation*

To explore the nature of physiological adaptation on the protein level, proteome expression at near zero growth in retentostats was analyzed and compared to chemostats at D of 0.023, 0.031, and 0.056 $h^{-1}$. In total, 1720 proteins were detected in all analyzed samples. Hierarchical clustering of detected proteins in all analyzed samples (1627 proteins) shows that most of the proteins in chemostats at D of 0.031 $h^{-1}$ had increased abundances (z-scores around 2) and a high number of the proteins in retentostats had decreased abundances (z-scores around -2) (Fig. S1 in Supporting Information). Surprisingly, although the dilution rate D 0.056 $h^{-1}$ was higher than 0.031 $h^{-1}$, proteome analysis at 0.056 $h^{-1}$ showed more proteins with decreased abundances than at the dilution rate 0.031 $h^{-1}$. This observation might suggest an uncoupling between translation and growth rate above D 0.31$h^{-1}$. $D_{high}$ may force *A. aurescens* TC1 to invest its energy into a response to higher flux associated with a shorter cell reproduction time (20-14 h) rather than into increased rates of translation.

Proteins detected at different D in chemostats were compared to proteins detected in retentostats. The highest number of differentially expressed proteins (230 proteins) was estimated in a pairwise comparison of those in the chemostat at dilution rate 0.031 with those in retentostat (Fig. S2 in supplementary material). Sixty-eight proteins were differentially expressed in all three pairwise comparisons. All differentially expressed proteins were hierarchically clustered and the clustering was visualized in the form of a heat map (Fig. 5). Hierarchical clustering visualizes a clear difference in the physiology of *A. aurescens* TC1 at high growth rates (chemostat) and near-zero growth rate (retentostat). Almost all differentially expressed proteins which were upregulated in retentostats had lower abundances in chemostats and vice versa (Table1). A distribution of proteins that



were differentially expressed in retentostats relative to dilution 0.031 $h^{-1}$in chemostats across functions using clusters of orthologous groups (COG) categories according to http://www.ncbi.nlm.nih.gov/COG [41] (Fig. 6) shows that the highest number of downregulated proteins belongs to such categories as [E] Amino acid transport and metabolism, [G] Carbohydrate transport and metabolism, [J] Translation, ribosomal structure and biogenesis, [O] Post-translational modification, protein turnover, chaperones. Although a lower number of differentially expressed proteins was detected for pairwise comparison of retentostat condition to other dilutions in chemostats (Fig. S2 in the supplementary material), overall a similar distribution of downregulated proteins across COG categories is observed (Fig. 6).

Analysis of the distribution of proteins across COG categories suggests that bacteria in retentostats allocated their energy flux in a different way than in chemostats. As has been presented above (Table S1), energy flow in retentostats went mainly (~97%) into maintenance. This allocation of energy flow could become possible via reduction of biosynthetic building block requirements. Protein synthesis is one of the most expensive anabolic reactions for biomass synthesis [14]. Among all cellular macromolecules, synthesis of protein consumes 90% of energy followed by RNA and DNA [1]. Several ribosomal proteins and other proteins related to anabolic reactions such as synthesis of amino acids and nucleotides had significantly decreased abundances in retentostats relative to chemostats at D = 0.031 $h^{-1}$ (Table 1). In addition, also a number of amino acid- and lipid metabolism-related proteins were significantly downregulated in retentostats relative to chemostats at D = 0.031 $h^{-1}$ (Fig. 6). Several transporters of sugars and ions decreased their abundances in retentostats (e.g., proteins A1R2F7, A1R437, A1RC00, and A1R375 in Table 1). Proteins with significantly decreased abundances from carbohydrate and energy metabolism belong to glycolysis (glyceraldehyde-3-phosphate dehydrogenase A1R7C8 in Table 1), pyruvate metabolism (pyruvate dehydrogenase E1 component A1R7E9 in Table 1), malate (malate dehydrogenase A1RBA3 in Table 1) and aldehyde conversions (aldehyde dehydrogenase in A1R953).

Although more proteins were downregulated than upregulated in retentostats, several upregulated proteins attracted our attention. For example, one of the most abundant

maintaining high metabolic fluxes at oligotrophic concentrations might be associated with a loss in the energetic efficiency of the overall metabolism [46].

At the end, survival under oligotrophic conditions depends on two factors: 1) capability to transport the substrate inside the cells 2) using the available catabolic energy to synthesize macromolecules or at least meet the maintenance demand. Since we did not observe evidence of an atrazine transporter that would "boost" intracellular concentrations (Ehrl et al., in communication) mass transfer must be diffusion-mediated meaning that the concentration inside the cell can never exceed the outside concentration. Though our study indicated that *A. aurescens* TC1 can scavenge atrazine from low concentration due to fast enzyme kinetics of TrZN and a low $m_E$ corresponding to low basal power requirement, the limitation imposed by transport is unavoidable. On one hand, isotope fractionation reveals that transport of substrate through cell membrane slow at physiological threshold condition and 60% of bulk concentration is available for energy metabolism. On the other hand, below physiological threshold concentration, the proton leakage rate might attribute to minimal or loss of pmf over time at extreme low energy flux leading to a halt in transport and eventually, shut-down of metabolism. Indeed, in a study with *Aminobacter* MSH1 Sjøholm et al. observed that >80% cells lost membrane potential under starvation and only intact cells with a polarized membrane resumed growth on micropollutant [47]. An adaptation in cell membrane such as reduction in permeability or utilizing other ions rather than proton (for eg. $Na^+$ has $10^2$ less trans-membrane diffusion rates) for chemiosmotic energy transduction would minimize the transport limitation [1], [44], [48] and trigger the physiological adaptation in terms of lowering the maintenance requirement. Moreover, the presence of alternative energy sources such as the metabolites generated by other bacteria present in nature would allow the atrazine degraders to adapt and survive at extreme low energy fluxes lowering the threshold.

[Figure S1 about here.]

[Figure S2 about here.]

[Figure 5 about here.]



[Figure 6 about here.]

[Table 1 about here.]

## 4. Conclusion

This work demonstrated that the minimization of maintenance energy is one of the adaptation strategies for survival under energy limitation and slowing down the metabolism is the biggest contributing factor behind this. With this adaptation developing a long-term bioremediation strategy for micropollutants even up to a concentration of 10 $\mu g\ L^{-1}$ is possible where the energy flux is sufficient to sustain cell viability i.e., maintenance energy requirement. Limitation imposed by transport either permeation through cell membrane or maintaining a pmf puts a constraint on physiological adaptation at a concentration below 10 $\mu g\ L^{-1}$. Transport limitation boosts the extreme low energy availability which will eventually lead to a "shut-down" of metabolism i.e. a halt in the degradation of micropollutants. Further work is needed to explore 1) whether the threshold can be further lowered by a co-substrate addition 2) adaptation of microorganisms to prevent the loss of ions by changing the permeability of membrane or by using a different, more effective ion pump 3) the degradation of atrazine as a sole source of energy with a microbial consortium to study the syntrophy lowering the threshold.

**Acknowledgment**

**Reference**

[1] T. M. Hoehler and B. B. Jørgensen, "Microbial life under extreme," *Nat. Rev. Microbiol.*, vol. 11, no. 2, pp. 83–94, 2013.

[2] M. A. Shannon, P. W. Bohn, M. Elimelech, J. G. Georgiadis, B. J. Mariñas, and A. M. Mayes, "Science and technology for water purification in the coming decades," *Nature*, vol. 452, no. 7185, pp. 301–310, 2008.

[3] K. Fenner, S. Canonica, L. P. Wackett, and M. Elsner, "Evaluating pesticide degradation in the environment: blind spots and emerging opportunities," *Science (80-. ).*, vol. 341, no. 6147, pp. 752–758, 2013.

[4] N. Shapir, E. F. Mongodin, M. J. Sadowsky, S. C. Daugherty, K. E. Nelson, and L. P. Wackett, "Evolution of catabolic pathways: genomic insights into microbial s-triazine

metabolism," *J. Bacteriol.*, vol. 189, no. 3, pp. 674–682, 2007.
[5] D. Vonberg, J. Vanderborght, N. Cremer, T. Pütz, M. Herbst, and H. Vereecken, "20 years of long-term atrazine monitoring in a shallow aquifer in western Germany," *Water Res.*, vol. 50, pp. 294–306, 2014.
[6] A. H. Meyer, H. Penning, and M. Elsner, "C and N isotope fractionation suggests similar mechanisms of microbial atrazine transformation despite involvement of different enzymes (AtzA and TrzN)," *Environ. Sci. Technol.*, vol. 43, no. 21, pp. 8079–8085, 2009.
[7] J. F. Douglass, M. Radosevich, and O. H. Tuovinen, "Microbial attenuation of atrazine in agricultural soils: Biometer assays, bacterial taxonomic diversity, and catabolic genes," *Chemosphere*, vol. 176, pp. 352–360, 2017.
[8] T. Egli, "How to live at very low substrate concentration," *water Res.*, vol. 44, no. 17, pp. 4826–4837, 2010.
[9] T. N. P. Bosma, P. J. M. Middeldorp, G. Schraa, and A. J. B. Zehnder, "Mass transfer limitation of biotransformation: quantifying bioavailability," *Environ. Sci. Technol.*, vol. 31, no. 1, pp. 248–252, 1996.
[10] H. P. Fuchslin, "Microbial competition and mixed substrate utilisation in the laboratory: Towards a better understanding of microbial behaviour in the environment (Chelatobacter heintzii, Ralstonia eutropha).," 2004.
[11] K. Kovar, V. Chaloupka, and T. Egli, "A Threshold Substrate Concentration Is Required to Initiate the Degradation of 3-Phenylpropionic Acid in Escherichia coli," *Eng. Life Sci.*, vol. 22, no. 3–4, pp. 285–298, 2002.
[12] M. Bucheli-Witschel, T. Hafner, I. Rüegg, and T. Egli, "Benzene degradation by Ralstonia pickettii PKO1 in the presence of the alternative substrate succinate," *Biodegradation*, vol. 20, no. 3, pp. 419–431, 2009.
[13] L. Tijhuis, M. C. M. Van Loosdrecht, and J. J. Heijnen, "A thermodynamically based correlation for maintenance Gibbs energy requirements in aerobic and anaerobic chemotrophic growth," *Biotechnol. Bioeng.*, vol. 42, no. 4, pp. 509–519, 1993.
[14] J. B. Russell and G. M. Cook, "Energetics of bacterial growth: balance of anabolic and catabolic reactions.," *Microbiol. Rev.*, vol. 59, no. 1, pp. 48–62, 1995.
[15] A. Konopka, "Microbial physiological state at low growth rate in natural and engineered ecosystems," *Curr. Opin. Microbiol.*, vol. 3, no. 3, pp. 244–247, 2000.
[16] O. Ercan, M. M. M. Bisschops, W. Overkamp, T. R. Jørgensen, A. F. Ram, E. J. Smid, J. T. Pronk, O. P. Kuipers, P. Daran-Lapujade, and M. Kleerebezem, "Physiological and transcriptional responses of different industrial microbes at near-zero specific growth rates," *Appl. Environ. Microbiol.*, vol. 81, no. 17, pp. 5662–5670, 2015.
[17] B. Lin, H. V Westerhoff, and W. F. M. Röling, "How Geobacteraceae may dominate subsurface biodegradation: physiology of Geobacter metallireducens in slow-growth habitat-simulating retentostats," *Environ. Microbiol.*, vol. 11, no. 9, pp. 2425–2433, 2009.
[18] S. Marozava, W. F. M. Röling, J. Seifert, R. Küffner, M. Von Bergen, and R. U. Meckenstock, "Physiology of Geobacter metallireducens under excess and limitation of electron donors. Part I. Batch cultivation with excess of carbon sources," *Syst. Appl. Microbiol.*, vol. 37, no. 4, pp. 277–286, 2014.
[19] L. C. Strong, C. Rosendahl, G. Johnson, M. J. Sadowsky, and L. P. Wackett, "Arthrobacter aurescens TC1 metabolizes diverse s-triazine ring compounds," *Appl. Environ. Microbiol.*,



vol. 68, no. 12, pp. 5973–5980, 2002.
[20] S. J. Pirt, "Maintenance energy: a general model for energy-limited and energy-sufficient growth," *Arch. Microbiol.*, vol. 133, no. 4, pp. 300–302, 1982.
[21] J. J. Heijnen, "Bioenergetics of microbial growth," *Encycl. bioprocess Technol.*, 1999.
[22] H. W. Van Verseveld, J. A. De Hollander, J. Frankena, M. Braster, F. J. Leeuwerik, and A. H. Stouthamer, "Modeling of microbial substrate conversion, growth and product formation in a recycling fermentor," *Antonie Van Leeuwenhoek*, vol. 52, no. 4, pp. 325–342, 1986.
[23] J. A. Nelder and R. Mead, "A Simplex Method for Function Minimization," *Comput. J.*, vol. 7, no. 4, pp. 308–313, 1965.
[24] R. Brun, P. Reichert, and H. R. Künsch, "Practical identifiability analysis of large environmental simulation models," *Water Resour. Res.*, vol. 37, no. 4, pp. 1015–1030, 2001.
[25] T. E. Oliphant, "Python for scientific computing," *Comput. Sci. Eng.*, vol. 9, no. 3, 2007.
[26] J. G. Speight and others, *Lange's handbook of chemistry*, vol. 1. McGraw-Hill New York, 2005.
[27] P. M. Gschwend and others, *Environmental organic chemistry*. John Wiley & Sons, 2016.
[28] N. Pfennig and S. Wagener, "An improved method of preparing wet mounts for photomicrographs of microorganisms," *J. Microbiol. Methods*, vol. 4, no. 5–6, pp. 303–306, 1986.
[29] J. R. Wiśniewski, A. Zougman, N. Nagaraj, and M. Mann, "Universal sample preparation method for proteome analysis," *Nat. Methods*, vol. 6, no. 5, p. 359, 2009.
[30] J. Merl, M. Ueffing, S. M. Hauck, and C. von Toerne, "Direct comparison of MS-based label-free and SILAC quantitative proteome profiling strategies in primary retinal Müller cells," *Proteomics*, vol. 12, no. 12, pp. 1902–1911, 2012.
[31] Y. Benjamini and Y. Hochberg, "Controlling the false discovery rate: a practical and powerful approach to multiple testing," *J. R. Stat. Soc. Ser. B*, pp. 289–300, 1995.
[32] J. S. Poindexter, "Fast and famine existence," *Adv. Microb. Ecol.*, vol. 5, pp. 63–89, 1981.
[33] H. V Westerhoff, K. J. Hellingwerf, and K. Van Dam, "Thermodynamic efficiency of microbial growth is low but optimal for maximal growth rate," *Proc. Natl. Acad. Sci.*, vol. 80, no. 1, pp. 305–309, 1983.
[34] H. V. Westerhoff, "Mosaic non-equilibrium thermodynamics and (the control of) biological free-energy transduction," 1983.
[35] M. T. Madigan, D. P. Clark, D. Stahl, and J. M. Martinko, *Brock Biology of Microorganisms 13th edition*. Benjamin Cummings, 2010.
[36] R. Otto, B. Brink, H. Veldkamp, and W. N. Konings, "The relation between growth rate and electrochemical proton gradient of Streptococcus cremoris," *FEMS Microbiol. Lett.*, vol. 16, no. 1, pp. 69–74, 1983.
[37] P. C. Maloney, "Membrane H+ conductance of Streptococcus lactis.," *J. Bacteriol.*, vol. 140, no. 1, pp. 197–205, 1979.
[38] R. López-Amorós, S. Castel, J. Comas-Riu, and J. Vives-Rego, "Assessment of E. coli and Salmonella viability and starvation by confocal laser microscopy and flow cytometry using rhodamine 123, DiBAC4 (3), propidium iodide, and CTC," *Cytom. Part A*, vol. 29, no. 4, pp. 298–305, 1997.
[39] R. Schumann, U. Schiewer, U. Karsten, and T. Rieling, "Viability of bacteria from different

aquatic habitats. II. Cellular fluorescent markers for membrane integrity and metabolic activity," *Aquat. Microb. Ecol.*, vol. 32, no. 2, pp. 137–150, 2003.

[40] M. Thullner, M. Kampara, H. H. Richnow, H. Harms, and L. Y. Wick, "Impact of bioavailability restrictions on microbially induced stable isotope fractionation. 1. Theoretical calculation," *Environ. Sci. Technol.*, vol. 42, no. 17, pp. 6544–6551, 2008.

[41] R. L. Tatusov, M. Y. Galperin, D. A. Natale, and E. V Koonin, "The COG database: a tool for genome-scale analysis of protein functions and evolution," *Nucleic Acids Res.*, vol. 28, no. 1, pp. 33–36, 2000.

[42] H. Nakayama, K. Kurokawa, and B. L. Lee, "Lipoproteins in bacteria: structures and biosynthetic pathways," *FEBS J.*, vol. 279, no. 23, pp. 4247–4268, 2012.

[43] D. E. LaRowe and J. P. Amend, "The energetics of anabolism in natural settings," *ISME J.*, vol. 10, no. 6, pp. 1285–1295, 2016.

[44] J. de Vossenberg, A. J. M. Driessen, and W. N. Konings, "Adaptations of the cell membrane for life in extreme environments," *Cell Mol. responses to Stress. Elsevier Sci. Ltd., Amsterdam*, pp. 71–88, 2000.

[45] C. P. Kempes, P. M. van Bodegom, D. Wolpert, E. Libby, J. Amend, and T. Hoehler, "Drivers of bacterial maintenance and minimal energy requirements," *Front. Microbiol.*, vol. 8, 2017.

[46] M. J. T. De Mattos and O. M. Neijssel, "Bioenergetic consequences of microbial adaptation to low-nutrient environments," *J. Biotechnol.*, vol. 59, no. 1, pp. 117–126, 1997.

[47] O. R. Sjøholm, O. Nybroe, J. Aamand, and J. Sørensen, "2, 6-Dichlorobenzamide (BAM) herbicide mineralisation by Aminobacter sp. MSH1 during starvation depends on a subpopulation of intact cells maintaining vital membrane functions," *Environ. Pollut.*, vol. 158, no. 12, pp. 3618–3625, 2010.

[48] J. L. C. M. Vossenberg, T. Ubbink-Kok, M. G. L. Elferink, A. J. M. Driessen, and W. N. Konings, "Ion permeability of the cytoplasmic membrane limits the maximum growth temperature of bacteria and archaea," *Mol. Microbiol.*, vol. 18, no. 5, pp. 925–932, 1995.



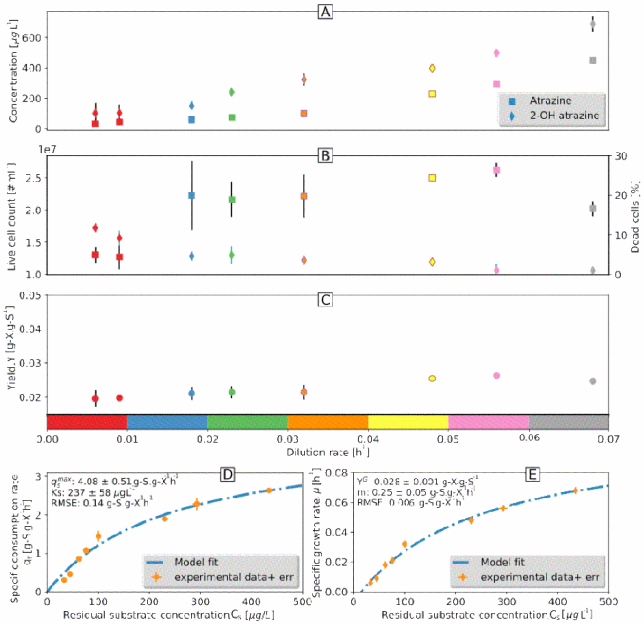


Figure 1: Growth parameters of *A. aurescens* TC1 plotted versus dilution rates indicate a high atrazine degradation capability under oligotrophic conditions and high maintenance demand. A: Live cell numbers per milliliter and percentage of dead cells; B: Concentration of residual atrazine and 2-OH atrazine C: Yield. D: The symbols indicate relationship between biomass-specific atrazine consumption rate ($q_S$) and residual substrate concentration at different dilution rates. The line indicates $q_s$ according to Michaelis-Menten type relation (eq. 3) using fitted growth parameters of maximum specific atrazine consumption rate ( $q_s^{max}$ ) and Monod affinity constant ($K_s$). E: The specific growth rates ($\mu$) dependence on substrate concentrations obtained experimentally is shown by symbols and the line indicates same relationship according to modified-Herbert-Pirt model (eq. 4) using fitted maintenance demand ($m_s$) and maximum growth yield ($Y_{x/s}^{max}$) . Data points represent the mean ± standard deviation of replicates.

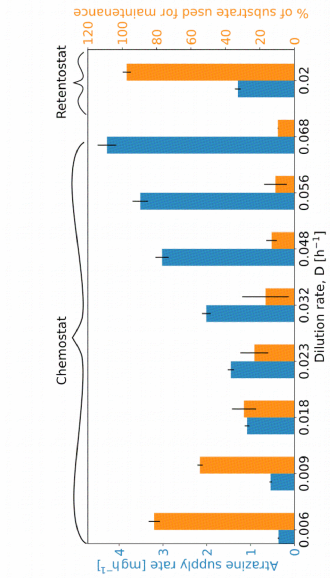


Figure 3: Allocation of energy fluxes to maintenance during chemostat and retentostat cultivation.

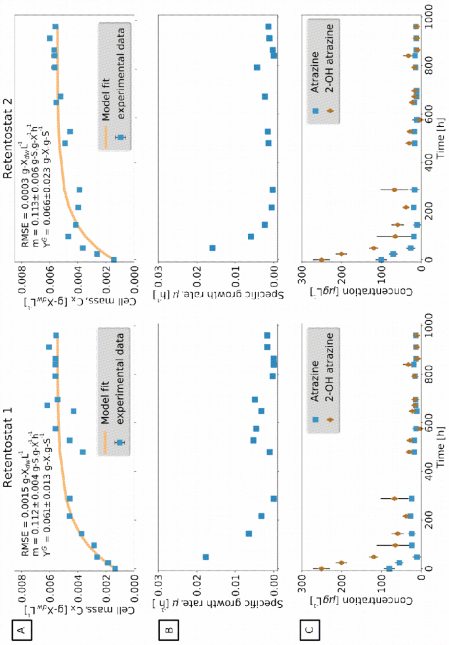


Figure 2: Retentostat cultivation reveals a different maintenance energy requirement of *A. aurescens* near zero growth rate in continuous culture with 100 % biomass retention. A: Measured biomass concentration (gdw/L) in retentostat 1 and 2 over time. Data points represent the mean ± standard deviation of duplicate samples. The line indicates biomass calculated with the fitted van Verseveld equation (Eq. 5). The fitted maintenance requirement is two times lower than in chemostat. B: Calculated specific growth rates ($h^{-1}$) over time. At the end of the experiment, near-zero growth condition was achieved corresponding to 225 days doubling time. C: Concentration of residual atrazine and its metabolite 2-OH atrazine were lower than in the chemostat experiment. Bars indicate the standard deviation of replicates.

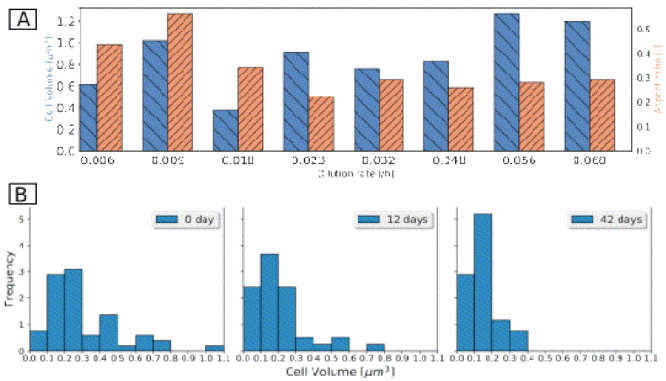


Figure 4: Morphological adaptation to limiting substrate condition in A. Chemostat and B. Retentostat. In chemostat, at low growth rates cells were smaller rods in comparison to high growth rates. In the retentostat, a transition from rod (0 d) to cocci shape was observed after 42 days at near-zero growth condition. This morphological change increases surface to volume ratio of the cells facilitating transport of substrates and nutrients.



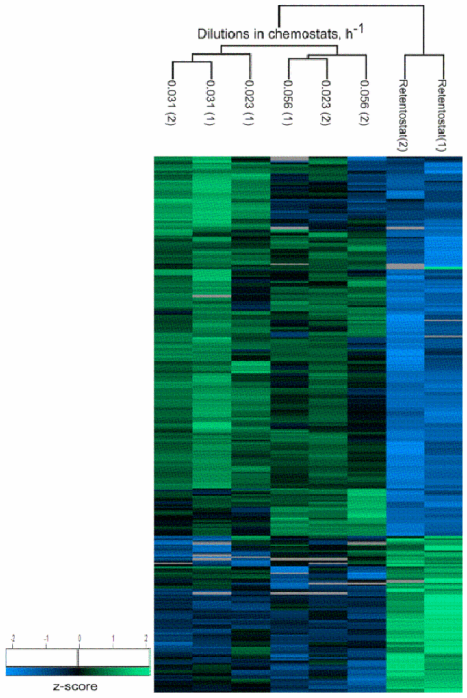


Figure 5: Heat map representing the clustering of differentially expressed proteins at dilution rates 0.023, 0.031, and 0.056/h relative to retentostat condition suggests allocation of energy flux is different in chemostat and retentostat. Proteins differentially expressed at least in one pairwise comparison (268 proteins) were used for heat map. Each chemostat and retentostat condition was performed in duplicates as indicated by dilution rates in the brackets above the heat map. Protein expression is displayed in the heat map as z-scores (i.e., calculated based on the mean and standard deviation of the protein) in the range between 2 (up-regulated, green) and -2 (down-regulated, blue).

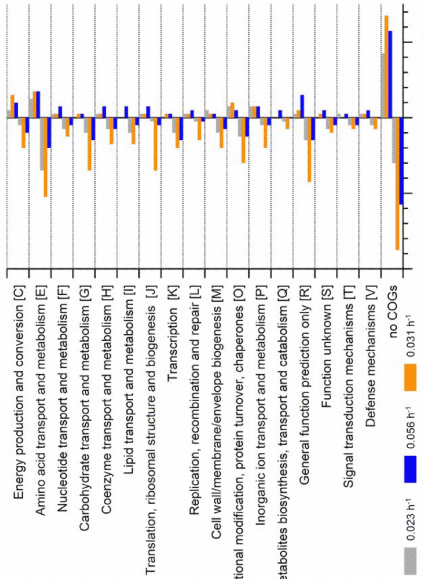


Figure 6: Distribution of significantly up-(shown as positive) and down-(shown as negative) regulated proteins across clusters of orthologous groups (COG) categories in retentostat relative to different dilution rates in chemostats (as indicated by different colors) suggests slow-down of metabolism under extreme energy limitation.



| Accession | Description | Rate of averaged protein abundance: Ret/D0.023 | Ret/D0.031 | Ret/D0.056 | p-values of corresponding pairwise comparisons: ret | ret | ret |
|---|---|---|---|---|---|---|---|
| | **Amino acid transport and metabolism** | | | | | | |
| A1R5B9 | Putative amino acid ABC transporter, permease protein | 0.03 | 0.03 | 0.06 | 0.04 | 0.03 | 0.07 |
| A1R8D0 | Putative L-asparagine permease | 0.25 | 0.08 | 0.29 | 0.20 | 0.23 | 0.21 |
| A1R3B2 | Aminotransferase, class I/II protein | 0.48 | 0.34 | 0.38 | 0.16 | 0.25 | 0.09 |
| A1R4B7 | Acetylornithine/succinyldiaminopimelate/ | 0.42 | 0.12 | 0.37 | 0.10 | 0.24 | 0.06 |
| A1R2R6 | Acetylornithine/succinyldiaminopimelate/ | 0.47 | 0.14 | 0.34 | 0.14 | 0.14 | 0.00 |
| A1R7M8 | Homoserine dehydrogenase | 0.47 | 0.74 | 0.79 | 0.10 | 0.10 | 0.14 |
| A1R3W0 | Pyridoxal-phosphate dependent enzyme | 0.01 | 0.01 | 0.02 | 0.04 | 0.03 | 0.05 |
| A1R8B4 | Serine hydroxymethyltransferase | 0.16 | 0.08 | 0.21 | 0.10 | 0.30 | 0.14 |
| A1R0Y6 | Putative glutamine amidotransferase | 0.33 | 0.20 | 0.32 | 0.07 | 0.30 | 0.07 |
| A1R8Z9 | Succinyldiaminopimelate desuccinylase | 0.06 | 0.11 | 0.22 | 0.03 | 0.23 | 0.09 |
| A1R5B6 | Putative amino acid permease | 0.09 | 0.08 | 0.18 | 0.03 | 0.21 | 0.05 |
| A1R4J6 | Putative branched-chain amino acid transport system, permease | 0.14 | 0.11 | 0.26 | 0.04 | 0.22 | 0.11 |
| A1R7C3 | Putative amino acid permease | 0.12 | 0.10 | 0.22 | 0.03 | 0.22 | 0.09 |
| A1R1D3 | Amino acid permease-like protein | 0.14 | 0.10 | 0.23 | 0.03 | 0.23 | 0.09 |
| A1R4T6 | O-acetylhomoserine sulfhydrylase | 0.29 | 0.26 | 0.34 | 0.15 | 0.28 | 0.05 |
| A1R8B7 | Glutamate permease | 0.18 | 0.19 | 0.19 | 0.3 | 0.32 | 0.01 |
| A1R8B8 | Glutamate permease | 0.22 | 0.23 | 0.29 | 0.04 | 0.28 | 0.05 |
| A1R4P9 | Putative 3-oxoacid CoA-transferase | 25.11 | 1829.52 | 42.56 | 0.11 | 0.23 | 0.27 |
| A1R2V6 | Putative amino acid decarboxylase, pyridoxal-dependent enzyme | 25.62 | 46.34 | 23.69 | 0.13 | 0.21 | 0.08 |
| A1R4E0 | Aminotransferase, class I/II protein | 4.23 | 1.39 | 7.01 | 0.14 | 0.25 | 0.08 |
| A1R4Z7 | Aspartate aminotransferase | 3.35 | 1.54 | 5.11 | 0.16 | 0.28 | 0.09 |
| A1R5S9 | Aminotransferase, class V | 3.35 | 1.26 | 5.09 | 0.15 | 0.23 | 0.06 |
| | **Carbohydrate transport and metabolism** | | | | | | |
| A1R2F7 | Putative ABC-type sugar transport system, permease component | 0.02 | 0.01 | 0.07 | 0.15 | 0.28 | 0.13 |
| A1R7C8 | Glyceraldehyde-3-phosphate dehydrogenase | 0.35 | 0.27 | 0.50 | 0.19 | 0.34 | 0.15 |
| A1R4S7 | Putative sugar ABC transporter, permease protein | 0.29 | 0.38 | 0.13 | 0.38 | 0.26 | 0.04 |
| | **Inorganic ion transport and metabolism** | | | | | | |
| A1R8R8 | P-type ATPase, cation transport | 647.25 | 791.11 | 34.29 | 0.13 | 0.22 | 0.09 |
| A1R6T1 | Putative ABC transporter, transport system, | 4.51 | 6.16 | 4.90 | 0.17 | 0.34 | 0.16 |
| A1R7Y7 | Putative cation ABC transporter, ATP-binding protein | 4.09 | 6.09 | 2.90 | 0.12 | 0.26 | 0.14 |
| A1R7C9 | Putative ABC transporter, ATP-binding protein | 3.13 | 2.58 | 4.69 | 0.08 | 0.15 | 0.08 |
| A1R5K7 | Putative membrane protein, cell surface res stance | 0.36 | 0.29 | 0.55 | 0.10 | 0.25 | 0.15 |
| A1R7B2 | Potassium/quanidocitial sialein-like family protein | 0.04 | 0.03 | 0.03 | 0.13 | 0.22 | 0.08 |
| A1R4D0 | Copper-translocating P-type ATPase | 0.08 | 0.06 | 0.18 | 0.17 | 0.34 | 0.16 |
| A1R3P5 | Phosphate-specific transport system accessory protein PhoU | 0.09 | 0.16 | 0.19 | 0.04 | 0.24 | 0.07 |
| | **Nucleotide transport and metabolism** | | | | | | |
| A1R1D6 | Uracil-xanthine permease | 0.08 | 0.08 | 0.47 | 0.13 | 0.32 | 0.23 |
| A1R7P3 | Putative nucleoside 2-deoxyribosyltransferase | 0.43 | 0.70 | 0.61 | 0.12 | 0.36 | 0.13 |
| A1R8Z | Adenylate kinase | 0.25 | 0.15 | 0.51 | 0.04 | 0.24 | 0.03 |
| | **Translation, ribosomal structure and biogenesis** | | | | | | |
| A1R8E5 | 30S ribosomal protein S5 | 0.37 | 0.23 | 0.56 | 0.12 | 0.24 | 0.23 |
| A1R8W6 | 30S ribosomal protein S11 | 0.31 | 0.04 | 1.66 | 0.50 | 0.33 | 0.72 |
| A1R8T4 | 50S ribosomal protein | 0.55 | 0.17 | 1.01 | 0.39 | 0.39 | 0.92 |
| A1R6X0 | 30S ribosomal protein S20 | 0.09 | 0.03 | 0.61 | 0.13 | 0.23 | 0.61 |
| A1R8U3 | 50S ribosomal protein L23 | 0.25 | 0.12 | 0.65 | 0.13 | 0.23 | 0.58 |
| A1R7W7 | 50S ribosomal protein L27 | 0.25 | 0.11 | 0.69 | 0.23 | 0.34 | 0.65 |
| A1R8Z1 | 30S ribosomal protein S14 | 0.07 | 0.02 | 0.54 | 0.24 | 0.28 | 0.73 |
| A1R8Y… | 30S ribosomal protein S7 | 0.30 | 0.14 | 0.71 | 0.22 | 0.34 | 0.68 |
| A1R8U… | 30S ribosomal protein S19 | 0.08 | 0.00 | 0.11 | 0.18 | 0.24 | 0.14 |
| A1R8S8 | 50S ribosomal protein L33 | 0.12 | 0.06 | 0.30 | 0.07 | 0.22 | 0.17 |
| A1R8N1 | Ribosomal protein S1 aa N-acetyltransferase | 0.23 | 0.20 | 0.18 | 0.06 | 0.24 | 0.04 |
| A1R568 | 50S ribosomal protein L21 | 0.22 | 0.19 | 0.21 | 0.16 | 0.24 | 0.05 |
| A1R4Q1 | 50S ribosomal protein L31 | 0.38 | 0.19 | 0.49 | 0.19 | 0.28 | 0.10 |
| | **Energy production and conversion** | | | | | | |
| A1R8A1 | NADH dehydrogenase | 0.33 | 0.12 | 0.26 | 0.17 | 0.28 | 0.05 |
| A1R5C7 | Aldehyde ferredoxin oxidoreductase, MOW family | 0.31 | 0.23 | 0.26 | 0.17 | 0.23 | 0.04 |
| A1R6J3 | Cytochrome c oxidase | 0.29 | 0.25 | 0.41 | 0.17 | 0.24 | 0.15 |
| A1R4B4 | Putative ferredoxin reductase | 27.51 | 54.11 | 20.47 | 0.13 | 0.31 | 0.03 |
| A1R4V5 | Putative iron-sulfur cluster-binding protein, rieske family | 2.95 | 1.84 | 8.41 | 0.19 | 0.17 | 0.06 |
| A1R7K1 | Pyruvate dehydrogenase E1 component | 0.19 | 0.16 | 0.44 | 0.16 | 0.23 | 0.11 |
| | **Putative cell wall related proteins** | | | | | | |
| A1R4J3 | Putative lipoprotein | 24.80 | 54.15 | 53.94 | 0.13 | 0.31 | 0.01 |
| A1R4K2 | Putative lipoprotein, putative | 6.21 | 24.79 | 24.76 | 0.12 | 0.29 | 0.04 |
| A1R1L8 | Putative lipoprotein | 14.55 | 16.95 | 27.10 | 0.15 | 0.28 | 0.03 |
| A1RCC1 | Putative lipoprotein | 5.41 | 4.13 | 7.27 | 0.04 | 0.24 | 0.03 |
| | **Enzyme transformation** | | | | | | |
| A1RCK5 | Hydroxylamine reductase | 2.59 | 2.40 | 3.68 | 0.10 | 0.15 | 0.05 |



Table 1: Selected proteins from Fig.5 with the indication of their annotation, ratios of averaged abundances in corresponding pairwise comparison and p-values. p-values <0.05 or=0.05 are significant. Underlined proteins are proteins which were significantly unregulated in retentostats.

**Supplementary material**

Table S1: Distribution of energy flux to maintenance during chemostat and retentostat cultivation. D-Dilution rate, HRT-Hydraulic retention time.

**Chemostat**

| D ($h^{-1}$) | HRT (h) | Atrazine supply rate mg $h^{-1}$ | % of flux used for maintenance |
|---|---|---|---|
| 0.006 | 166 | 0.36 | 81 |
| 0.009 | 111 | 0.54 | 54 |
| 0.018 | 55 | 1.08 | 29 |
| 0.023 | 43 | 1.45 | 23 |
| 0.032 | 31 | 2.01 | 16 |
| 0.048 | 20 | 3.02 | 13 |
| 0.056 | 17 | 3.52 | 10. |
| 0.068 | 14 | 4.28 | 9. |

**Retentostat**

| D (/h) | Time (h) | Atrazine supply rate mg $h^{-1}$ | % of flux used for maintenance |
|---|---|---|---|
| 0.02 | 0 | 1.29 | 26 |
| 0.02 | 216 | 1.29 | 73. |
| 0.02 | 528 | 1.29 | 84 |
| 0.02 | 912 | 1.29 | 97 |




Figure S1: Heat map representing the clustering of 1627 proteins detected in all analyzed conditions: at dilution rates 0.023, 0.031, and 0.056/h and retentostat. Each chemostat and retentostat condition was performed in duplicates as indicated by dilution rates in the brackets above the heat map. Protein expression is displayed in the heat map as z-scores (i.e., calculated based on the protein's mean and standard deviation) in the range between 2 (up-regulated, green) and -2 (down-regulated, blue).





mm Pt-100 temperature sensor was used to monitor the temperature inside the

bioreactor. The bioreactor was kept at room temperature (25 °C). The culture volume was kept constant at 2000 mL with a level sensor.

**C: 1.3 Determining concentrations with HPLC-UV-DAD**

Atrazine and 2-hydroxyatrazine concentrations in the bioreactor were measured using a Prominence HPLC system (Shimadzu Corp., Japan) together with a 100 x 4.6 mm Kinetex 5 µ Biphenyl 100 Å column equipped with a SecurityGuard ULTRA Biphenyl cartridge (both Phenomenex Inc., USA). The injected sample volume was 50 µL. Peak separation was achieved by 1 mL/min isocratic flow of 51 % 5 mM $KH_2PO_4$ buffer pH 7 and 49 % methanol for 9 min. The compounds were detected by UV absorbance at 222 nm and the peaks were quantified using LabSolutions V 5.71 SP2 (Shimadzu Corp., Japan). HPLC standards contained atrazine and 2-hydroxyatrazine (Riedel-de Haën, supplied by Sigma Aldrich, Germany) dissolved in 25 % methanol and 75 % water. Standard concentrations were 10.5, 21, 63, and 210 µg/L for atrazine and 7, 14, 42, and 140 µg/L for 2-hydroxyatrazine.

**C: 1.4 Cell counting by flow cytometry**

To count the cells, they were first fixed with 2.5 % glutaraldehyde, then stained with SYBR Green I (total cells) and propidium iodide (dead cells). To compare measurements over the long cultivation period, reference beads (Trucount™ Absolute Counting Tubes, BD Bioscience, USA) were added to the samples in two technical replicates. The cells were counted on a Cytomics FC 500 flow cytometer (Beckmann Coulter, Germany) equipped with a 488 nm (40 mW) and a 638 nm (25 mW) laser. For detection following parameters were applied: SYBR Green I: discriminator FL1 (green fluorescence) /0, forward scatter 178 V/ gain 2.0, side scatter 624 V/ gain 2.0, FL1 397 V/ gain 1.0, and FL3 (red fluorescence) 572 V/ gain 1.0. Propidium iodide: discriminator FL3 /1, forward scatter 745 V/ gain 1.0, side scatter 693 V/ gain 2.0, FL1 350/ gain 1.0, FL2 (yellow fluorescence) 527 V/ gain 1.0, and FL3 517 V/ gain 1.0. The data was analyzed with CXP software (version 2.2; Beckmancoulter, Germany).

**C: 1.5 Microscopy**

The fixed cells were analyzed on agar glass slides by light microscopy with an Axioscope 2 Plus microscope (Carl Zeiss AG, Germany). For imaging, pictures were

taken with the digital camera AxioCam HRm (Carl Zeiss AG, Germany) and the software AxioVision (Version 4.8.2; Carl Zeiss AG, Germany).

### C: 1.6 Determination of carbon and nitrogen enrichment factors

The GC-IRMS system consisted of a TRACE GC Ultra gas chromatograph (GC; Thermo Fisher Scientific, Milan, Italy) linked to a Finnigan MAT 253 isotope ratio mass spectrometer (IRMS) (Thermo Fisher Scientific, Germany) by a Finnigan GC Combustion III Interface (Thermo Fisher Scientific, Germany). The emission energy was set to 1.5 mA for carbon isotope analysis and 2 mA for nitrogen isotope analysis. Helium (grade 5.0) was used as carrier gas and the injector was controlled by an Optic 3 device (ATAS GL, distributed by Axel Semrau, Germany). The samples were injected using a GC Pal autosampler (CTC, Switzerland) onto a 60-m DB-5 (60 m × 0.25 mm; 1 µm film; Restek GmbH, Germany) analytical column. An on-column liner (custom made by a glassblower) was pressed directly onto a CS-fused-silica-methyl-sil retention gap (3 m × 0.53 mm inner diameter) (Chromatographie Service GmbH, Germany).

Isotope values were determined as $\delta^{13}C$ and $\delta^{15}N$ values in per mill relatively to Vienna PeeDee Belemnite (V-PDB)[77], and Air-$N_2$[78]. The $\delta^{13}C$ and $\delta^{15}N$ values were assessed in relation to a monitoring gas ($CO_2$ and $N_2$, respectively) which was measured alongside each run at the beginning and the end. Calibration of monitoring gases was performed in a Finnigan MAT Delta S isotope ratio mass spectrometer with dual inlet system (Thermo Fisher Scientific, Germany). The gases were measured against V-PDB and air, respectively, by use of international reference materials: the $CO_2$ gases RM 8562, RM 8563, and RM 8564 for $CO_2$ and NSVEC ($N_2$ gas) for $N_2$. Reference standards were provided by the IAEA.

The GC oven started at 35 °C (hold 30 s), ramp 5 °C/min to 80 °C to ensure complete solvent evaporation during the transfer of the sample from the retention gap to analytical column. This was followed by a temperature ramp of 100 °C/min to 160 °C, a ramp of 10 °C/min to 220 °C, then a ramp 2 °C/min up to 250 °C. The initial injector temperature at the Optic 3 was set to 40 °C, 300 s hold, then ramped to 250 °C at 2 °C/s. The initial column flow was set to 0.3 mL/min (hold 120 s), then ramped to 1.4 mL/min within 120 s so that a flow of 1.4 mL/min was established before the GC temperature was raised.

Isotopic enrichment factors were determined by determining the difference of the isotope ratios between the inflow and the outflow: Alternating measurements of the inflow and the bioreactor multiple times allowed the determination of the difference

without additional uncertainty of the instrument. The obtained values for the replicates at each residual atrazine concentration were compared by a two-sample t-test. For statistically indistinguishable replicates ($p > 0.1$) the individual values were combined and the average, standard error of mean, and the 95 % confidence intervals were calculated.

**C: 1.7 Growth in fed batch**

Empty 200 mL erlenmayer flasks were autoclaved and 150 µL of a 10 g/L atrazine solution in ethyl acetate were added each. The ethyl acetate was evaporated under a sterile nitrogen stream to yield 1.5 mg solid atrazine in each flask. 75 mL of mineral salt media (see above) were added to the first flask and the atrazine was dissolved by shaking for 24 h. A fresh culture of *Arthrobacter aurescens* TC1 was used to inoculate with a known amount of biomass. The degradation was followed by HPLC concentration measurements and cell counting by flow cytometry (see above). Upon atrazine consumption, the media was transferred to a new flask for two times. After both, atrazine and 2-hydroxyatrazine, had been consumed, the biomass was determined.

## C: 2 Supporting Information Figures and Tables

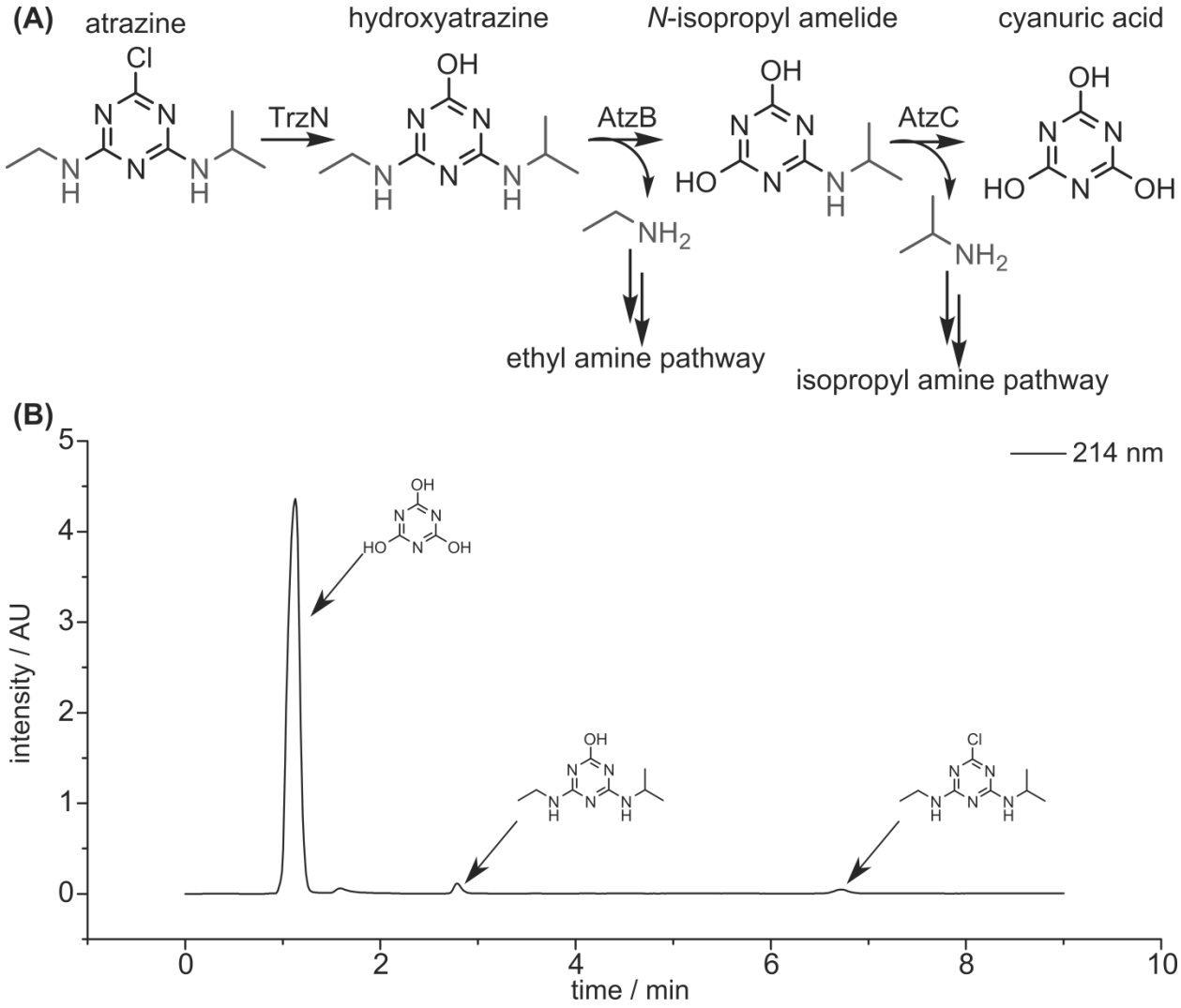


**Figure C1: Atrazine metabolism of *Arthrobacter aurescens* TC1. (A)** Atrazine is first hydrolyzed by TrzN to hydroxyatrazine. Then, ethyl amine is cleaved of by hydrolysis with AtzB and AtzC catalyses the hydrolysis to cyanuric acid and cleaves of isopropylamine. Both, ethyl amine and isopropyl amine, are further metabolized [63]. Cyanuric acid is not further degraded and accumulates in the medium. **(B)** High pressure liquid chromatography (HPLC) chromatogram of bioreactor samples with detection of analytes by their UV absorbance at 222 nm. The atrazine of the inflow is almost quantitatively degraded to cyanuric acid (>99.5 % degradation). Hydroxyatrazine (retention time 2.7 min) and atrazine (retention time 6.8 min) are detected and can be quantified via external calibration.

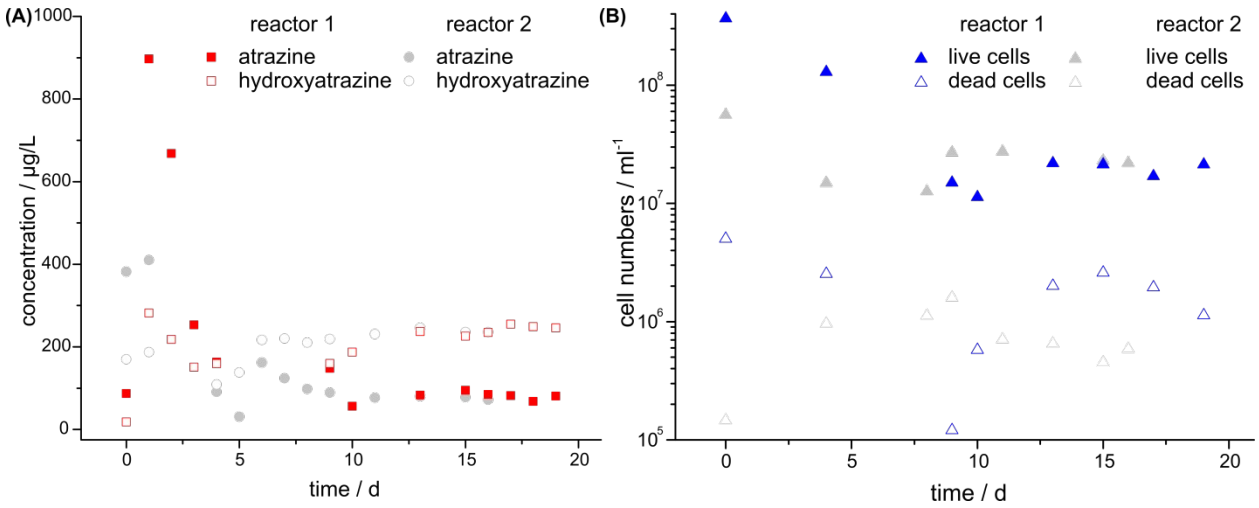


**Figure C2: Growth of *Arthrobacter aurescens* TC1 in aerobic, atrazine limited chemostat during initial high dilution rate.** (A) Residual concentrations of atrazine and the first metabolite 2-hydroxyatrazine. The reactors achieved steady state after 13 and 10 days, respectively, with approximately identical atrazine and hydroxyatrazine concentrations. Samples for isotope analysis were taken at the end of the cultivation (replicate 1: day 19; replicate 2: day 16) (B) cell numbers during cultivation in chemostat.

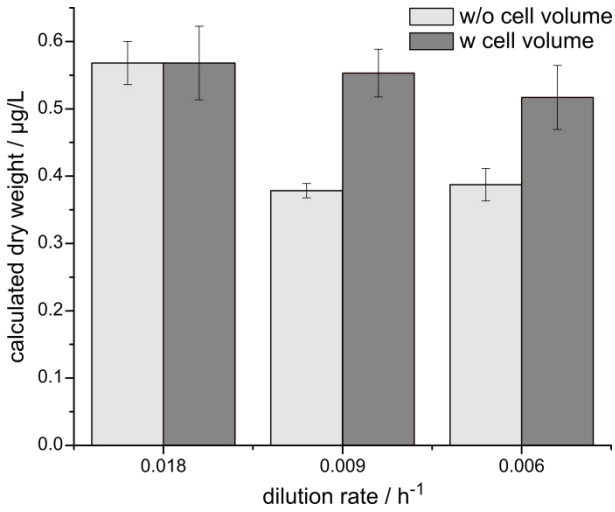

**Figure C3: Calculated dry weight for three dilution rates** (± SD): Since the biomass in the bioreactor was too low for a direct determination, the dry weight was instead calculated (i) by multiplying the cell number with the dry weight per cell reported by Strong *et al.* [63] and (ii) by correcting this number in addition with the observation that cell volumes increased at low dilution rates. According to (i) a decreased cell number at low dilution rates ($\mu_{low}$ and $\mu_{min}$) would lead to a decreased biomass ("w/o cell volume"), whereas after consideration of the increased cell volume (ii) the biomass is constant for all dilution rates.

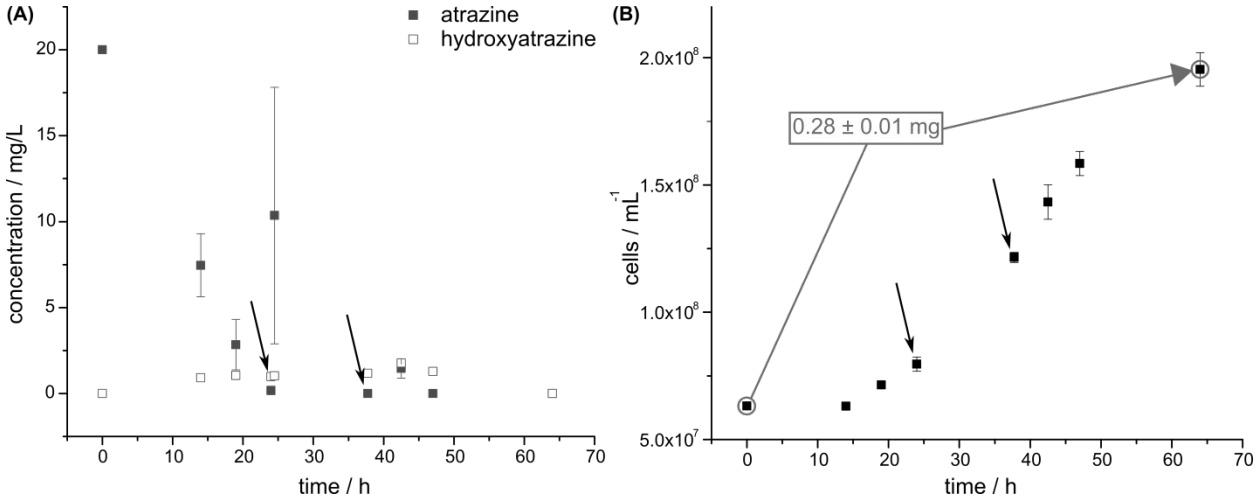


**Figure C4: Growth of *Arthrobacter aurescens* TC1 on atrazine in fed batch.** (± SD) (A) Residual concentration of atrazine and its first metabolite 2-hydroxyatrazine. The black arrows indicate time points at which the media was exchanged. The variability of the atrazine concentrations is quite high due to slightly different atrazine dissolution upon atrazine addition (black arrows). In contrast, the hydroxyatrazine concentration is similar in the replicates indicating similar degradation and metabolic activity and thus similar growth. This is also verified by the cell numbers (B). The dry weight was measured in the beginning and in the end of the cultivation. Degradation of 4.5 mg atrazine equals an uptake of 1.05 mg carbon leading to formation of 0.28 ± 0.01 mg biomass. This corresponds to a yield of Y = 0.27 ± 0.01 $g_{biomass}$/ $g_{carbon}$.

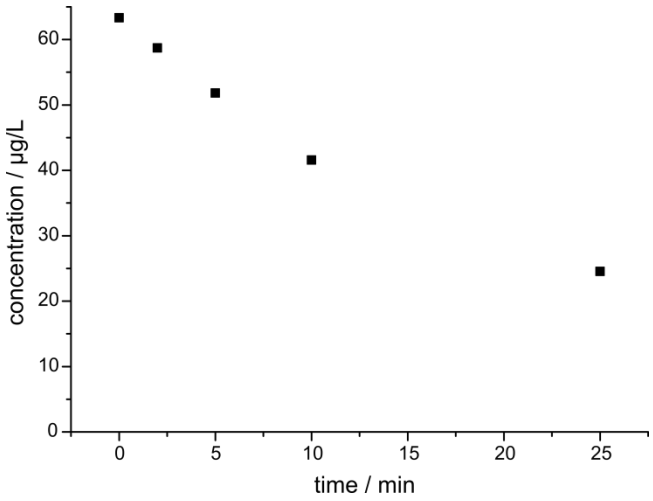


**Figure C5: Degradation of atrazine in a sample taken from the bioreactor when not sterilized by filtration immediately.** This degradation would lead to isotope fractionation and thus a change in the measured concentrations and isotope ratios of bioreactor samples in the time span before filtration. Since samples were filter-sterilized after at most 1 minute, the data indicates that such degradation-induced artifacts were always lower than 5 %.

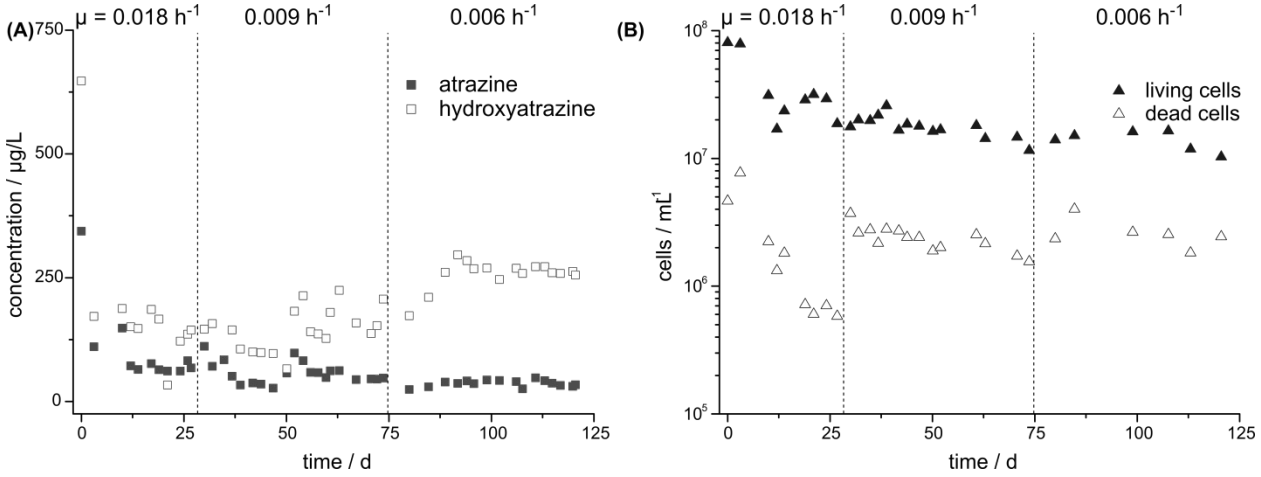


**Figure C6: Growth of *Arthrobacter aurescens* TC1 in aerobic, atrazine limited chemostat during stepwise decrease of the dilution rate - replicate 2.** (A) Residual concentration of atrazine and the first metabolite 2-hydroxyatrazine. (B) Cell numbers in chemostat. Both, residual atrazine concentrations and cell numbers are identical to the values of the first biological replicate. In day 46 of the cultivation, we observed that the flow rate was decreased due to a pump failure and thus a dilution rate lower than the desired dilution rate of $\mu$ = 0.009 $h^{-1}$

was the consequence. Upon adjustment and calibration of the pump, it took two weeks to achieve steady state again.

**Table C1 Concentration comparison of numerical model with and without a bioavailability term**

| | experimental | model with bioavailability term | | model without bioavailability term | |
|---|---|---|---|---|---|
| dilution rate / $h^{-1}$ | c(atrazine) / $\mu gL^{-1}$ | c(atrazine) / $\mu gL^{-1}$ | offset / $\mu gL^{-1}$ | c(atrazine) / $\mu gL^{-1}$ | offset / $\mu gL^{-1}$ |
| 0.018 | 61.5 | 58.3[1] | 3.2 | 45.3 | -16.2 |
| 0.009 | 44.5 | 50.7[2] | 6.2 | 20.6 | -23.9 |
| 0.006 | 31.9 | 33.5[2] | 2.4 | 13.4 | -18.9 |

[1] $k_{tr}$ = 0.0125 $s^{-1}$ (onset of mass transfer limitation) [2] $k_{tr}$ = 0.025 $s^{-1}$ (strong mass transfer limitation)

The residual atrazine concentrations in the chemostat calculated by the numerical model for the different dilution rates are compared with experimental values. The model without bioavailability term overestimates the degradation. In contrast, by including a bioavailability term, the concentrations of the numerical model match the experimental values. Two different values for the mass transfer term were used to mimic potential bacterial adaptation: $k_{tr}$ = 0.0125 $s^{-1}$ (onset of mass transfer limitation at c(atrazine) = 58.3 µgL-1); $k_{tr}$ = 0.025 s-1 (strong mass transfer limitation at c(atrazine) = 33.3 to 50.7 µgL-1).

# Appendix D: Supporting Information Chapter 4

## D: 1 Experimental Section

### D: 1.1Chemicals

Chemicals used were atrazine (97 %, Cfm Oskar Tropitzsch GmbH), potassium dihydrogenphosphate (99 %, AppliChem), sodium hydrogenphosphate (98 %, Sigma Aldrich), sodium hydroxide (99 %, Sigma Aldrich), potassium nitrate (99 %, Merck), ammonium sulfate (99.5 %, Sigma Aldrich), magnesium sulfate heptahydrate (99 %, Fluka), calcium chloride dihydrate (94 %, Roth), boric acid (99.8 %, Merck), manganese sulfate monohydrate (99 %, Sigma Aldrich), copper sulfate pentahydrate (99 %, Merck), zinc chloride (99 %, Fisher Scientific), cobalt chloride hexahydrate (99 %, Merck) sodium molybdate dihydrate (99.5 %, Merck), iron chloride hexahydrate (98 %, Sigma Aldrich), and potassium cyanide (99 %, Merck). Solvents used were ethyl acetate (99.7 %, Sigma Aldrich), dichloromethane (99.9 %, Roth), and methanol (99.9 %, Sigma Aldrich).

### D: 1.2 Media preparation

For the mineral salt media, MilliQ water with a low total organic carbon content of <10 µg/L was used. First 100X and 1000X solutions of the respective salts were prepared. 136 g $KH_2PO_4$ and 178 g $Na_2HPO_4 \cdot 2\ H_2O$ were dissolved in 1 L water and the pH was adjusted with NaOH topH = 7.2 and autoclaved to give the 100X buffer solution. Furthermore 5 g $KNO_3$, 23.8 g $(NH_4)_2SO_4$, 5 g $MgSO_4 \cdot 7\ H_2O$ and 1.32 g $CaCl_2 \cdot 2\ H_2O$ were dissolved in 1 L water and autoclaved to give the 100X mineral solution. To give the 1000X trace element solution, 2.86 g $H_3BO_3$, 1.54 g $MnSO_4 \cdot H_2O$, 0.039 g $CuSO_4 \cdot 5\ H_2O$, 0.021 g $ZnCl_2$, 0.041 g $CoCl_2 \cdot 6\ H_2O$, and 0.025 g $Na_2MoO_4 \cdot 2\ H_2O$ were dissolved in1 L water and autoclaved. Furthermore, a 1000X iron solution was prepared by dissolving 0.514 g $FeCl_3 \cdot 6\ H_2O$ in water and filter sterilization (0.22µm, PES). Empty 5 L bottles containing only a magnetic stir bar were autoclaved. Then, 15 mL of a solution of 10 g/L atrazine in ethyl acetate were added to each bottle and the ethyl acetate was evaporated under a sterile nitrogen stream to leave 150 mg solid atrazine. Afterwards, the solid atrazine was dissolved again in 5 L autoclaved water by stirring 48

h on a magnetic stirrer. This 30 mg/L atrazine solution was filter sterilized (0.22 µm, PES) to remove remaining atrazine particles. Finally, 50 mL 100X buffer solution, 50 mL 100X mineral solution, 5 mL 1000X trace element solution, and 5 mL 1000X iron solution were added.

## D: 2Supporting Figures and Table

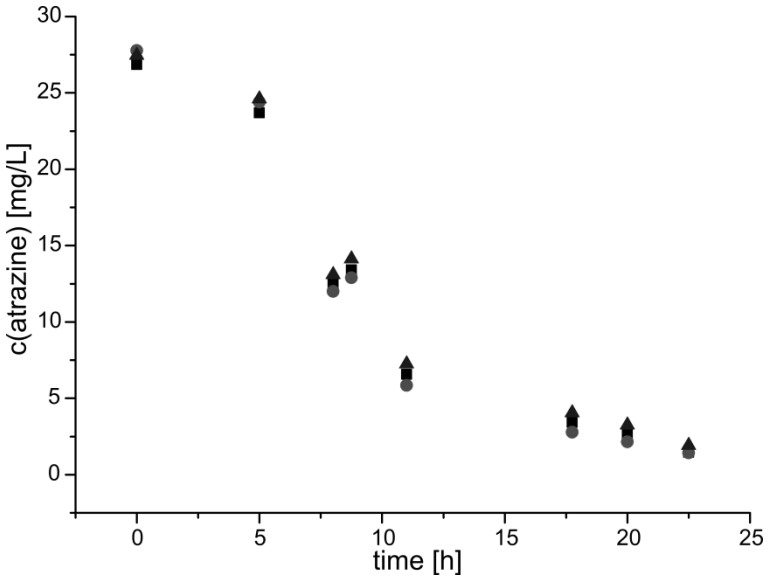


**Figure D1: Atrazine degradation by whole cells of *Polaramonas sp.* Nea-C of three biological replicates.**

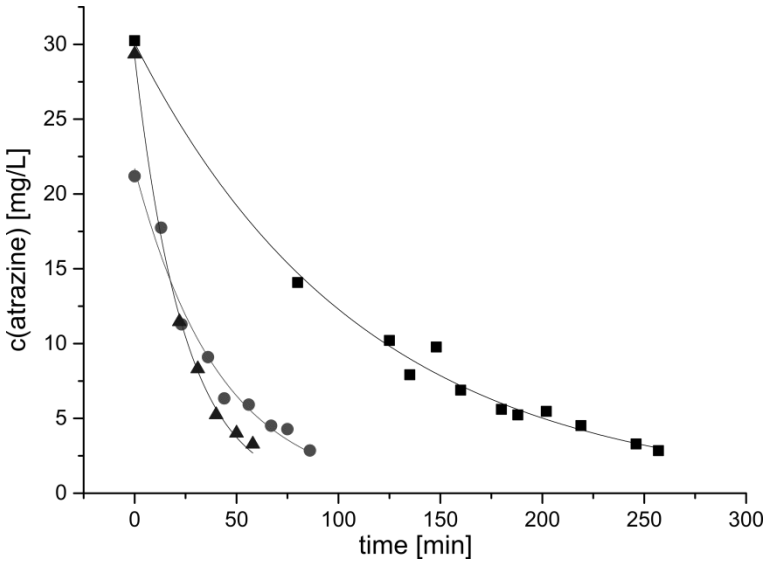


**Figure D2: Atrazine degradation by cell free extracts of three biological replicates.** The different degradation rates are a consequence of imperfect cell lysis in the french pressure cell.

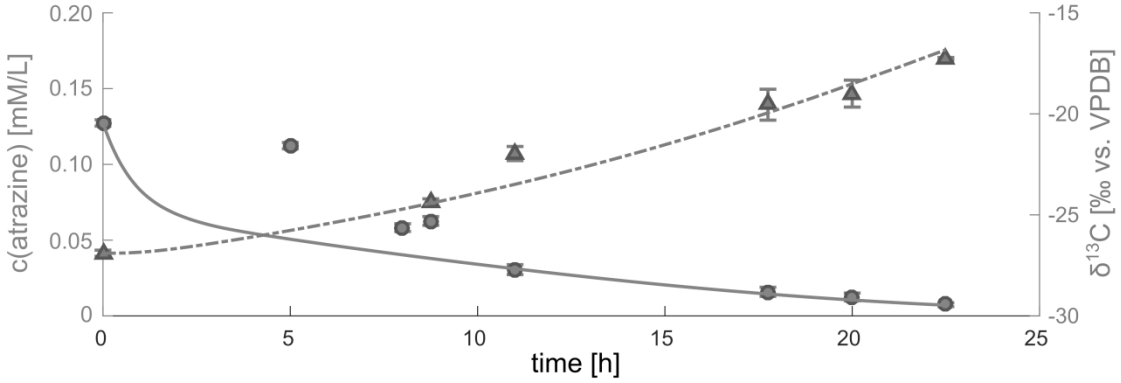


**Figure D3: Solution and fit of the experimental data including a bioavailability term.** The right axis illustrates the δ13C data (blue) and the left one shows the atrazine concentrations (orange). This led to estimation of $k_{tr}$ = 0.16 ± 0.02 × $10^{-3}$ $s^{-1}$ and $q_{max}$ = 2.7 ± 1.4 nmol $L^{-1}s^{-1}$. The norm of residuals for this fit is 2.3 × $10^{-8}$.

**Table D1: Similarity of published sequences of the atrazine hydrolase gene *trzN***

| Species | accession number | similarity [%] | coverage [%] |
|---|---|---|---|
| *Nocardioides sp.* MTD22 | AB427183.1 | 99.9 | 100 |
| *Arthrobacter sp.* AD26-2 | EU400620.1 | 99.9 | 100 |
| *Arthrobacter sp.* AD26 | EU091479.1 | 99.9 | 100 |
| *Arthrobacter sp.* AD25 | DQ989289.1 | 99.9 | 100 |
| *Arthrobacter sp.* ZXY-2 | CP017421.1 | 99.8 | 100 |
| *Acinetobacter lwoffii* | JQ360632.1 | 99.8 | 100 |
| *Pseudomonas sp.* AD39 | FJ161692.1 | 99.8 | 100 |
| *Arthrobacter sp.* DNS10 | KF453507.1 | 99.7 | 100 |
| *Arthrobacter sp.* T3AB1 | GU459314.1 | 99.7 | 100 |
| *Nocardioides sp.* AN3 | AB427184.1 | 99.7 | 100 |
| *Arthrobacter sp.* AD30 | FJ161691.1 | 98.8 | 100 |
| *Arthrobacter sp.* C3 | KR263873.1 | 98.7 | 93.3 |
| *Citricoccus sp.* | MF063313.1 | 99.8 | 33.3 |
| *Nocardioides sp.* DN36 | AB539567.1 | 100 | 31.5 |
| *Arthrobacter sp.* T3AB1 | KR349129.1 | 100 | 31.4 |
| Bacterium TN43 clone B | KT346393.1 | 99.8 | 31.5 |
| Bacterium TN98 clone II | KP339975.1 | 100 | 31.3 |
| *Nocardioides sp.* SP12 | AF537328.1 | 99.8 | 31.5 |
| Bacterium TN98 clone I | KP339976.1 | 99.3 | 31.1 |
| *Nocardioides sp.* CMU5 | EF088652.1 | 100 | 28.2 |

# Appendix E: Supporting Information Chapter 5

## E: 1 Supporting experimental section

### E: 1.1 Chemicals and media composition

The following chemicals were used in the liposome permeation study: glyphosate (98%, Sigma Aldrich), $D_2O$ (99.9%, Sigma Aldrich), sodium hydroxide (97%, Fisher scientific), 1-palmitoyl-2-oleoyl-*sn*-glycero-3-phosphocholine (99%, Avanti Polar Lipids), praseodymium(III)-chloride (99.99%, Fisher scientific), and 3-(trimethylsilyl)-2,2,3,3-tetradeuteropropionic acid (98 atom % D, Sigma Aldrich).

The following chemicals were used for the isolation of *Ochrobactrum sp*. FrEM and for glyphosate degradation: glyphosate (99%, Sigma Aldrich), ammonium acetate (99%, Sigma Aldrich), sodium glutamate (99%, Sigma-Aldrich), sodium peroxodisulfate (99%, Fluka), potassium hydroxide (99%, Fluka), phosphoric acid (99%, Fluka), , potassium dihydrogenphosphate (99%, AppliChem), sodium hydrogenphosphate (98%, Sigma Aldrich), sodium hydroxide (99%, Sigma Aldrich), potassium sulfate (99%, Merck), ammonium chloride (99.5%, Sigma Aldrich), magnesium sulfate heptahydrate (99%, Fluka), calcium chloride hexahydrate (94%, Roth), boric acid (99.8%, Merck), manganese sulfate monohydrate (99%, Sigma Aldrich), zinc sulfate heptahydrate (99%, Fisher Scientific), nickel chloride hexahydrate (99%, Merck) sodium molybdate dihydrate (99.5%, Merck), and iron sulfate heptahydrate (98%, Sigma Aldrich).

The medium contained (in $gL^{-1}$): $NH_4Cl$, 2.0; $MgSO_4 \times 7\ H_2O$, 0.2; $K_2SO_4$, 0.5; as well as trace elements (in $mgL^{-1}$): $FeSO_4 \times 7H_2O$, 2.5; $CaCl_2 \times 6H_2O$,10.0; $CuSO_4 \times 5H_2O$, 2.0; $H_3BO_3$, 0.06; $ZnSO_4 \times 7\ H_2O$,20.0; $MnSO_4 \times H_2O$, 1.0; $NiCl_2 \times 6H_2O$, 0.05; $Na_2MoO_4 \times 2H_2O$, 0.3.

### E: 1.2 Bacterial isolation and characterization

The soil samples were collected from different plots (and later combined) on a vineyard site in northern France (Agricultural and Viticultural College of Rouffach - Rouffach soil) where glyphosate was the most frequently used herbicide with a yearly application of

between 18 and 61 $kg \cdot ha^{-1}$.[224] Soil samples from each plot location were thoroughly mixed in sterile bottles, sealed, transported to the laboratory and stored at 4 °C until use.

For bacterial isolation from soil, a medium (see above) containing 60 mM sodium glutamate as carbon source were used. Ammonium chloride was used as nitrogen source, and glyphosate was the sole phosphorous source. Soil samples (10 g) were first sieved (> 2 mm). Then, 5 g of soil were suspended in 10 mL sterile water and centrifuged. A 1 mL aliquot of the supernatant was used to inoculate 50 mL medium containing 3 mM glyphosate and incubated at 30 °C at 160 rpm for 24 h. Several transfers were made and later streaked on agar plates containing 3 mM glyphosate. The single colonies formed were inoculated on agar plate to represent the pure isolated strain. The isolated bacteria were identified using 16S rRNA gene sequencing. For 16S rRNA gene amplification, the chromosomal DNA was isolated using a bacterial DNA extraction kit (Roche Applied Science, Germany) following the protocol of the manufacturer. PCR amplification was performed using universal primers (forward 27f and reverse 1492r). Standard PCR conditions was carried out in a 50 µL volume containing 1× PCR buffer, 1.5 mM $MgCl_2$, 2 mM dNTP mixture, 1 µM primers, 1 µM of P*f*u DNA polymerase (Fermentas, St. Leon-Rot, Germany), and 2 ng of template DNA. DNA was purified from a gel using an Agarose Gel Extraction kit (Roche Applied Sciences, Germany) and sequenced. Sequence homologies were evaluated using BLAST software (version 2.2.12). ClustalQ software was used to align the sequences. A neighbour-joining tress was constructed using Molecular Evolution Genetic Analysis (MEGA) software (version 6.0).

## E: 2 Supporting Figures and Tables

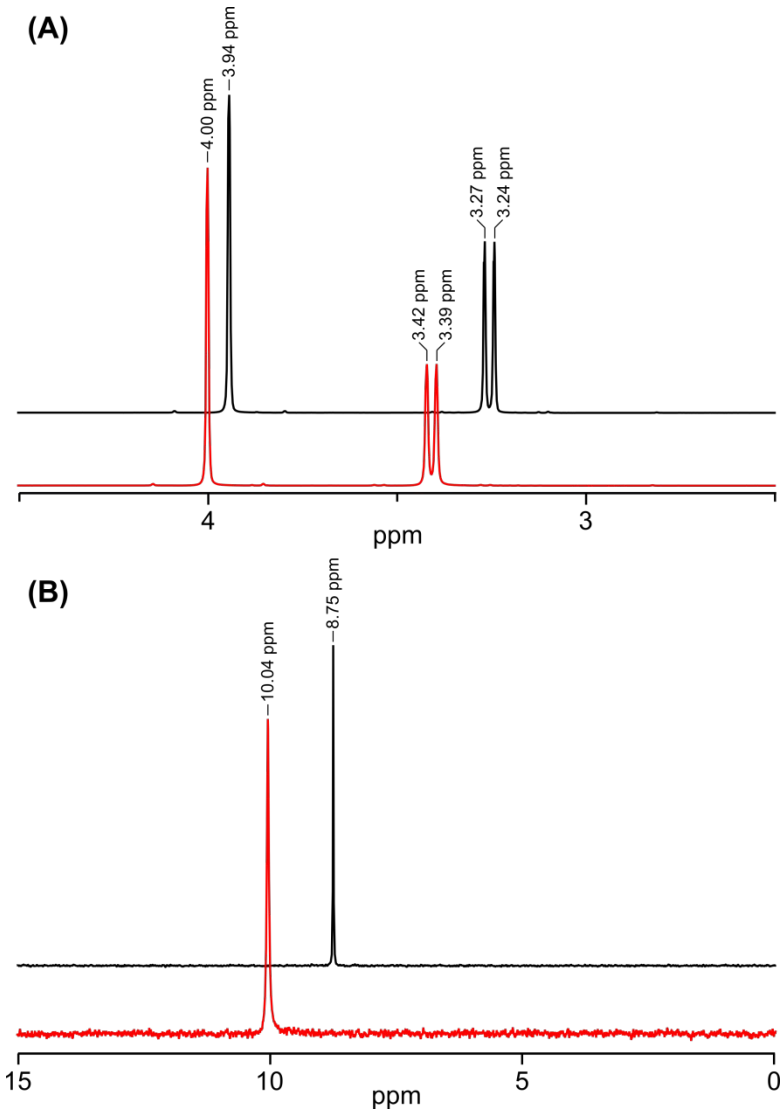


**Figure E1: (A)** $^{1}H$ with solvent suppression and **(B)** $^{31}P\{^{1}H\}$ spectra of glyphosate without (black) and with addition of 1 mM $PrCl_3$ (red). The NMR spectra were obtained glyphosate in $D_2O$ without pH adjustment where glyphosate dissociates into the monoanionic and the zwitterionic form.[28] The chemical shifts of glyphosate depend on pH. Therefore, the chemical shifts in these spectra differ from those presented in **Figure 10** and **Figure 11**.

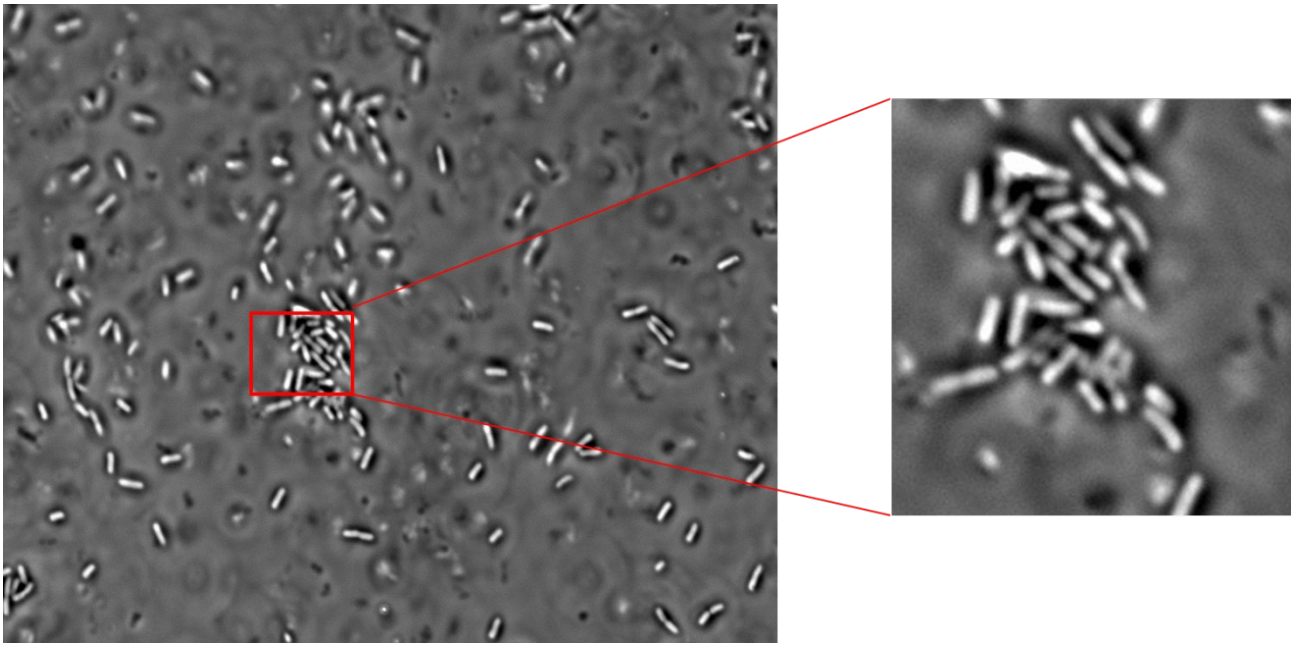

**Figure E2:** Micrograph of *Ochrobactrum sp* FrEM cells by light microscope (Axioskop Plus2, ZEISS, Germany (×100 resolution oil emulsion), AxioVision 4.1

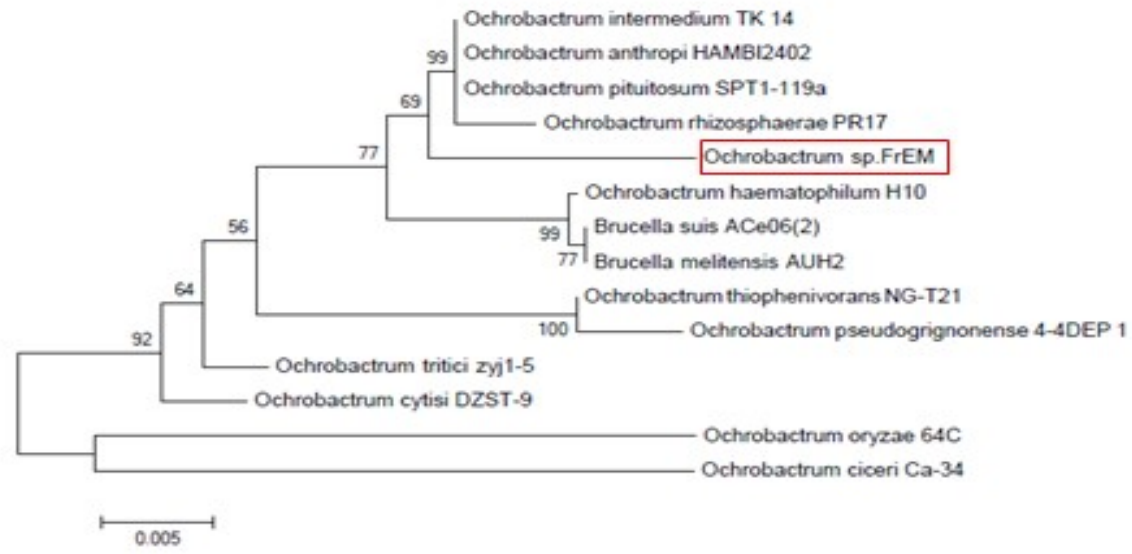


**Figure E3:** Phylogenetic position of the strain FrEM within *Ochrobactrum* species. Neighbour-joining tree based on partial 16S rRNA sequence. The bar indicates 0.005 substitutions per nucleotide.

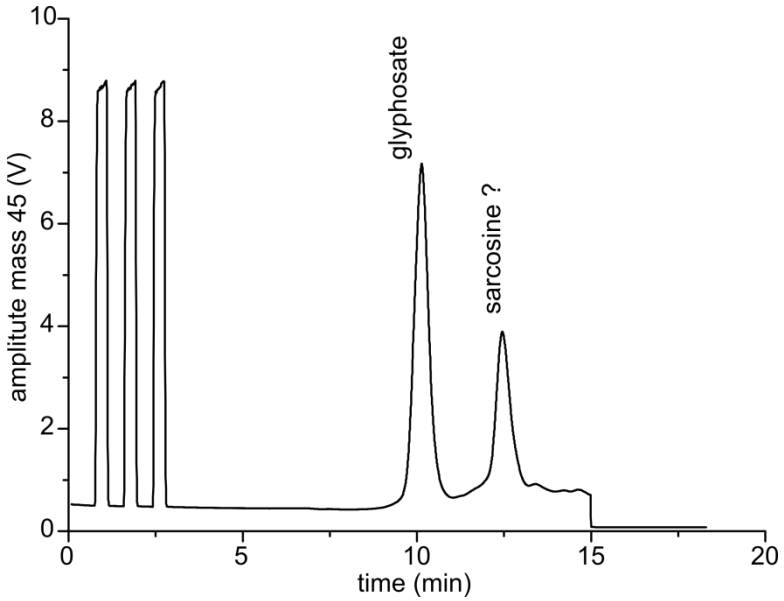


**Figure E4:** LC-IRMS chromatogram of ongoing glyphosate biodegradation. The three peaks between 0 s and 200 s are the $CO_2$ peaks of the reference gas. Glyphosate elutes around 600 s and is separated from the peak around 780 s which could be the metabolite sarcosine. The carbon source glutamate elutes after 900 s when the split to the IRMS is already closed.

**Table E1.Summary of NMR spectra collection parameters**

| experiment | transmitter frequency offset | relaxation delay (s) | spectral width (Hz) | acquisition time (s) | number of scans |
|---|---|---|---|---|---|
| $^{1}H$ Standard | 3165.1 Hz | 1.0 | 9973.4 | 2.855 | 8 |
| $^{31}P\{^{1}H\}$ Standard | 10028.7 Hz | 2.0 | 81521.7 | 0.99 | 16 |
| $^{1}H$ with solvent suppression (watergate W5) | HOD freq. | 1.5 | 7978.7 | 2.4009 | 128 |
| $^{1}H\{^{31}P\}$ with solvent suppression prior $PrCl_3$ addition | HOD freq. | 1.5 | 10000.0 | 1.499 | 16 |
| $^{1}H\{^{31}P\}$ with solvent suppression after $PrCl_3$ addition | HOD freq. | 1.5 | 10000.0 | 1.499 | 64 |

## Abbreviations

| | |
|---|---|
| % | per centum (Latin) — percent; parts per hundred |
| ‰ | pro mille (Latin) — per mil; parts per thousand |
| δ | chemical shift (in ppm) |
| µg | microgram; 1 µg = $1\times10^{-9}$ kg |
| µL | microliter; 1 µL = $1\times10^{-9}$ $m^3$ |
| µmol | micromole; 1 µmol = $1\times10^{-6}$ mol |
| AKIE | Apparent Kinetic Isotope Effect |
| ATP | adenosine triphosphate |
| d | day |
| DNA | deoxyribonucleic acid |
| Dr. rer. nat. | doctor rerum naturalium (Latin) — Doctor of Natural Science |
| Dr. | Doktor (German) — Doctor, equivalent to PhD |
| e.g. | exempli gratia (Latin) — for example |
| et al. | et alii (Latin) — and others |
| g | gram; 1 g = $1\times10^{-3}$ kg |
| *g* | gravitational acceleration; 1 *g* = 9.81 $m\cdot s^{-2}$ |
| GC | Gas Chromatography |
| h | hour; 1h = 3600 s |
| HPLC | high performance liquid chromatography |
| i.e. | id est (Latin) — that is |
| IRMS | isotope ratio mass spectrometry |
| kg | kilogram |
| KIE | kinetic isotope effect |
| L | liter; 1 L = $1\times10^{-3}$ $m^3$ |
| LC | liquid chromatography |
| M | molar; 1 $mol\cdot L^{-1}$ |
| mg | milligram; 1 mg = $1\times10^{-6}$ kg |
| min | minute; 1 min = 60 s |
| mL | milliliter; 1 mL = $1\times10^{-6}$ $m^3$ |
| mM | millimolar; 1mM = $1\times10^{-3}$ M |
| mol | mole |
| MSM | mineral salt medium |
| MW | molecular weight (in $g\cdot mol^{-1}$) |
| nmol | nanomole; 1 nmol = $1\times10^{-9}$ mol |
| NMR | nuclear magnetic resonance spectroscopy |
| pH | potential hydrogenii (Latin) — decimal logarithm of the reciprocal of the proton activity in water |
| ppm | parts per million |
| RNA | ribonucleic acid |
| rpm | rounds per minute |
| rRNA | ribosomal ribonucleic acid |
| s | second |
| UV | ultraviolet |

| | |
|---|---|
| vs. | versus (Latin) — compared to, against |
| V-PDB | Vienne PeeDee Belemnite |

## References

1. Schwarzenbach, R. P.; Escher, B. I.; Fenner, K.; Hofstetter, T. B.; Johnson, C. A.; von Gunten, U.; Wehrli, B., The Challenge of Micropollutants in Aquatic Systems. *Science* **2006,** *313*, (5790), 1072-1077.

2. Schwarzenbach, R. P.; Egli, T.; Hofstetter, T. B.; von Gunten, U.; Wehrli, B., Global Water Pollution and Human Health. *Annual Review of Environment and Resources* **2010,** *35*, (1), 109-136.

3. Johnsen, A. R.; Wick, L. Y.; Harms, H., Principles of microbial PAH-degradation in soil. *Environmental Pollution* **2005,** *133*, (1), 71-84.

4. Moreels, D.; Bastiaens, L.; Ollevier, F.; Merckx, R.; Diels, L.; Springael, D., Evaluation of the intrinsic methyl-*tert*-butyl ether (MTBE) biodegradation potential of hydrocarbon contaminated subsurface soils in batch microcosm systems. *FEMS Microbiol. Ecol.* **2004,** *49*, (1), 121-128.

5. Vila, M.; Lorber-Pascal, S.; Laurent, F., Fate of RDX and TNT in agronomic plants. *Environmental Pollution* **2007,** *148*, (1), 148-154.

6. Carreón-Diazconti, C.; Santamaría, J.; Berkompas, J.; Field, J. A.; Brusseau, M. L., Assessment of In-Situ Reductive Dechlorination Using Compound-Specific Stable Isotopes, Functional-Gene Pcr, and Geochemical Data. *Environ. Sci. Technol.* **2009,** *43*, (12), 4301-4307.

7. Bagby, S. C.; Reddy, C. M.; Aeppli, C.; Fisher, G. B.; Valentine, D. L., Persistence and biodegradation of oil at the ocean floor following Deepwater Horizon. *Proceedings of the National Academy of Sciences* **2017,** *114*, (1), E9-E18.

8. Gavrilescu, M.; Demnerová, K.; Aamand, J.; Agathos, S.; Fava, F., Emerging pollutants in the environment: present and future challenges in biomonitoring, ecological risks and bioremediation. *New Biotechnology* **2015,** *32*, (1), 147-156.

9. Martin Ruel, S.; Esperanza, M.; Choubert, J.-M.; Valor, I.; Budzinski, H.; Coquery, M., On-site evaluation of the efficiency of conventional and advanced secondary processes for the removal of 60 organic micropollutants. *Water Science and Technology* **2010,** *62*, (12), 2970-2978.

10. Barbieri, M.; Carrera, J.; Ayora, C.; Sanchez-Vila, X.; Licha, T.; Noedler, K.; Osorio, V.; Perez, S.; Koeck-Schulmeyer, M.; Lopez de Alda, M.; Barcelo, D., Formation of diclofenac and sulfamethoxazole reversible transformation products in aquifer material under denitrifying conditions: Batch experiments. *Science of the Total Environment* **2012,** *426*, 256-263.

11. Tixier, C.; Singer, H. P.; Oellers, S.; Muller, S. R., Occurrence and fate of carbamazepine, clofibric acid, diclofenac, ibuprofen, ketoprofen, and naproxen in surface waters. *Environ. Sci. Technol.* **2003,** *37*, (6), 1061-1068.

12. Drewes, J. E.; Heberer, T.; Rauch, T.; Reddersen, K., Fate of pharmaceuticals during ground water recharge. *Ground Water Monitoring and Remediation* **2003,** *23*, (3), 64-72.

13. Rosal, R.; Rodríguez, A.; Perdigón-Melón, J. A.; Petre, A.; García-Calvo, E.; Gómez, M. J.; Agüera, A.; Fernández-Alba, A. R., Occurrence of emerging pollutants in urban wastewater

and their removal through biological treatment followed by ozonation. *Water Research* **2010,** *44*, (2), 578-588.

14. Dai, N.; Mitch, W. A., Relative Importance of N-Nitrosodimethylamine Compared to Total N-Nitrosamines in Drinking Waters. *Environ. Sci. Technol.* **2013,** *47*, (8), 3648-3656.

15. Ying, G. G.; Kookana, R. S.; Mallavarpu, M., Release behavior of triazine residues in stabilised contaminated soils. *Environmental Pollution* **2005,** *134*, (1), 71-77.

16. Dai, M.; Copley, S. D., Genome shuffling improves degradation of the anthropogenic pesticide pentachlorophenol by *Sphingobium chlorophenolicum* ATCC 39723. *Applied and Environmental Microbiology* **2004,** *70*, (4), 2391-2397.

17. Kjær, J.; Olsen, P.; Ullum, M.; Grant, R., Leaching of Glyphosate and Amino-Methylphosphonic Acid from Danish Agricultural Field Sites. *J. Environ. Qual.* **2005,** *34*, (2), 608-620.

18. Schriever, C. A.; von der Ohe, P. C.; Liess, M., Estimating pesticide runoff in small streams. *Chemosphere* **2007,** *68*, (11), 2161-2171.

19. Battaglin, W. A.; Meyer, M. T.; Kuivila, K. M.; Dietze, J. E., Glyphosate and Its Degradation Product AMPA Occur Frequently and Widely in U.S. Soils, Surface Water, Groundwater, and Precipitation. *J. Am. Water Resour. Assoc.* **2014,** *50*, (2), 275-290.

20. Torrentó, C.; Bakkour, R.; Ryabenko, E.; Ponsin, V.; Prasuhn, V.; Hofstetter, T. B.; Elsner, M.; Hunkeler, D., Fate of Four Herbicides in an Irrigated Field Cropped with Corn: Lysimeter Experiments. *Procedia Earth and Planetary Science* **2015,** *13*, 158-161.

21. Morvan, X.; Mouvet, C.; Baran, N.; Gutierrez, A., Pesticides in the groundwater of a spring draining a sandy aquifer: Temporal variability of concentrations and fluxes. *Journal of Contaminant Hydrology* **2006,** *87*, (3-4), 176-190.

22. Tappe, W.; Groeneweg, J.; Jantsch, B., Diffuse atrazine pollution in German aquifers. *Biodegradation* **2002,** *13*, (1), 3-10.

23. (LfU), B. L. f. U. *Pflanzenschutzmittel-Metaboliten Vorkommen und Bewertung: Fachtagung des Bayerischen Landesamtes für Umwelt* 2008.

24. Le Baron, H. M.; McFarland, J. E.; Burnside, O. C., *The triazine herbicides*. 1 ed.; Elsevier: Oxford, 2008; p 600.

25. Franz, J. E.; Mao, M. K.; Sikorski, J. A., *Glyphosate: a unique global herbicide*. American Chemical Society: 1997.

26. Duke, S. O.; Powles, S. B., Glyphosate: a once-in-a-century herbicide. *Pest Management Science* **2008,** *64*, (4), 319-325.

27. Samsel, A.; Seneff, S., Glyphosate, pathways to modern diseases II: Celiac sprue and gluten intolerance. *Interdisciplinary Toxicology* **2013,** *6*, (4), 159-184.

28. Sprankle, P.; Meggitt, W.; Penner, D., Adsorption, mobility, and microbial degradation of glyphosate in the soil. *Weed Science* **1975**, 229-234.

29. Dill, G. M., Glyphosate-resistant crops: history, status and future. *Pest Management Science* **2005,** *61*, (3), 219-224.

30. Solomon, K. R.; Baker, D. B.; Richards, R. P.; Dixon, K. R.; Klaine, S. J.; La Point, T. W.; Kendall, R. J.; Weisskopf, C. P.; Giddings, J. M.; Giesy, P.; Hall, L. W., Jr.; Williams, W. M.,

Ecological risk assessment of atrazine in North American surface waters. *Environmental Toxicology and Chemistry* **1996,** *15*, (1), 31-76.

31. Giesy, J. P.; Dobson, S.; Solomon, K. R., Ecotoxicological Risk Assessment for Roundup® Herbicide. In *Reviews of Environmental Contamination and Toxicology: Continuation of Residue Reviews*, Ware, G. W., Ed. Springer New York: New York, NY, 2000; pp 35-120.

32. Bi, E.; Schmidt, T. C.; Haderlein, S. B., Practical issues relating to soil column chromatography for sorption parameter determination. *Chemosphere* **2010,** *80*, (7), 787-793.

33. Qiu, S.; Eckert, D.; Cirpka, O. A.; Huenniger, M.; Knappett, P.; Maloszewski, P.; Meckenstock, R. U.; Griebler, C.; Elsner, M., Direct Experimental Evidence of Non-first Order Degradation Kinetics and Sorption-Induced Isotopic Fractionation in a Mesoscale Aquifer: 13C/12C Analysis of a Transient Toluene Pulse. *Environ. Sci. Technol.* **2013,** *47*, (13), 6892-6899.

34. Einsiedl, F.; Radke, M.; Maloszewski, P., Occurrence and transport of pharmaceuticals in a karst groundwater system affected by domestic wastewater treatment plants. *Journal of Contaminant Hydrology* **2010,** *117*, (1-4), 26-36.

35. Bouchard, D.; Hunkeler, D.; Gaganis, P.; Aravena, R.; Höhener, P.; Broholm, M. M.; Kjeldsen, P., Carbon Isotope Fractionation during Diffusion and Biodegradation of Petroleum Hydrocarbons in the Unsaturated Zone: Field Experiment at Vaerlose Airbase, Denmark, and Modeling. *Environ. Sci. Technol.* **2008,** *42*, (2), 596-601.

36. Aitken, C. M.; Jones, D. M.; Larter, S. R., Anaerobic hydrocarbon biodegradation in deep subsurface oil reservoirs. *Nature* **2004,** *431*, (7006), 291-294.

37. Cribbin, L. B.; Winstanley, H. F.; Mitchell, S. L.; Fowler, A. C.; Sander, G. C., Reaction front formation in contaminant plumes. *Journal of Contaminant Hydrology* **2014,** *171*, (0), 12-21.

38. Rosenstock, B.; Simon, M., Sources and sinks of dissolved free amino acids and protein in a large and deep mesotrophic lake. *Limnology and Oceanography* **2001,** *46*, (3), 644-654.

39. Jaisi, D. P.; Kukkadapu, R. K.; Stout, L. M.; Varga, T.; Blake, R. E., Biotic and Abiotic Pathways of Phosphorus Cycling in Minerals and Sediments: Insights from Oxygen Isotope Ratios in Phosphate. *Environ. Sci. Technol.* **2011,** *45*, (15), 6254-6261.

40. Egli, T., How to live at very low substrate concentration. *Water Research* **2010,** *44*, (17), 4826-4837.

41. Wu, M.; Quirindongo, M.; Sass, J.; Wetzler, A., Still poisoning the well: atrazine continues to conatminate surface water and drinking water in the United States. *New York (NY): Natural Resources Defense Council* **2010**.

42. LfU, Bayerisches Landesamt für Umwelt Grundwasser für die öffentliche Wasserversorgung: Nitrat und Pflanzenschutzmittel In Bayerisches Landesamt für Umwelt: 2015.

43. Button, D. K., Nutrient uptake by microorganisms according to kinetic parameters from theory as related to cytoarchitecture. *Microbiology and Molecular Biology Reviews* **1998,** *62*, (3), 636-645.

44. Ferenci, T.; Robert, K. P., Bacterial Physiology, Regulation and Mutational Adaptation in a Chemostat Environment. In *Advances in Microbial Physiology*, Academic Press: 2008; Vol. Volume 53, pp 169-315.

45. Bosma, T. N. P.; Middeldorp, P. J. M.; Schraa, G.; Zehnder, A. J. B., Mass Transfer Limitation of Biotransformation: Quantifying Bioavailability. *Environ. Sci. Technol.* **1997,** *31*, (1), 248-252.

46. Wick, A.; Wagner, M.; Ternes, T. A., Elucidation of the Transformation Pathway of the Opium Alkaloid Codeine in Biological Wastewater Treatment. *Environ. Sci. Technol.* **2011,** *45*, (8), 3374-3385.

47. Locher, H. H.; Poolman, B.; Cook, A. M.; Konings, W. N., Uptake of 4-toluene sulfonate by Comamonas testosteroni T-2. *Journal of Bacteriology* **1993,** *175*, (4), 1075-1080.

48. Delcour, A. H., Outer Membrane Permeability and Antibiotic Resistance. *Biochimica et biophysica acta* **2009,** *1794*, (5), 808-816.

49. Beate I. Escher, L. S., Chemical Speciation of Organics and of Metals at Biological Interphases. In *Physicochemical Kinetics and Transport at Biointerfaces*, Hermann P. Van Leeuwen, W. K., Ed. Wiley: 2004; Vol. 9, pp 205-269.

50. Parales, R. E.; Ditty, J. L., Substrate Transport. In *Handbook of Hydrocarbon and Lipid Microbiology*, Timmis, K. N., Ed. Springer Berlin Heidelberg: Berlin, Heidelberg, 2010; pp 1545-1553.

51. Qiu, S.; Gözdereliler, E.; Weyrauch, P.; Lopez, E. C. M.; Kohler, H.-P. E.; Sørensen, S. R.; Meckenstock, R. U.; Elsner, M., Small 13C/12C Fractionation Contrasts with Large Enantiomer Fractionation in Aerobic Biodegradation of Phenoxy Acids. *Environ. Sci. Technol.* **2014,** *48*, (10), 5501-5511.

52. Marozava, S.; Röling, W. F.; Seifert, J.; Küffner, R.; Von Bergen, M.; Meckenstock, R. U., Physiology of *Geobacter metallireducens* under excess and limitation of electron donors. Part II. Mimicking environmental conditions during cultivation in retentostats. *Syst Appl Microbiol* **2014,** *37*, (4), 287-295.

53. Konopka, A., Microbial physiological state at low growth rate in natural and engineered ecosystems. *Current Opinion in Microbiology* **2000,** *3*, (3), 244-247.

54. Harder, J., Species-independent maintenance energy and natural population sizes. *FEMS Microbiol. Ecol.* **1997,** *23*, 39-44.

55. Kovarova-Kovar, K.; Egli, T., Growth kinetics of suspended microbial cells: From single-substrate-controlled growth to mixed-substrate kinetics. *Microbiology and Molecular Biology Reviews* **1998,** *62*, (3), 646-666.

56. Wang, Y.; Hammes, F.; Boon, N.; Chami, M.; Egli, T., Isolation and characterization of low nucleic acid (LNA)-content bacteria. *ISME J* **2009,** *3*, (8), 889-902.

57. Yanze-Kontchou, C.; Gschwind, N., Mineralization of the herbicide atrazine as a carbon source by a Pseudomonas strain. *Appl. Environ. Microbiol.* **1994,** *60*, (12), 4297-4302.

58. Sviridov, A. V.; Shushkova, T. V.; Zelenkova, N. F.; Vinokurova, N. G.; Morgunov, I. G.; Ermakova, I. T.; Leontievsky, A. A., Distribution of glyphosate and methylphosphonate

catabolism systems in soil bacteria Ochrobactrum anthropi and Achromobacter sp. *Applied Microbiology and Biotechnology* **2012,** *93*, (2), 787-796.

59. Mandelbaum, R. T.; Wackett, L. P.; Allan, D. L., Mineralization of the s-triazine ring of atrazine by stable bacterial mixed cultures. *Appl. Environ. Microbiol.* **1993,** *59*, (6), 1695-1701.

60. Rosenthal, H.; Adrian, L.; Steiof, M., Dechlorination of PCE in the presence of Fe0 enhanced by a mixed culture containing two Dehalococcoides strains. *Chemosphere* **2004,** *55*, (5), 661-669.

61. Marozava, S.; Röling, W. F.; Seifert, J.; Küffner, R.; Von Bergen, M.; Meckenstock, R. U., Physiology of Geobacter metallireducens under excess and limitation of electron donors. Part I. Batch cultivation with excess of carbon sources. *Systematic and applied microbiology* **2014,** *37*, (4), 277-286.

62. Devers, M.; El Azhari, N.; Kolic, N.-U.; Martin-Laurent, F., Detection and organization of atrazine-degrading genetic potential of seventeen bacterial isolates belonging to divergent taxa indicate a recent common origin of their catabolic functions. *FEMS Microbiology Letters* **2007,** *273*, (1), 78-86.

63. Strong, L. C.; Rosendahl, C.; Johnson, G.; Sadowsky, M. J.; Wackett, L. P., *Arthrobacter aurescens* TC1 metabolizes diverse s-triazine ring compounds. *Appl. Environ. Microbiol.* **2002,** *68*, (12), 5973-5980.

64. Lin, C.; Gu, J.-G.; Qiao, C.; Duan, S.; Gu, J.-D., Degradability of atrazine, cyanazine, and dicamba in methanogenic enrichment culture microcosms using sediment from the Pearl River of Southern China. *Biology and Fertility of Soils* **2006,** *42*, (5), 395-401.

65. Kunkel, U.; Radke, M., Biodegradation of acidic pharmaceuticals in bed sediments: Insight from a laboratory experiment. *Environ. Sci. Technol.* **2008,** *42*, (19), 7273-7279.

66. Li, D.; Sharp, J. O.; Saikaly, P. E.; Ali, S.; Alidina, M.; Alarawi, M. S.; Keller, S.; Hoppe-Jones, C.; Drewes, J. E., Dissolved Organic Carbon Influences Microbial Community Composition and Diversity in Managed Aquifer Recharge Systems. *Applied and Environmental Microbiology* **2012,** *78*, (19), 6819–6828.

67. Mellage, A.; Eckert, D.; Grösbacher, M.; Inan, A. Z.; Cirpka, O. A.; Griebler, C., Dynamics of Suspended and Attached Aerobic Toluene Degraders in Small-Scale Flow-through Sediment Systems under Growth and Starvation Conditions. *Environ. Sci. Technol.* **2015,** *49*, (12), 7161-7169.

68. Schürner, H. K.; Maier, M. P.; Eckert, D.; Brejcha, R.; Neumann, C.-C.; Stumpp, C.; Cirpka, O. A.; Elsner, M., Compound-Specific Stable Isotope Fractionation of Pesticides and Pharmaceuticals in a Mesoscale Aquifer Model. *Environ. Sci. Technol.* **2016,** *50*, (11), 5729-5739.

69. Eckert, D.; Qiu, S.; Elsner, M.; Cirpka, O. A., Model Complexity Needed for Quantitative Analysis of High Resolution Isotope and Concentration Data from a Toluene-Pulse Experiment. *Environ. Sci. Technol.* **2013,** *47*, (13), 6900-6907.

70. Trautwein, K.; Lahme, S.; Wöhlbrand, L.; Feenders, C.; Mangelsdorf, K.; Harder, J.; Steinbüchel, A.; Blasius, B.; Reinhardt, R.; Rabus, R., Physiological and Proteomic Adaptation of *Aromatoleum aromaticum* EbN1 to Low Growth Rates in Benzoate-Limited, Anoxic Chemostats. *Journal of Bacteriology* **2012,** *194*, (9), 2165-2180.

71. Devers, M.; Rouard, N.; Martin-Laurent, F., Fitness drift of an atrazine-degrading population under atrazine selection pressure. *Environmental Microbiology* **2008,** *10*, (3), 676-684.

72. Lin, B.; Westerhoff, H. V.; Röling, W. F. M., How Geobacteraceae may dominate subsurface biodegradation: physiology of Geobacter metallireducens in slow-growth habitat-simulating retentostats. *Environmental Microbiology* **2009,** *11*, (9), 2425-2433.

73. Brenna, J. T.; Corso, T. N.; Tobias, H. J.; Caimi, R. J., High-precision continuous-flow isotope ratio mass spectrometry. *Mass Spectrometry Reviews* **1997,** *16*, (5), 227-258.

74. Meier-Augenstein, W., A Reference Gas Inlet Module for Internal Isotopic Calibration in High Precision Gas Chromatography/Combustion-Isotope Ratio Mass Spectrometry. *Rapid Commun. Mass Spectrom.* **1997,** *11*, 1775-1780.

75. Clark, I.; Fritz, P., *Environmental Isotopes in Hydrogeology*. Lewis Pubishers: New York, 1997; p 328.

76. Hoefs, J., *Stable Isotope Geochemistry*. Springer-Verlag: Berlin, 1997.

77. Coplen, T. B., Guidelines and recommended terms for expression of stable-isotope-ratio and gas-ratio measurement results. *Rapid Communications in Mass Spectrometry* **2011,** *25*, (17), 2538-2560.

78. Coplen, T. B.; Krouse, H. R.; Boehlke, J. K., Reporting of nitrogen-isotope abundances. *Pure & Applied Chemistry* **1992,** *64*, 907-908.

79. Westheimer, F. H., The magnitude of the primary kinetic isotope effect for compounds of hydrogen and deuterium. *Chemical Reviews* **1961,** *61*, 265-273.

80. Kirsch, J. F., Secondary Kinetic Isotope Effects. In *Isotope Effects on Enzyme-Catalyzed Reactions*, Cleland, W. W.; O'Leary, M. H.; Northrop, D. B., Eds. University Park Press: Baltimore, London, Tokyo, 1977; pp 100-121.

81. Churchill, D. G.; Janak, K. E.; Wittenberg, J. S.; Parkin, G., Normal and Inverse Primary Kinetic Deuterium Isotope Effects for C−H Bond Reductive Elimination and Oxidative Addition Reactions of Molybdenocene and Tungstenocene Complexes: Evidence for Benzene σ-Complex Intermediates. *J. Am. Chem. Soc.* **2003,** *125*, (5), 1403-1420.

82. Sherwood Lollar, B.; Slater, G. F.; Ahad, J.; Sleep, B.; Spivack, J.; Brennan, M.; MacKenzie, P., Contrasting carbon isotope fractionation during biodegradation of trichloroethylene and toluene: implications for intrinsic bioremediation. *Organic Geochemistry* **1999,** *30*, (8), 813-820.

83. Hunkeler, D.; Aravena, R.; Butler, B. J., Monitoring microbial dechlorination of tetrachloroethene (PCE) using compound-specific carbon isotope ratios: Microcosms and field experiments. *Environ. Sci. Technol.* **1999,** *33*, (16), 2733-2738.

84. Meckenstock, R. U.; Morasch, B.; Griebler, C.; Richnow, H. H., Stable isotope fractionation analysis as a tool to monitor biodegradation in contaminated acquifers. *J.Contam.Hydrol.* **2004,** *75*, (3-4), 215-255.

85. Farquhar, G. D.; Ehleringer, J. R.; Hubick, K. T., Carbon Isotope Discrimination and Photosynthesis. *Ann. Rev. Plant Physiol. Plant Mol. Biol.* **1989,** *40*, 503-537.

86. O'Leary, M. H., Carbon Isotopes in Photosynthesis. *Bioscience* **1988,** *38*, (5), 328-336.

87. Rees, C. E., A steady-state model for sulphur isotope fractionation in bacterial reduction processes. *Geochimica et Cosmochimica Acta* **1973,** *37*, (5), 1141-1162.

88. Brunner, B.; Bernasconi, S. M.; Kleikemper, J.; Schroth, M. H., A model for oxygen and sulfur isotope fractionation in sulfate during bacterial sulfate reduction processes. *Geochimica et Cosmochimica Acta* **2005,** *69*, (20), 4773-4785.

89. Wing, B. A.; Halevy, I., Intracellular metabolite levels shape sulfur isotope fractionation during microbial sulfate respiration. *Proceedings of the National Academy of Sciences* **2014,** *111*, (51), 18116-18125.

90. Wunderlich, A.; Meckenstock, R.; Einsiedl, F., Effect of Different Carbon Substrates on Nitrate Stable Isotope Fractionation During Microbial Denitrification. *Environ. Sci. Technol.* **2012,** *46*, (9), 4861-4868.

91. Kritee, K.; Sigman, D. M.; Granger, J.; Ward, B. B.; Jayakumar, A.; Deutsch, C., Reduced isotope fractionation by denitrification under conditions relevant to the ocean. *Geochimica et Cosmochimica Acta* **2012,** *92*, (0), 243-259.

92. Thullner, M.; Kampara, M.; Richnow, H. H.; Harms, H.; Wick, L. Y., Impact of Bioavailability Restrictions on Microbially Induced Stable Isotope Fractionation. 1. Theoretical Calculation. *Environ. Sci. Technol.* **2008,** *42*, (17), 6544-6551.

93. Kampara, M.; Thullner, M.; Harms, H.; Wick, L. Y., Impact of cell density on microbially induced stable isotope fractionation. *Applied Microbiology and Biotechnology* **2009,** *81*, (5), 977-985.

94. Aeppli, C.; Berg, M.; Cirpka, O. A.; Holliger, C.; Schwarzenbach, R. P.; Hofstetter, T. B., Influence of Mass-Transfer Limitations on Carbon Isotope Fractionation during Microbial Dechlorination of Trichloroethene. *Environ. Sci. Technol.* **2009,** *43*, (23), 8813-8820.

95. Renpenning, J.; Rapp, I.; Nijenhuis, I., Substrate hydrophobicity and cell composition influence the extent of rate limitation and masking of isotope fractionation during microbial reductive dehalogenation of chlorinated ethenes. *Environ. Sci. Technol.* **2015,** *49*, (7), 4293-4301.

96. Wohnsland, F.; Faller, B., High-Throughput Permeability pH Profile and High-Throughput Alkane/Water log P with Artificial Membranes. *Journal of Medicinal Chemistry* **2001,** *44*, (6), 923-930.

97. Passeleu-Le Bourdonnec, C.; Carrupt, P.-A.; Scherrmann, J. M.; Martel, S., Methodologies to Assess Drug Permeation Through the Blood–Brain Barrier for Pharmaceutical Research. *Pharmaceutical Research* **2013,** *30*, (11), 2729-2756.

98. Males, R. G.; Herring, F. G., A 1H-NMR study of the permeation of glycolic acid through phospholipid membranes. *Biochimica et Biophysica Acta (BBA) - Biomembranes* **1999,** *1416*, (1–2), 333-338.

99. Naderkhani, E.; Vasskog, T.; Flaten, G. E., Biomimetic PVPA in vitro model for estimation of the intestinal drug permeability using fasted and fed state simulated intestinal fluids. *European Journal of Pharmaceutical Sciences* **2015,** *73*, 64-71.

100. Fujikawa, M.; Nakao, K.; Shimizu, R.; Akamatsu, M., QSAR study on permeability of hydrophobic compounds with artificial membranes. *Bioorganic & Medicinal Chemistry* **2007,** *15*, (11), 3756-3767.

101. Whitman, B. E.; Lueking, D. R.; Mihelcic, J. R., Naphthalene uptake by a Pseudomonas fluorescens isolate. *Canadian Journal of Microbiology* **1998,** *44*, (11), 1086-1093.

102. Bateman, J. N.; Speer, B.; Feduik, L.; Hartline, R. A., Naphthalene association and uptake in Pseudomonas putida. *Journal of Bacteriology* **1986,** *166*, (1), 155-161.

103. Lande, M. B.; Donovan, J. M.; Zeidel, M. L., The relationship between membrane fluidity and permeabilities to water, solutes, ammonia, and protons. *The Journal of General Physiology* **1995,** *106*, (1), 67-84.

104. Kallimanis, A.; Frillingos, S.; Drainas, C.; Koukkou, A. I., Taxonomic identification, phenanthrene uptake activity, and membrane lipid alterations of the PAH degrading Arthrobacter sp. strain Sphe3. *Applied Microbiology and Biotechnology* **2007,** *76*, (3), 709-717.

105. Ultee, A.; Kets, E. P. W.; Alberda, M.; Hoekstra, F. A.; Smid, E. J., Adaptation of the food-borne pathogen Bacillus cereus to carvacrol. *Archives of Microbiology* **2000,** *174*, (4), 233-238.

106. Nielsen, L. E.; Kadavy, D. R.; Rajagopal, S.; Drijber, R.; Nickerson, K. W., Survey of Extreme Solvent Tolerance in Gram-Positive Cocci: Membrane Fatty Acid Changes in Staphylococcus haemolyticus Grown in Toluene. *Applied and Environmental Microbiology* **2005,** *71*, (9), 5171-5176.

107. Dietrich, C.; Bagatolli, L. A.; Volovyk, Z. N.; Thompson, N. L.; Levi, M.; Jacobson, K.; Gratton, E., Lipid Rafts Reconstituted in Model Membranes. *Biophysical Journal* **2001,** *80*, (3), 1417-1428.

108. Prestegard, J. H.; Cramer, J. A.; Viscio, D. B., Nuclear magnetic resonance determinations of permeation coefficients for maleic acid in phospholipid vesicles. *Biophysical Journal* **1979,** *26*, (3), 575-584.

109. Xiang, T.-X.; Anderson, B. D., Development of a combined NMR paramagnetic ion-induced line-broadening/dynamic light scattering method for permeability measurements across lipid bilayer membranes. *Journal of Pharmaceutical Sciences* **1995,** *84*, (11), 1308-1315.

110. Millet, O.; Loria, J. P.; Kroenke, C. D.; Pons, M.; Palmer, A. G., The Static Magnetic Field Dependence of Chemical Exchange Linebroadening Defines the NMR Chemical Shift Time Scale. *J. Am. Chem. Soc.* **2000,** *122*, (12), 2867-2877.

111. Meyer, A. H.; Penning, H.; Elsner, M., C and N isotope fractionation suggests similar mechanisms of microbial atrazine transformation despite involvement of different Enzymes (AtzA and TrzN). *Environ. Sci. Technol.* **2009,** *43*, (21), 8079-8085.

112. Schürner, H. K. V.; Seffernick, J. L.; Grzybkowska, A.; Dybala-Defratyka, A.; Wackett, L. P.; Elsner, M., Characteristic Isotope Fractionation Patterns in s-Triazine Degradation Have Their Origin in Multiple Protonation Options in the s-Triazine Hydrolase TrzN. *Environ. Sci. Technol.* **2015,** *49*, (6), 3490-3498.

113. Shapir, N.; Pedersen, C.; Gil, O.; Strong, L.; Seffernick, J.; Sadowsky, M. J.; Wackett, L. P., TrzN from Arthrobacter aurescens TC1 Is a zinc amidohydrolase. *J. Bacteriol.* **2006,** *188*, (16), 5859-5864.

114. Seffernick, J. L.; Reynolds, E.; Fedorov, A. A.; Fedorov, E.; Almo, S. C.; Sadowsky, M. J.; Wackett, L. P., X-ray Structure and Mutational Analysis of the Atrazine Chlorohydrolase TrzN. *Journal of Biological Chemistry* **2010,** *285*, (40), 30606-30614.

115. Tran, N. H.; Urase, T.; Ngo, H. H.; Hu, J.; Ong, S. L., Insight into metabolic and cometabolic activities of autotrophic and heterotrophic microorganisms in the biodegradation of emerging trace organic contaminants. *Bioresource technology* **2013,** *146*, 721-731.

116. Melander, L.; Saunders, W. H., *Reaction rates of isotopic molecules*. John Wiley: New York, 1980; p 331.

117. McKelvie, J. R.; Mackay, D. M.; de Sieyes, N. R.; Lacrampe-Couloume, G.; Sherwood Lollar, B., Quantifying MTBE biodegradation in the Vandenberg Air Force Base ethanol release study using stable carbon isotopes. *Journal of Contaminant Hydrology* **2007,** *94*, (3-4), 157-165.

118. Chartrand, M.; Passeport, E.; Rose, C.; Lacrampe-Couloume, G.; Bidleman, T. F.; Jantunen, L. M.; Lollar, B. S., Compound specific isotope analysis of hexachlorocyclohexane isomers: a method for source fingerprinting and field investigation of in situ biodegradation. *Rapid Communications in Mass Spectrometry* **2015,** *29*, (6), 505-514.

119. Braeckevelt, M.; Fischer, A.; KÃ¤stner, M., Field applicability of Compound-Specific Isotope Analysis (CSIA) for characterization and quantification of in situ contaminant degradation in aquifers. *Applied Microbiology and Biotechnology* **2012,** *94*, (6), 1401-1421.

120. Smith, D.; Artursson, P.; Avdeef, A.; Di, L.; Ecker, G. F.; Faller, B.; Houston, J. B.; Kansy, M.; Kerns, E. H.; Krämer, S. D.; Lennernäs, H.; Van De Waterbeemd, H.; Sugano, K.; Testa, B., Passive lipoidal diffusion and carrier-mediated cell uptake are both important mechanisms of membrane permeation in drug disposition. *Molecular Pharmaceutics* **2014,** *11*, (6), 1727-1738.

121. Reinnicke, S.; Simonsen, A.; Sørensen, S. R.; Aamand, J.; Elsner, M., C and N Isotope Fractionation during Biodegradation of the Pesticide Metabolite 2,6-Dichlorobenzamide (BAM): Potential for Environmental Assessments. *Environ. Sci. Technol.* **2012,** *46*, (3), 1447-1454.

122. Clingenpeel, S. R.; Moan, J. L.; McGrath, D. M.; Hungate, B. A.; Watwood, M. E., Stable carbon isotope fractionation in chlorinated ethene degradation by bacteria expressing three toluene oxygenases. *Frontiers in Microbiology* **2012,** *3*, 63.

123. Elsner, M.; Imfeld, G., Compound-specific isotope analysis (CSIA) of micropollutants in the environment — current developments and future challenges. *Curr. Opin. Biotechnol.* **2016,** *41*, 60-72.

124. Sajjaphan, K.; Shapir, N.; Wackett, L. P.; Palmer, M.; Blackmon, B.; Sadowsky, M. J., *Arthrobacter aurescens* TC1 atrazine catabolism genes trzN, atzB, and atzC are linked on a 160-kilobase region and are functional in *Escherichia coli.* . *Appl. Environ. Microbiol.* **2004,** *70*, (7), 4402-4407.

125. Graymore, M.; Stagnitti, F.; Allinson, G., Impacts of atrazine in aquatic ecosystems. *Environ. Int.* **2001,** *26*, (7-8), 483-495.

126. Münster, U., Concentrations and fluxes of organic carbon substrates in the aquatic environment. *Antonie van Leeuwenhoek* **1993,** *63*, (3-4), 243-274.

127. Davidson, M. M.; Bisher, M. E.; Pratt, L. M.; Fong, J.; Southam, G.; Pfiffner, S. M.; Reches, Z.; Onstott, T. C., Sulfur Isotope Enrichment during Maintenance Metabolism in the Thermophilic Sulfate-Reducing Bacterium Desulfotomaculum putei. *Applied and Environmental Microbiology* **2009,** *75*, (17), 5621-5630.

128. Penning, H.; Plugge, C. M.; Galand, P. E.; Conrad, R., Variation of carbon isotope fractionation in hydrogenotrophic methanogenic microbial cultures and environmental samples at different energy status. *Global Change Biology* **2005,** *11*, (12), 2103-2113.

129. Hoefs, J., Theoretical and Experimental Principles. In *Stable isotope geochemistry*, 3rd ed.; Wyllie, P. J., Ed. Springer-Verlag: Chicago, 1987; pp 1-25.

130. Schmidt, T. C.; Zwank, L.; Elsner, M.; Berg, M.; Meckenstock, R. U.; Haderlein, S. B., Compound-specific stable isotope analysis of organic contaminants in natural environments: a critical review of the state of the art, prospects, and future challenges. *Anal. Bioanal. Chem.* **2004,** *378*, (2), 283-300.

131. Gharasoo, M.; Ehrl, B. N.; Cirpka, O. A.; Elsner, M., Modeling mechanisms that control contaminant biodegradation in chemostats at extremely low dilution rates. *Ecological Modeling* **in preparation, attached as supporting information for review only**. **See Appendix A.**

132. Mongodin, E. F.; Shapir, N.; Daugherty, S. C.; DeBoy, R. T.; Emerson, J. B.; Shvartzbeyn, A.; Radune, D.; Vamathevan, J.; Riggs, F.; Grinberg, V.; Khouri, H.; Wackett, L. P.; Nelson, K. E.; Sadowsky, M. J., Secrets of Soil Survival Revealed by the Genome Sequence of Arthrobacter aurescens TC1. *PLoS Genetics* **2006,** *2*, (12), e214.

133. Best, J. B., The inference of intracellular enzymatic properties from kinetic data obtained on living cells. I. Some kinetic considerations regarding an enzyme enclosed by a diffusion barrier. *Journal of Cellular and Comparative Physiology* **1955,** *46*, (1), 1-27.

134. Stenzel, A.; Goss, K. U.; Endo, S., Determination of Polyparameter Linear Free Energy Relationship (pp-LFER) Substance Descriptors for Established and Alternative Flame Retardants. *Environ. Sci. Technol.* **2013,** *47*, (3), 1399.

135. Van Meer, G.; Voelker, D. R.; Feigenson, G. W., Membrane lipids: where they are and how they behave. *Nature reviews Molecular cell biology* **2008,** *9*, (2), 112-124.

136. Schreglmann, K.; Hoeche, M.; Steinbeiss, S.; Reinnicke, S.; Elsner, M., Carbon and nitrogen isotope analysis of atrazine and desethylatrazine at sub-microgram per liter concentrations in groundwater. *Anal. Bioanal. Chem.* **2013,** *405*, (9), 2857-2867.

137. Loos, R.; Locoro, G.; Comero, S.; Contini, S.; Schwesig, D.; Werres, F.; Balsaa, P.; Gans, O.; Weiss, S.; Blaha, L.; Bolchi, M.; Gawlik, B. M., Pan-European survey on the occurrence of selected polar organic persistent pollutants in ground water. *Water Research* **2010,** *44*, (14), 4115-4126.

138. Selim, H. M., Modelling kinetic retention of atrazine and metribuzin in soil 1. *Soil Science* **2004,** *169*, 25-34.

139. Button, D. K.; Robertson, B.; Gustafson, E.; Zhao, X. M., Experimental and theoretical bases of specific affinity, a cytoarchitecture-based formulation of nutrient collection proposed to supercede the Michaels-Menten paradigm of microbial kinetics. *Applied and Environmental Microbiology* **2004,** *70*, (9), 5511-5521.

140. Wick, L. M.; Quadroni, M.; Egli, T., Short- and long-term changes in proteome composition and kinetic properties in a culture of Escherichia coli during transition from glucose-excess to glucose-limited growth conditions in continuous culture and vice versa. *Environmental Microbiology* **2001,** *3*, (9), 588-599.

141. Hunkeler, D.; Elsner, M., Principles and Mechanisms of Isotope Fractionation. In *Environmental Isotopes in Biodegradation and Bioremediation*, Aelion, C. M.; Hohener, P.; Hunkeler, D.; Aravena, R., Eds. CRC Press: Boca Raton, London, New York, 2010.

142. Schmidt, H. L., Fundamentals and systematics of the non-statistical distributions of isotopes in natural compounds. *Naturwissenschaften* **2003,** *90*, (12), 537-552.

143. Northrop, D. B., The expression of isotope effects on enzyme-catalyzed reactions. *Annu. Rev. Biochem.* **1981,** *50*, 103-131.

144. Nijenhuis, I.; Andert, J.; Beck, K.; Kastner, M.; Diekert, G.; Richnow, H. H., Stable isotope fractionation of tetrachloroethene during reductive dechlorination by *Sulfurospirillum multivorans* and *Desulfitobacterium* sp. Strain PCE-S and abiotic reactions with cyanocobalamin. *Appl. Environ. Microbiol.* **2005,** *71*, (7), 3413-3419.

145. Kampara, M.; Thullner, M.; Richnow, H. H.; Harms, H.; Wick, L. Y., Impact of Bioavailability Restrictions on Microbially Induced Stable Isotope Fractionation. 2. Experimental Evidence. *Environ. Sci. Technol.* **2008,** *42*, (17), 6552-6558.

146. Ehrl, B. N.; Kundu, K.; Gharasoo, M.; Marozava, S.; Elsner, M., Rate limiting mass transfer in micropollutant degradation revealed by isotope fractionation. *Nature Geoscience* **in review, attached as supporting information for review only**. **See chapter 3.**

147. Bernstein, A.; Ronen, Z.; Adar, E.; Nativ, R.; Lowag, H.; Stichler, W.; Meckenstock, R. U., Compound-Specific Isotope Analysis of RDX and Stable Isotope Fractionation during Aerobic and Anaerobic Biodegradation. *Environ. Sci. Technol.* **2008,** *42*, (21), 7772-7777.

148. Hunkeler, D.; Van Breukelen, B. M.; Elsner, M., Modeling Chlorine Isotope Trends during Sequential Transformation of Chlorinated Ethenes. *Environ. Sci. Technol.* **2009,** *43*, (17), 6750-6756.

149. Maier, M. P.; De Corte, S.; Nitsche, S.; Spaett, T.; Boon, N.; Elsner, M., C & N Isotope Analysis of Diclofenac to Distinguish Oxidative and Reductive Transformation and to Track Commercial Products. *Environ. Sci. Technol.* **2014,** *48*, (4), 2312-2320.

150. Devers, M.; Azhari, N. E.; Kolic, N.-U.; Martin-Laurent, F., Detection and organization of atrazine-degrading genetic potential of seventeen bacterial isolates belonging to divergent taxa indicate a recent common origin of their catabolic functions. *FEMS Microbiology Letters* **2007,** *273*, (1), 78-86.

151. Reinnicke, S.; Juchelka, D.; Steinbeiss, S.; Meyer, A. H.; Hilkert, A.; Elsner, M., Gas chromatography-isotope ratio mass spectrometry (GC-IRMS) of recalcitrant target compounds: performance of different combustion reactors and strategies for standardization. *Rapid. Commun. Mass. Sp.* **2012,** *26*, (9), 1053-1060.

152. Michaelis, L. M., M.L., Die Kinetik der Invertinbindung. *Biochemische Zeitschrift* **1913,** *49*, 333-369.

153. Gharasoo, M.; Centler, F.; Van Cappellen, P.; Wick, L. Y.; Thullner, M., Kinetics of Substrate Biodegradation under the Cumulative Effects of Bioavailability and Self-Inhibition. *Environ. Sci. Technol.* **2015,** *49*, (9), 5529-5537.

154. Gharasoo, M.; Thullner, M.; Elsner, M., Introduction of a new platform for parameter estimation of kinetically complex environmental systems. *Environmental Modelling & Software* **2017,** *98*, (Supplement C), 12-20.

155. Zhang, Z.; Schwartz, S.; Wagner, L.; Miller, W., A Greedy Algorithm for Aligning DNA Sequences. *Journal of Computational Biology* **2000,** *7*, (1-2), 203-214.

156. Endo, S.; Escher, B. I.; Goss, K.-U., Capacities of Membrane Lipids to Accumulate Neutral Organic Chemicals. *Environ. Sci. Technol.* **2011,** *45*, (14), 5912-5921.

157. Deutscher, J.; Francke, C.; Postma, P. W., How Phosphotransferase System-Related Protein Phosphorylation Regulates Carbohydrate Metabolism in Bacteria. *Microbiology and Molecular Biology Reviews* **2006,** *70*, (4), 939-1031.

158. Nichols, N. N.; Harwood, C. S., PcaK, a high-affinity permease for the aromatic compounds 4-hydroxybenzoate and protocatechuate from Pseudomonas putida. *Journal of Bacteriology* **1997,** *179*, (16), 5056-61.

159. Groenewegen, P. E.; Driessen, A. J.; Konings, W. N.; de Bont, J. A., Energy-dependent uptake of 4-chlorobenzoate in the coryneform bacterium NTB-1. *Journal of Bacteriology* **1990,** *172*, (1), 419-423.

160. Lambert, P. A., Cellular impermeability and uptake of biocides and antibiotics in Gram-positive bacteria and mycobacteria. *Journal of Applied Microbiology* **2002,** *92*, 46S-54S.

161. Mancini, S. A.; Hirschorn, S. K.; Elsner, M.; Lacrampe-Couloume, G.; Sleep, B. E.; Edwards, E. A.; SherwoodLollar, B., Effects of Trace Element Concentration on Enzyme Controlled Stable Isotope Fractionation during Aerobic Biodegradation of Toluene. *Environ. Sci. Technol.* **2006,** *40*, (24), 7675-7681.

162. Sikkema, J.; de Bont, J. A.; Poolman, B., Mechanisms of membrane toxicity of hydrocarbons. *Microbiological Reviews* **1995,** *59*, (2), 201-22.

163. Isken, S.; de Bont, J. A. M., Bacteria tolerant to organic solvents. *Extremophiles* **1998,** *2*, (3), 229-238.

164. Dill, G. M.; Sammons, R. D.; Feng, P. C. C.; Kohn, F.; Kretzmer, K.; Mehrsheikh, A.; Bleeke, M.; Honegger, J. L.; Farmer, D.; Wright, D.; Haupfear, E. A., Glyphosate: Discovery, Development, Applications, and Properties. In *Glyphosate Resistance in Crops and Weeds*, John Wiley & Sons, Inc.: 2010; pp 1-33.

165. Bøhn, T.; Cuhra, M.; Traavik, T.; Sanden, M.; Fagan, J.; Primicerio, R., Compositional differences in soybeans on the market: Glyphosate accumulates in Roundup Ready GM soybeans. *Food Chemistry* **2014,** *153*, 207-215.

166. Woodburn, A. T., Glyphosate: production, pricing and use worldwide. *Pest Management Science* **2000,** *56*, (4), 309-312.

167. Sullivan, T. P.; Sullivan, D. S., Vegetation management and ecosystem disturbance: impact of glyphosate herbicide on plant and animal diversity in terrestrial systems. *Environmental Reviews* **2003,** *11*, (1), 37-59.

168. Mamy, L.; Gabrielle, B.; Barriuso, E., Comparative environmental impacts of glyphosate and conventional herbicides when used with glyphosate-tolerant and non-tolerant crops. *Environmental Pollution* **2010,** *158*, (10), 3172-3178.

169. Firbank, L. G.; Forcella, F., Genetically Modified Crops and Farmland Biodiversity. *Science* **2000,** *289*, (5484), 1481-1482.

170. WHO, IARC Monographs: evaluation of five organophosphate insecticides and herbicides. *WHO* **2015,** *112*.

171. Chang, E. T.; Delzell, E., Systematic review and meta-analysis of glyphosate exposure and risk of lymphohematopoietic cancers. *Journal of Environmental Science and Health, Part B* **2016,** *51*, (6), 402-434.

172. Andreotti, G.; Koutros, S.; Hofmann, J. N.; Sandler, D. P.; Lubin, J. H.; Lynch, C. F.; Lerro, C. C.; De Roos, A. J.; Parks, C. G.; Alavanja, M. C.; Silverman, D. T.; Beane Freeman, L. E., Glyphosate Use and Cancer Incidence in the Agricultural Health Study. *Journal of the National Cancer Institute* **2017**.

173. Mamy, L.; Barriuso, E.; Gabrielle, B., Environmental fate of herbicides trifluralin, metazachlor, metamitron and sulcotrione compared with that of glyphosate, a substitute broad spectrum herbicide for different glyphosate-resistant crops. *Pest management science* **2005,** *61*, (9), 905-916.

174. Horth, H.; Blackmore, K., Survey of glyphosate and AMPA in groundwaters and surface waters in Europe. *Report by WRc plc, Swindon, Swindon, Wiltshire, United Kingdom. No.: UC8073* **2009,** *2*.

175. Ermakova, I.; Kiseleva, N.; Shushkova, T.; Zharikov, M.; Zharikov, G.; Leontievsky, A., Bioremediation of glyphosate-contaminated soils. *Applied Microbiology and Biotechnology* **2010,** *88*, (2), 585-594.

176. Pipke, R.; Amrhein, N., Degradation of the Phosphonate Herbicide Glyphosate by Arthrobacter atrocyaneus ATCC 13752. *Applied and Environmental Microbiology* **1988,** *54*, (5), 1293-1296.

177. Borggaard, O. K.; Gimsing, A. L., Fate of glyphosate in soil and the possibility of leaching to ground and surface waters: a review. *Pest Management Science* **2008,** *64*, (4), 441-456.

178. Button, D. K., Kinetics of nutrient-limited transport and microbial growth. *Microbiol. Rev.* **1985**, (49), 270-297.

179. Ehrl, B. N.; Gharasoo, M.; Elsner, M., Isotope fractionation pinpoints membrane permeability as barrier to atrazine biodegradation in Gram-negative Polaromonas sp. Nea-C. *Environ. Sci. Technol.* **in review, attached as supporting information for review only**. **See chapter 4.**

180. Thullner, M.; Fischer, A.; Richnow, H. H.; Wick, L. Y., Influence of mass transfer on stable isotope fractionation. *Applied Microbiology and Biotechnology* **2013,** *97*, (2), 441-452.

181. Kujawinski, D. M.; Wolbert, J. B.; Zhang, L.; Jochmann, M. A.; Widory, D.; Baran, N.; Schmidt, T. C., Carbon isotope ratio measurements of glyphosate and AMPA by liquid chromatography coupled to isotope ratio mass spectrometry. *Analytical and Bioanalytical Chemistry* **2013,** *405*, (9), 2869-2878.

182. Moncelli, M. R.; Becucci, L.; Guidelli, R., The intrinsic pKa values for phosphatidylcholine, phosphatidylethanolamine, and phosphatidylserine in monolayers deposited on mercury electrodes. *Biophysical Journal* **1994,** *66*, (6), 1969-1980.

183. Viscio, D. B.; Prestegard, J. H., NMR studies of 5-hydroxytryptamine transport through large unilamellar vesicle membranes. *Proceedings of the National Academy of Sciences of the United States of America* **1981,** *78*, (3), 1638-1642.

184. Kell, D. B.; Dobson, P. D.; Oliver, S. G., Pharmaceutical drug transport: the issues and the implications that it is essentially carrier-mediated only. *Drug Discovery Today* **2011,** *16*, (15–16), 704-714.

185. Males, R. G.; Phillips, P. S.; Herring, F. G., Equations describing passive transport through vesicular membranes. *Biophysical Chemistry* **1998,** *70*, (1), 65-74.

186. Kopinke, F.-D.; Georgi, A.; Roland, U., Isotope fractionation in phase-transfer processes under thermodynamic and kinetic control – Implications for diffusive fractionation in aqueous solution. *Science of The Total Environment* **2018,** *610-611*, (Supplement C), 495-502.

187. Elsner, M.; Zwank, L.; Hunkeler, D.; Schwarzenbach, R. P., A new concept linking observable stable isotope fractionation to transformation pathways of organic pollutants. *Environ. Sci. Technol.* **2005,** *39*, (18), 6896-6916.

188. Mancini, S. A.; Ulrich, A. C.; Lacrampe-Couloume, G.; Sleep, B.; Edwards, E. A.; Lollar, B. S., Carbon and hydrogen isotopic fractionation during anaerobic biodegradation of benzene. *Appl. Environ. Microbiol.* **2003,** *69*, (1), 191-198.

189. Pipke, R.; Amrhein, N.; Jacob, G. S.; Schaefer, J.; Kishore, G. M., Metabolism of glyphosate in an Arthrobacter sp. GLP-1. *European Journal of Biochemistry* **1987,** *165*, (2), 267-273.

190. Erickson, L. E., Degradation of atrazine and related s-triazines. *Crit. Rev. Env. Con.* **1989,** *19*, 1-14.

191. Behki, R. M.; Shahamat, K. U., Degradation of atrazine by *Pseudomonas*: N-dealkylation and dehalogenation of atrazine and its metabolites. *Journal of Agriculture and Food Chemistry* **1986,** *34*, 746-749.

192. Behki, R.; Topp, E.; Dick, W.; Germon, P., Metabolism of the herbicide atrazine by *Rhodococcus* strains. *Applid Environmental Microbiology* **1993,** *59*, (6), 1955-1959.

193. Nagy, I.; Compernolle, F.; Ghys, K.; Vanderleyden, J.; De Mot, R., A single cytochrome P-450 system is involved in degradation of the herbicides EPTC (S-ethyl dipropylthiocarbamate) and atrazine by Rhodococcus sp. strain NI86/21. *Appl. Environ. Microbiol.* **1995,** *61*, (5), 2056-2060.

194. de Souza , M. L.; Seffernick, J.; Martinez, B.; Sadowsky, M. J.; Wackett, L. P., The atrazine catabolism genes atzABC are widespread and highly conserved. *Journal of Bacteriology* **1998,** *180*, (7), 1951-1954.

195. Seffernick, J. L.; Johnson, G.; Sadowsky, M. J.; Wackett, L. P., Substrate specificity of atrazine chlorohydrolase and atrazine-catabolizing bacteria. *Applied Environmental Microbiology* **2000,** *66*, (10), 4247-4252.

196. Topp, E.; Mulbry, W. M.; Zhu, H.; Nour, S. M.; Cuppels, D., Characterization of S-Triazine Herbicide Metabolism by a Nocardioides sp. Isolated from Agricultural Soils. *Appl. Environ. Microbiol.* **2000,** *66*, (8), 3134-3141.

197. Rousseaux, S.; Hartmann, A.; Soulas, G., Isolation and characterisation of new Gram-negative and Gram-positive atrazine degrading bacteria from different French soils. *FEMS Microbiol. Ecol.* **2001,** *36*, (2-3), 211-222.

198. Satsuma, K., Complete biodegradation of atrazine by a microbial community isolated from a naturally derived river ecosystem (microcosm). *Chemosphere* **2009,** *77*, (4), 590-596.

199. Vibber, L.; Pressler, M.; Colores, G., Isolation and characterization of novel atrazine-degrading microorganisms from an agricultural soil. *Applied Microbiology and Biotechnology* **2007,** *75*, (4), 921-928.

200. Piutti, S.; Semon, E.; Landry, D.; Hartmann, A.; Dousset, S.; Lichtfouse, E.; Topp, E.; Soulas, G.; Martin-Laurent, F., Isolation and characterisation of Nocardioides sp SP12, an atrazine-degrading bacterial strain possessing the gene trzN from bulk- and maize rhizosphere soil. *Fems Microbiology Letters* **2003,** *221*, (1), 111-117.

201. Holler, T.; Wegener, G.; Niemann, H.; Deusner, C.; Ferdelman, T. G.; Boetius, A.; Brunner, B.; Widdel, F., Carbon and sulfur back flux during anaerobic microbial oxidation of methane and coupled sulfate reduction. *Proceedings of the National Academy of Sciences* **2011,** *108*, (52), E1484-E1490.

202. Pipke, R.; Schulz, A.; Amrhein, N., Uptake of Glyphosate by an Arthrobacter sp. *Applied and Environmental Microbiology* **1987,** *53*, (5), 974-978.

203. Pilloni, G.; von Netzer, F.; Engel, M.; Lueders, T., Electron acceptor-dependent identification of key anaerobic toluene degraders at a tar-oil-contaminated aquifer by Pyro-SIP. *FEMS Microbiol Ecol* **2011,** *78*, (1), 165-175.

204. Radajewski, S.; Ineson, P.; Parekh, N. R.; Murrell, J. C., Stable-isotope probing as a tool in microbial ecology. *Nature* **2000,** *403*, (6770), 646-649.

205. Tratnyek, P. G.; Johnson, T. L.; Scherer, M. M.; Eykholt, G. R., Remediating ground water with zero-valent metals: Chemical considerations in barrier design. *Ground Water Monitoring and Remediation* **1997,** *17*, (4), 108-114.

206. Li, X. Q.; Elliott, D. W.; Zhang, W. X., Zero-valent iron nanoparticles for abatement of environmental pollutants: Materials and engineering aspects. *Critical Reviews in Solid State and Materials Sciences* **2006,** *31*, (4), 111-122.

207. Anneser, B.; Einsiedl, F.; Meckenstock, R. U.; Richters, L.; Wisotzky, F.; Griebler, C., High-resolution monitoring of biogeochemical gradients in a tar oil-contaminated aquifer. *Appl Geochem* **2008,** *23*, (6), 1715-1730.

208. Kotte, O.; Zaugg, J. B.; Heinemann, M., Bacterial adaptation through distributed sensing of metabolic fluxes. *Molecular Systems Biology* **2010,** *6*, (1).

209. Unell, M.; Kabelitz, N.; Jansson, J. K.; Heipieper, H. J., Adaptation of the psychrotroph Arthrobacter chlorophenolicus A6 to growth temperature and the presence of phenols by changes in the anteiso/iso ratio of branched fatty acids. *FEMS Microbiology Letters* **2006,** *266*, (2), 138-143.

210. Zhu, W.; Smith, J. W.; Huang, C.-M., Mass Spectrometry-Based Label-Free Quantitative Proteomics. *Journal of Biomedicine and Biotechnology* **2010,** *2010*, 6.

211. Dieterich, D. C.; Link, A. J.; Graumann, J.; Tirrell, D. A.; Schuman, E. M., Selective identification of newly synthesized proteins in mammalian cells using bioorthogonal noncanonical amino acid tagging (BONCAT). *Proc Natl Acad Sci USA* **2006,** *103*, (25), 9482-9487.

212. Landgraf, P.; Antileo, E. R.; Schuman, E. M.; Dieterich, D. C., BONCAT: metabolic labeling, click chemistry, and affinity purification of newly synthesized proteomes. *Site-Specific Protein Labeling: Methods and Protocols* **2015**, 199-215.

213. Glenn, W. S.; Stone, S. E.; Ho, S. H.; Sweredoski, M. J.; Moradian, A.; Hess, S.; Bailey-Serres, J.; Tirrell, D. A., Bioorthogonal Noncanonical Amino Acid Tagging (BONCAT) Enables Time-Resolved Analysis of Protein Synthesis in Native Plant Tissue. *Plant Physiol.* **2017,** *173*, (3), 1543-1553.

214. Herbst, F.-A.; Bahr, A.; Duarte, M.; Pieper, D. H.; Richnow, H.-H.; von Bergen, M.; Seifert, J.; Bombach, P., Elucidation of in situ polycyclic aromatic hydrocarbon degradation by functional metaproteomics (protein-SIP). *PROTEOMICS* **2013,** *13*, (18-19), 2910-2920.

215. Wilson, M. S.; Bakermans, C.; Madsen, E. L., In Situ, Real-Time Catabolic Gene Expression: Extraction and Characterization of Naphthalene Dioxygenase mRNA Transcripts from Groundwater. *Applied and Environmental Microbiology* **1999,** *65*, (1), 80-87.

216. Bligh, E. G.; Dyer, W. J., A RAPID METHOD OF TOTAL LIPID EXTRACTION AND PURIFICATION. *Canadian Journal of Biochemistry and Physiology* **1959,** *37*, (8), 911-917.

217. Lennen, R. M.; Pfleger, B. F., Modulating Membrane Composition Alters Free Fatty Acid Tolerance in Escherichia coli. *PLOS ONE* **2013,** *8*, (1), e54031.

218. vanBodegom, P., Microbial Maintenance: A Critical Review on Its Quantification. *Microbial Ecology* **2007,** *53*, (4), 513-523.

219. Pirt, S. J., The maintenance energy of bacteria in growing cultures. *Proceedings of the Royal Society of London. Series B. Biological Sciences* **1965,** *163*, (991), 224-231.

220. Kotte, O.; Volkmer, B.; Radzikowski, J. L.; Heinemann, M., Phenotypic bistability in Escherichia coli's central carbon metabolism. *Molecular systems biology* **2014,** *10*, (7), 736.

221. de Poorter, L. M. I.; Geerts, W. J.; Keltjens, J. T., Coupling of Methanothermobacter thermautotrophicus Methane Formation and Growth in Fed-Batch and Continuous Cultures under Different H2 Gassing Regimens. *Appl. Environ. Microbiol.* **2007,** *73*, (3), 740-749.

222. Muller, R. H.; Rohwerder, T.; Harms, H., Carbon Conversion Efficiency and Limits of Productive Bacterial Degradation of Methyl tert-Butyl Ether and Related Compounds. *Appl. Environ. Microbiol.* **2007,** *73*, (6), 1783-1791.

223. Christensen, T. H.; Bjerg, P. L.; Banwart, S. A.; Jakobsen, R.; Heron, G.; Albrechtsen, H. J., Characterization of redox conditions in groundwater contaminant plumes. *Journal of Contaminant Hydrology* **2000,** *45*, (3-4), 165-241.

224. Gregoire, C.; Payraudeau, S.; Domange, N., Use and fate of 17 pesticides applied on a vineyard catchment. *International Journal of Environmental and Analytical Chemistry* **2010,** *90*, (3-6), 406-420.